Innate Immune Consequences of Hepatocyte Injury

Katherine J. Brempelis

A dissertation

submitted in partial fulfillment of the

requirements for the degree of

Doctor of Philosophy

University of Washington

2016

Reading Committee:

Ian N. Crispe, Chair

Jessica Hamerman

Stephen Polyak

Program Authorized to Offer Degree:

Pathobiology

University of Washington

Abstract

Innate Immune Consequences of Hepatocyte Injury

Katherine J. Brempelis

Chair of the supervisory committee:

Professor Ian N. Crispe

Department of Pathology

Acute and chronic liver disease are estimated to have caused more than two million deaths in 2013, accounting for 4% of total worldwide deaths. The etiologies of acute and chronic liver injury are varied and include insult from pathogens, toxins, diet, and mechanical stresses. A common feature of both infectious and non-infectious liver injury is the death of hepatocytes, the dominant cell population in the liver. The innate inflammatory response to hepatocyte death plays an important role in the outcome of liver injury and can determine whether inflammation is resolved or progresses to chronic disease. This dissertation outlines research to identify innate immune signaling pathways involved in the response to hepatocyte death. To this end, we have developed a mouse model of hepatocyte-specific death to induce acute liver injury by expressing the human diphtheria toxin receptor specifically in hepatocytes. Upon administration of diphtheria toxin and induction of hepatocyte death, we found that the Toll/IL-1 receptor domain-containing adapter protein inducing IFN-β (TRIF) was a central mediator in the resulting inflammatory response and signaled by Toll-like receptor 4- and type I

interferon-independent mechanisms. Hepatocytes were the main responders to cell death and up-regulated chemokine (*Ccl2*, *Ccl5*, *Ccl7*, *Cxcl1*, *Cxcl2*, *Cxcl10*), cell adhesion (*Icam1*, *Vcam1*), and inflammatory (*Tnf*, *Ifnb1*) genes more than either liver sinusoidal endothelial cells or Kupffer cells. We also employed a diet- and alcohol-induced model of liver injury to study the effects of hepatocyte death in a chronic setting. We found that increased liver steatosis, or fatty liver, correlated with increased amounts of dietary carbohydrates, and specifically glucose. Furthermore, similar to our model of acute liver injury, we found that hepatocytes were central responders to liver injury and up-regulated the expression of chemokine (*Ccl2*, *Ccl5*, *Cxcl10*), cell adhesion (*Vcam1*), inflammatory (*Il1a*, *Il1b*), and fibrosis (*Mmp9*, *Mmp12*, *Pdgfra*, *Tgfb1*) genes more than either liver sinusoidal endothelial cells or Kupffer cells. Finally, ethanol exposure increased the recruitment of neutrophils to the liver but down-regulated expression of *Tgfb1* and reduced the overall pathology.

The unifying theme we demonstrate in this thesis is the previously-underappreciated central role that hepatocytes play in the response to non-infectious liver injury. Hepatocytes are both the targets of insult and the primary mediators of the innate immune response in models of acute and chronic inflammation, suggesting a conserved mechanism in the response to liver injury.

TABLE OF CONTENTS

LIST OF FIGURES ..... **IV**

LIST OF TABLES ..... **VI**

LIST OF ABBREVIATIONS ..... **VIII**

CHAPTER 1: INTRODUCTION **1**

Overview 1
The global burden of liver disease 2
Non-infectious modes of liver injury: Acute and chronic pathologies 3
Acute inflammation 4
Chronic inflammation 5
The central role of hepatocytes in non-infectious modes of liver injury 6
Non-infectious modes of liver injury: The immune machinery 7
Indicators of injury: DAMPs and PAMPs 7
Sensors of injury: TLRs 8
Non-infectious modes of liver injury: TLR-driven inflammation in acute and chronic injury 11
Acetaminophen hepatotoxicity 11
Ischemia-reperfusion injury 13
Non-alcoholic liver disease and non-alcoholic steatohepatitis 15
Alcoholic liver disease and alcoholic steatohepatitis 16
Dissertation Aims 18

CHAPTER 2: MATERIALS AND METHODS **19**

Shared Methods 19
Liver perfusion 19
Flow cytometry and cell sorting 19
Cell purity 20
Measurement of liver enzymes 20
Quantitative real-time PCR (qRT-PCR) expression analysis 23
Histology 24
Materials and Methods for Chapter 3 25
Plasmids for rAAV vectors 26
rAAV production and purification 26
Mice 27
Quantification of rAAV 28
Model of hepatocyte-specific death 29
Measurement of protein 29
Western blot analysis 29
Statistical analysis 30
Materials and Methods for Chapter 4 33
Mice 33
Description of diets 33
Preparation of diets 34

Administration of diets 34
Measurement of mouse weight 36
Statistical methods 36

CHAPTER 3: HEPATOCYTE-SPECIFIC DEATH AS A MODEL OF ACUTE, STERILE LIVER INJURY 37

Abstract 37
Introduction 38
Results 39
Model of hepatocyte-specific death 39
Neutrophils and monocytes are recruited to the liver following hepatocyte death 43
Type I interferon expression is increased following hepatocyte death 48
TRIF plays a larger role than MyD88 in the inflammatory response to hepatocyte death 50
TRIF is not required for increased expression of myeloid cell-recruiting chemokines or cell-adhesion molecules, nor for increased production of CCL2 and CXCL1 protein 52
TRIF is required for increased production of IL-1β, IL-10, and IL-6 56
Type I IFN signaling does not mediate the inflammation that follows hepatocyte death 61
TLR4 does not mediate the inflammation that follows hepatocyte death 61
Discussion 65

CHAPTER 4: DIET- AND ALCOHOL-INDUCED DAMAGE AS A MODEL OF CHRONIC LIVER INJURY 70

Abstract 70
Introduction 71
Results 74
6.7% vol/vol ethanol resulted in early, unexpected mouse mortality 74
5.0% vol/vol ethanol prevented unexpected mouse mortality 76
Ethanol-fed mice had lower measures of liver damage than control-fed mice at 8 weeks 76
Low-fat diets increased ALT and AST serum levels in mice 77
Low-fat diets increased monocyte and neutrophil infiltrate in mice 80
Low-fat diets caused increased pathology in the liver 82
Mid-fat and low-fat diets caused up-regulation of inflammatory genes in hepatocytes 85
Ethanol down-regulated chemokine and fibrosis gene expression in hepatocytes 86
Discussion 91

CHAPTER 5: CONCLUSIONS AND FUTURE DIRECTIONS 95

Overview 95
Discussion 96
Conclusion 102
Acknowledgements 102

APPENDIX: ISOLATION OF NON-PARENCHYMAL CELLS FROM THE MOUSE LIVER 103

REFERENCES 125

LIST OF FIGURES

Figure 1-1. Toll-like receptor signaling pathways. 9
Figure 2-1. Enrichment of cell-specific genes in total liver, hepatocyte, LSEC, and KC populations for Chapter 3. 22
Figure 2-2. Enrichment of cell-specific genes in total liver, hepatocyte, LSEC, KC, and HSC populations for Chapter 4. 23
Figure 2-3. Expression of *hDTR* as a criteria to eliminate mice from the analyses for Chapter 3. 32
Figure 3-1. Hepatocyte-specific expression of rAAV8.pAlb.mCherry.hDTR results in peak liver damage 48 hours following diphtheria toxin injection. 41
Figure 3-2. Preliminary experiments using rAAV8.pAlb.OVA.hDTR support findings from rAAV8.pAlb.mCherry.hDTR experiments. 42
Figure 3-3. Preliminary gating strategy. 44
Figure 3-4. Hepatocyte death promotes the infiltration of neutrophils and monocytes. 45
Figure 3-5. Ly6C(+) monocytes are the predominant monocyte population in the liver at 24 hours but by 48 hours Ly6C(-) monocytes dominate. 46
Figure 3-6. Hepatocyte death up-regulates genes associated with myeloid cell-recruitment, predominantly in hepatocytes. 48
Figure 3-7. Hepatocyte death induces expression of the TRIF-pathway cytokine IFN-β, predominantly in hepatocytes, and only minimally induces expression of MyD88-pathway cytokines. 49
Figure 3-8. $TRIF^{-/-}$ mice exhibit less inflammation than $MyD88^{-/-}$ mice following hepatocyte death. 51
Figure 3-9. TRIF is dispensable for increased expression of myeloid cell-recruiting chemokines and cell-adhesion molecules, as well as increased production of CCL2 and CXCL1 protein. 55
Figure 3-10. The increased production of IL-10, IL-6, and IL-1β depends on TRIF. 58
Figure 3-11. *Il10*, *Il6*, *Il1b*, and *Tnf* are expressed most highly by Kupffer cells and levels decrease 48-72 hours following diphtheria toxin injection. 59
Figure 3-12. TRIF is required for the down-regulation of *Il10*, *Il6*, and *Il1b* in Kupffer cells. 60
Figure 3-13. Type I IFN does not contribute to the inflammation induced by hepatocyte death. 62
Figure 3-14. TLR4 signaling is not required for the inflammation induced by hepatocyte death. 63
Figure 3-15. Reduced transduction of $TLR3^{-/-}$ hepatocytes by rAAV. 64
Figure 4-1. A 6.7% vol/vol ethanol diet caused early mouse mortality. 75
Figure 4-2. Ethanol-fed mice had lower levels of ALT, AST, and monocytes than control-fed mice. 77
Figure 4-3. Low-fat control and ethanol diets induced more damage in mice than mid-fat control and chow diets. 80
Figure 4-4. Low-fat diets induce greater monocyte and neutrophil infiltrate than mid-fat control and chow diets. 81

Figure 4-5. Hematoxylin and eosin-stained liver sections, 8 weeks. 84
Figure 4-6. Mid-fat and low-fat Lieber-DeCarli control diets induce greater up-regulation of genes related to inflammation, oxidative stress, and fibrosis, predominantly in hepatocytes..... 87
Figure 4-7. Mid-fat and low-fat Lieber-DeCarli diets cause up-regulation of inflammatory and fibrosis genes in hepatocytes. 88
Figure 4-8. Ethanol suppresses gene expression in hepatocytes to a greater extent than in LSECs or KCs. 89
Figure 4-9. Ethanol suppresses *Tgfb1* expression in hepatocytes. 90
Figure A-1. Suggested workspace set-up. 119
Figure A-2. General perfusion anatomy and procedure. 120
Figure A-3. NPC sort strategy. 121
Figure A-4. Quality control by qRT-PCR of hepatocytes and sorted liver NPCs. 123

LIST OF TABLES

Table 2-1. Caloric profile for diets used in Chapter 4 experiments. 34
Table 2-2. Experimental design for Chapter 4 experiments. 34
Table 4-1. Caloric profile and carbohydrate composition for diets. 79
Table 4-2. Histological scores for hematoxylin and eosin stained sections, 8 weeks. 83
Table A-1. Antibodies for FACS-based purification of some of the major liver NPC and leukocytes. 124

Dedication

To my family,
thank you.

This is for you.

LIST OF ABBREVIATIONS

pAlb or Alb^P = Albumin promotor

ALD = Alcoholic fatty liver disease

ALF = Acute liver failure

ALT = Alanine aminotransferase

APAP = Acetaminophen

ASH = Alcoholic steatohepatitis

AST = Aspartate aminotransferase

Ccl = Chemokine (C-C) motif ligand

Cxcl = C-X-C motif chemokine

DAMP = Damage-associated molecular pattern

DT = Diphtheria toxin

HBV = Hepatitis B virus

HCC = Hepatocellular carcinoma

HCV = Hepatitis C virus

hDTR = Human diphtheria toxin receptor

Hepa = Hepatocyte

HMGB1 = High mobility group box 1

HSC= Hepatic stellate cell

HSPs = Heat shock proteins

ICAM1 = Intercellular adhesion molecule 1

IFNAR1 = Interferon (α and β) receptor 1

IFN = Interferon

IL = Interleukin

IRF= Interferon regulatory factor

IR = Ischemia-reperfusion

KC = Kupffer cell

LPS = Lipopolysaccharide

LSEC = Liver sinusoidal endothelial cell

MMPs = Matrix metalloproteinases

MyD88 = Myeloid differentiation primary response protein 88

NAFLD = Non-alcoholic fatty liver disease

NASH = Non-alcoholic steatohepatitis

NF-kB = Nuclear factor κB

NK = Natural killer

NPC = Non-parenchymal cell

PAMP = Pathogen-associated molecular pattern

PRR = Pattern recognition receptor

rAAV = Recombinant adeno-associated virus

ROS = Reactive oxygen species

TGF-β = Transforming growth factor beta

TIMPs = Tissue inhibitors of metalloproteinases

TLR = Toll-like receptor

TNF-α = Tumor necrosis factor alpha

TRIF = Toll/IL-1 receptor domain-containing adapter protein inducing IFN-β

VCAM1 = Vascular cell adhesion molecule 1

v/v or vol/vol = volume/volume

CHAPTER 1: INTRODUCTION

Overview

Liver disease is a serious concern in both developing and developed nations, contributing to 4% of deaths worldwide [1]. Liver damage can be caused by pathogens, toxins, diet, or mechanical stress and initiates an inflammatory response by innate immune cells. The outcome of the initial innate immune response dictates whether inflammation is acute and resolved or chronic with potential progression to fibrosis, cirrhosis, and/or hepatocellular carcinoma. Inflammation is often complicated by the fact that more than one cause, for example hepatitis C virus infection combined with chronic alcohol consumption, contributes to the resulting pathology. The inflammatory responses to liver damage in the presence and absence of pathogen utilize shared signaling pathways. As a result, the contribution of specific factors to the inflammation can be difficult to disentangle. In this dissertation, I use two models of liver injury, and specifically of hepatocyte death, to understand the role non-infectious modes of injury play in acute and chronic inflammatory responses in the liver. The remainder of this introductory chapter will provide the context for the studies outlined in this dissertation. Chapter 2 describes methods critical for the understanding and execution of Chapters 3 and 4. Chapter 3 describes an acute mouse model of liver injury induced by hepatocyte death. Chapter 4 describes a diet- and ethanol-induced mouse model of chronic liver injury. Finally, Chapter 5 provides a synthesis of the major findings in this dissertation, and elaborates on one of the unexpected and interesting connecting themes that emerged through the use of these distinct models of injury: the hepatocyte is a key mediator of the immune response to liver injury.

The global burden of liver disease

Worldwide, viral hepatitis contributes heavily to the burden of liver pathologies. Two-hundred and forty million people are chronically infected with hepatitis B virus (HBV) and 130-150 million people with hepatitis C virus (HCV) [2, 3]. Fifty-five to seventy-five percent of people infected with HCV will progress to chronic infection and of those, 15-30% will develop cirrhosis within 20-30 years [3, 4]. Once cirrhosis is established, the risk of developing hepatocellular carcinoma (HCC), the leading form of liver cancer, is 5-7% per year [5]. While only 5% of adults with HBV infections develop chronic infection, up to 90% of infants who vertically acquire HBV progress to chronic disease [4]. Chronic HBV infection also predisposes people to develop fibrosis, cirrhosis, and HCC, contributing to 30% of cirrhosis cases and 53% of HCC cases [6]. Overall, HBV and HCV contribute to 57% of cirrhosis cases and 78% of HCC cases, respectively [6].

While HBV and HCV are leading causes of liver disease in resource-poor nations, drug- and diet-induced pathologies are the main contributing factors to liver disease in developed nations. In Western nations, the main cause of acute liver failure (ALF) is acetaminophen (APAP) overdose, accounting for nearly 50% of ALF cases [7]. Ischemia-reperfusion (IR) injury contributes to up to 10% of early organ failure following liver transplant and can ultimately lead to increased risk of short-term and long-term organ rejection [8]. Damage induced by diet results in non-alcoholic fatty liver disease (NAFLD), the most common chronic liver disease in Western nations, which can progress to non-alcoholic steatohepatitis (NASH). Damage induced by alcohol results in alcoholic liver disease (ALD), which can progress to alcoholic steatohepatitis (ASH). NAFLD and ALD are characterized by fatty liver, or steatosis, and with the development of fibrosis and inflammation, can progress to NASH and ASH, respectively. Current studies suggest that between 20-30% of the population of the United States and other

Western nations is afflicted by fatty liver [9]. Chronic alcohol abuse is a global issue with studies estimating the presence of 140 million alcoholics worldwide [10]. In the United States alone, chronic alcohol consumption contributed to 13,050 deaths in 2006, approximately 47% of all deaths attributable to chronic liver disease and cirrhosis [11].

Non-infectious modes of liver injury: Acute and chronic pathologies

The innate immune system has evolved to identify and respond to pathogens through the recognition of conserved microbial motifs known as pathogen-associated molecular patterns (PAMPs) [12]; however, innate immune-mediated inflammation also occurs in the absence of pathogen, as with APAP-induced injury or IR injury during organ transplant [13]. Termed sterile inflammation, this state is induced by the release of host-derived products, called damage associated-molecular patterns (DAMPs), during tissue damage. DAMPs, which are normally sequestered inside cells, interact with the pattern recognition receptors (PRRs) of the innate immune system and initiate an inflammatory response.

Liver injury is not monolithic, and there are several pathologies that straddle the border between sterile inflammation and pathogen-induced inflammation. One such example is ALD. In ALD, ethanol-induced damage results in the release of various DAMPs; however, ethanol exposure also increases intestinal permeability and results in increased leakage of lipopolysaccharide (LPS), a bacterial PAMP, from the commensal intestinal flora into the blood supply to the liver. Once in the liver, LPS binds to and activates liver resident macrophages, known as Kupffer cells (KCs), which then produce inflammatory cytokines that promote hepatocyte damage [14-16].

While some forms of sterile liver injury may in fact respond solely to DAMPs released from dying cells, many forms of “sterile” injury are complicated by a response to

PAMPs. The response to PAMPs from the normal gut flora as a component of “sterile” inflammation is increasingly thought to play an important role in pathologies of the liver. The unifying feature of both of true sterile inflammation and inflammation involving an additional PAMP component is that they are non-infectious modes of liver injury.

Acute inflammation

Non-infectious liver injury can induce an acute immune response that either resolves or results in death of the host, or a chronic immune response that produces continual cycles of cell death and inflammation. In the liver, acute inflammation is characterized by the production of cytokines—interleukin (IL)-6, IL-1β, and tumor necrosis factor (TNF)-α—and chemokines—chemokine (C-C motif) ligand (CCL) and C-X-C motif chemokine (CXCL) family chemokines—in response to liver injury which is largely composed of, but not limited to, hepatocyte death [17, 18]. KCs play a central role in the induction and propagation of acute liver injury. Activation of KCs by dying hepatocytes and their released DAMPs drives the production of mediators that can directly induce hepatocyte death (TNF-α, Fas ligand, and reactive oxygen species (ROS)) or indirectly induce hepatocyte death through the recruitment of neutrophils (IL-1β, CXCL1, and CXCL2) [17, 19]. KCs also produce the anti-inflammatory cytokine IL-10, which exerts indirect protective effects on hepatocytes [17]. The influx of neutrophils and monocytes is a hallmark of acute liver injury, with various studies noting the importance of infiltrating monocytes in the production of inflammatory chemokines, a role which is often attributed solely to the hepatic KCs [17]. Classic examples of acute liver inflammation are APAP hepatotoxicity and IR injury.

Chronic inflammation

In many cases, the acute inflammation described above is not resolved and a state of chronic inflammation is established in the liver. For this reason, acute and chronic inflammation can be considered on a spectrum and the events initiating a state of chronic inflammation are the same as those just described for acute inflammation. The difference between acute and chronic liver injury lies in failure of the immune system to resolve the inflammation due to repeated insult and re-injury. With enough time, chronic inflammation can progress to fibrosis, cirrhosis, and ultimately the irreversible state of HCC.

Hepatic stellate cells (HSCs) are central mediators of the progression to fibrosis. Dying cells and chemokines produced in the response to injury activate HSCs which then secrete transforming growth factor beta (TGF-β). TGF-β induces the transdifferentiation of HSCs into activated myofibroblasts, which promote deposition of extracellular matrix and collagen, leading to fibrosis of the liver. During inflammatory responses, KCs produce matrix metalloproteinases (MMPs) to degrade collagen and extracellular matrix components that have been deposited, but myofibroblasts counteract MMPs by producing tissue inhibitors of metalloproteinases (TIMPs) which degrade MMPs [20]. This cycle of matrix deposition, production of TIMPs, and inhibition of MMPs leads to scarring of the liver. The cycle is further perpetuated by TNF-α and IL-1β, inflammatory cytokines produced during the response to liver injury, which promote myofibroblast survival [20]. Examples of chronic liver inflammation include the NAFLD and ALD spectrums. In these and related indications, the interplay of cell types, inflammatory signaling molecules, and molecular effectors underscore the complexity of acute-to-chronic liver inflammation.

The central role of hepatocytes in non-infectious modes of liver injury

The liver is comprised mainly of parenchymal cells, called hepatocytes, and several types of non-parenchymal cells (NPCs): liver sinusoidal endothelial cells (LSECs), the resident macrophage population called KCs, HSCs, liver dendritic cells (DCs), and intrahepatic lymphocytes dominated by Natural Killer (NK) and NKT cell populations. Hepatocytes, which make up ~90% of the total liver mass, comprise only 60-80% of the total cell number in the liver [21, 22]. The remainder is made up of the NPC populations. LSECs account for ~50% of the NPCs and KCs for about 20%, with the remainder made up by lymphocytes (~25%), hepatic DCs (<1%), and HSCs (<1%) [21].

A defining feature of non-infectious liver injury is the death of hepatocytes. In APAP-mediated toxicity, the main mechanism of injury is damage to the endothelial cell microvasculature followed by extensive hepatocyte death in the centrilobular regions of the liver [23]. Historically there has been controversy as to whether the mode of hepatocyte death is predominantly apoptosis or necrosis, though increasing evidence supports necrosis as the dominant mechanism [24-26]. Metabolic disorders such as insulin resistance and obesity also ultimately result in hepatocyte damage, via an excess of free fatty acids (FFA) which contribute to the development of steatosis and NAFLD [27, 28]. Progression to NASH occurs with the development of persistent inflammation and increased hepatocyte death, and in some cases leads to cirrhosis [28]. During ASH, TNF-α released by activated KCs mediates the death of hepatocytes, mainly through apoptotic mechanisms [29, 30]. Finally, in IR injury following liver transplant, hepatocyte death is a central feature, though there is disagreement as to the extent and mode of death [31-33]. In future chapters in this dissertation, I describe work to define pathways of inflammation induced following hepatocyte death in a model of acute, sterile inflammation and also in a model of chronic, non-infectious inflammation.

Non-infectious modes of liver injury: The immune machinery

Indicators of injury: DAMPs and PAMPs

After barrier defenses such as skin and antimicrobial peptides, the next line of defense against foreign microorganisms is the innate immune system. The innate immune system recognizes conserved pathogen components called PAMPs. PAMPs include: components of bacterial cell walls (such as LPS and peptidoglycan); lipopeptides from bacteria, mycobacteria, and mycoplasma; flagellin; DNA from bacteria and viruses, and single- and double-stranded viral RNA; viral envelope proteins; fungal glycolipids and polysaccharides; and finally, a variety of parasitic components including glycolipids [12]. In the liver, one of the most important PAMPs in non-infectious injury is LPS derived from the gut microbiome, with multiple studies demonstrating its importance in inflammation in ALD and more recently, that it may also contribute to the inflammation seen in NAFLD [34, 35].

The innate response against PAMPs allows the immune system to discriminate self from non-self and respond quickly to potentially dangerous foreign material. In 1994, to address short-comings of the “self versus non-self” model of immunity, Polly Matzinger proposed the Danger model, the concept that the immune system responds to danger signals, or DAMPs, released from damaged tissues [36, 37]. While there were no described DAMPs at the time this model was first proposed, many have since been identified, including: endogenous DNA and RNA, ATP, uric acid, high mobility group box 1 (HMGB1), heat-shock proteins (HSPs), and extracellular matrix fragments [13, 27]. HMGB1, a DNA chaperone released during necrotic and apoptotic cell death plays a role in many types of non-infectious liver injury including IR injury and APAP-induced toxicity following its release from dying hepatocytes [25, 38-40].

PAMPs and DAMPs serve as the ligand for PRRs, which are characterized into five families: Toll-like receptors (TLRs), RIG-I-like receptors (RLRs), NOD-like receptors

(NLRs), C-type lectin receptors (CLRs), and absence in melanoma 2 (AIM2)-like receptors (ALRs) [13]. RLRs, CLRs, NLRs and ALRs play an important role in the ecosystem of liver injury; however, this dissertation will expand on the role of TLRs as they directly relate to the studies described in this dissertation.

Sensors of injury: TLRs

Structurally, TLRs are characterized by an intracellular Toll/interleukin (IL)-1 receptor (TIR) signaling domain, a transmembrane region, and an extracellular leucine-rich repeat (LRR) domain that interacts with ligand [41]. In humans, 10 TLRs have been identified (TLRs 1-10), while in mice 12 TLRs have been identified (TLRs 1-13, excluding TLR10) [21]. TLR1, TLR2, TLR4, TLR5, and TLR6 are expressed on the cellular membrane where they interact with external PAMPs and extracellular DAMPs and TLR3, TLR7, TLR8, and TLR9 are expressed within intracellular compartments on the endosome-lysosome membrane, where they interact with nucleic acids, of host or pathogen origin [41].

Binding of ligand to the TLR initiates a signaling cascade through one of two primary adaptor proteins, namely Toll/IL-1 receptor domain-containing adapter protein inducing IFN-β (TRIF) or myeloid differentiation primary response protein 88 (MyD88). TLR3 and TLR4 are the only TLRs known to signal via TRIF while all of the TLRs, with the exception of TLR3, signal through MyD88 [42, 43]. There are two additional adaptors, Toll/interleukin (IL)-1 receptor (TIR) domain containing adaptor protein (TIRAP), used by TLR2 and TLR4 to recruit MyD88 and TRIF-related adaptor molecule (TRAM), used by TLR4 to signal via TRIF [41, 44-46]. In general, the TRIF-dependent pathway results in the translocation of interferon-regulatory factor (IRF)3 and IRF7 to the nucleus and induces transcription of type I interferon (IFN); however, it also has a late-phase response in which nuclear factor κB (NF-κB) is translocated to the nucleus and

induces transcription of pro-inflammatory cytokines such as IL-1β, TNF, and IL-6. The MyD88-dependent pathway generally results in NF-κB translocation to the nucleus and the induction of pro-inflammatory cytokines; however, signaling through endosomal TLRs also induces IRF3 and IRF7 translocation to the nucleus and induction of type I IFN (Figure 1-1) [21, 41].

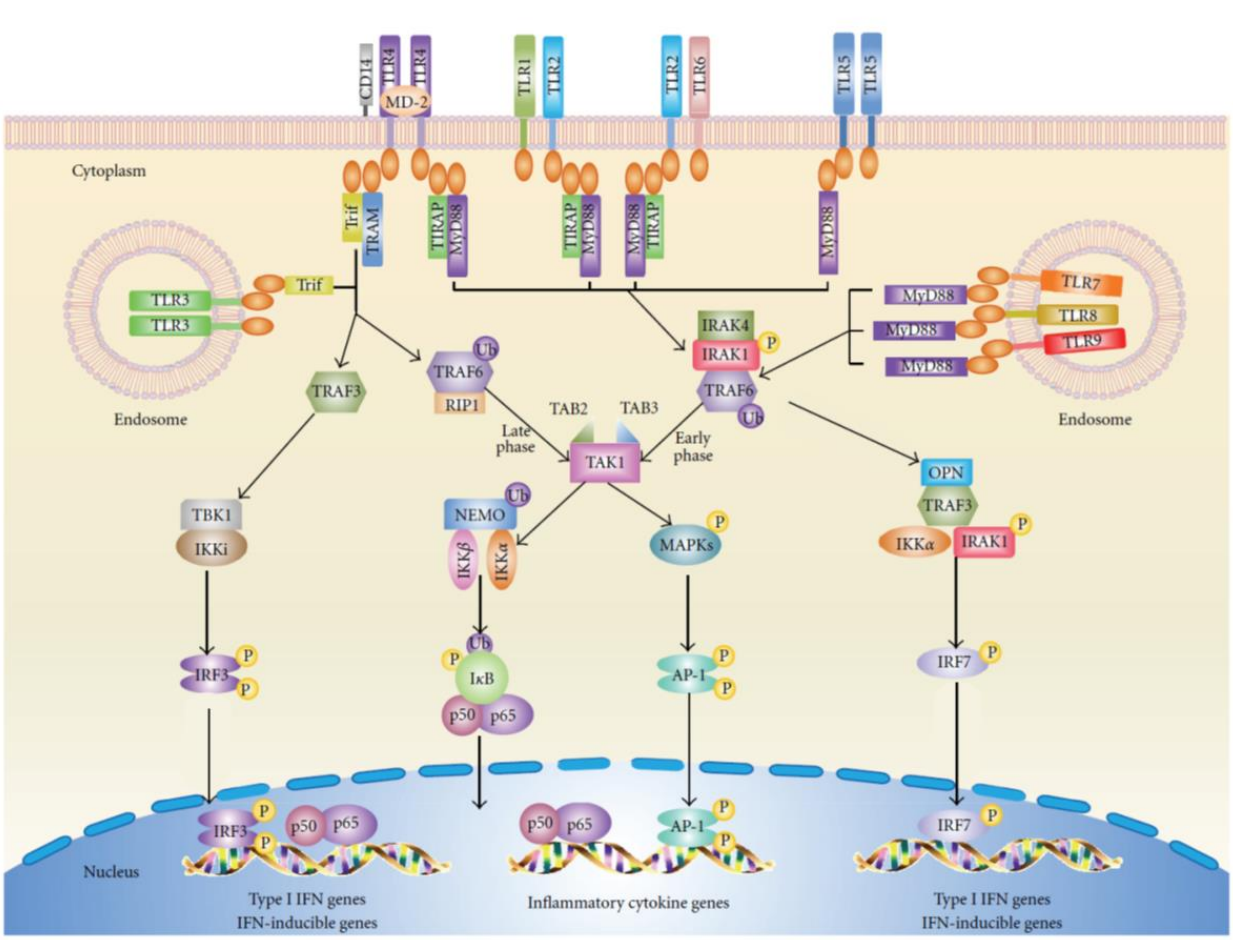

Figure 1-1. Toll-like receptor signaling pathways.
Reprinted from International Journal of Inflammation, 2011, Yan Feng and Wei Chao, "Toll-like Receptors and Myocardial Inflammation", 1-21, Copyright (2011). [12, 47]

The liver is a complex environment where TLR signaling can occur simultaneously by multiple cell populations. Mouse hepatocytes, LSECs, KCs, and HSCs express mRNA for TLRs 1-9, though expression of mRNA does not equate to functional use of the receptor [48-50]. Hepatocytes respond to TLR2, TLR3, and TLR4 ligands *in vitro*, producing IFN-β in response to poly-IC stimulation of TLR3 and activating NF-κB in response to stimulation of TLR2 and TLR4, but show limited or no responses by the other TLRs [44, 51, 52]. A comprehensive study of mouse LSECs and KCs showed that KCs produce either IL-6 or TNF-α in response to stimulation of TLRs 1-9 and additionally, IFN-β following stimulation of TLR3 and TLR4 [49]. LSECs produce TNF-α in response to stimulation of TLRs 1, 2, 4, 6, 8, and 9; IL-6 following stimulation of TLR3 and TLR4; and IFN-β in response to TLR3 [49]. Additionally, the response of KCs to TLR4 ligation, largely by LPS, results in the production of TNF-α, IL-1β, IL-6, IL-12, IL-18, as well as IL-10 [44]. Activated HSCs also respond to TLR ligation, modulating expression of IL-6, intercellular adhesion molecule (ICAM)-1, vascular cell adhesion molecule (VCAM)-1, TGF-β, and CCL2 following stimulation of TLR2, TLR3, TLR4, TLR7, and TLR9 [53]. The TLR pathways in LSECs, KCs, and HSCs that lead to the induction of TNF-α, IFN-β, and IL-6 highlight the importance of these cytokines as central mediators of liver pathology.

In addition to the liver-resident LSECs, KCs, and HSCs, the liver also contains a sizeable population of intrahepatic lymphocytes, which are dominated by NK and NKT cells, and liver DCs. NK cells express mRNA for TLRs 1-4 and 6-9 and respond to TLR stimuli in combination with IL-12 to produce IFN-γ, CCL3, CCL4, and CCL5 [54]. Finally, hepatic conventional DCs (cDCs) and plasmacytoid DCs (pDCs) from mice express TLRs 2, 4, 7, and 9 while cDCs also express TLR3 [21]. TLR7 and TLR9 in pDCs are largely responsible for the production of IFN-α; however, stimulation of TLR7, TLR8, and TLR9 also produces the inflammatory cytokines, TNF-α, IL-6, and IL-12 [55, 56]. cDCs,

on the other hand, respond to ligation of TLRs 2, 3, 4, 7, 8, and 9 by production of TNF-α and IL-6 and additionally produce IL-12 in response to TLR7, TLR8, and TLR9 ligation [56]. Mouse NK cells and liver DCs are important in driving adaptive immune responses, though in comparison to LSECs, KCs, and HSCs, their roles in non-infectious liver injury are less understood [57, 58]. The aggregate of parenchymal, NPC, and other professional immune cells expressing suites of TLR molecules suggests a milieu that is primed to respond to insult; however, the mediators and mechanisms of those responses—for example to non-infectious modes of liver injury—are areas of active research.

Non-infectious modes of liver injury: TLR-driven inflammation in acute and chronic injury

In both acute and chronic pathologies, binding of DAMPs and PAMPs to TLRs is a central mechanism whereby inflammation is initiated, resolved, and/or propagated. In the liver, TLR2, TLR4, and TLR9 are the critical TLRs involved in signaling initiated by currently identified DAMPs. HMGB1, HSPs, and extracellular matrix components bind to both TLR2 and TLR4, whereas cellular DNA binds to TLR9 [13]. In terms of PAMPs in non-infectious liver injury, LPS interacting with and signaling via TLR4 is the best-characterized partnership. As case studies for the role of TLRs in mediating liver injury, what follows is a more detailed expansion on four of the most important types of non-infectious liver injury: acetaminophen hepatotoxicity, ischemia-reperfusion injury, non-alcoholic steatohepatitis, and finally, alcoholic steatohepatitis.

Acetaminophen hepatotoxicity

Inflammation following APAP overdose is dominated by extensive damage to the sinusoids followed by hepatocyte death and release of multiple DAMPs including

HMGB1, HSP-70, hyaluronic acid, and DNA [25, 59]. The recruitment of myeloid cell populations to the liver is also a key feature and may act to both resolve and perpetuate inflammation. Ly6C(hi) monocytes are recruited by CCL2 and are largely involved in tissue repair [60, 61]. The role of neutrophils is controversial. Mice deficient for CD18, the β-chain of the $\alpha_M\beta_2$ integrin critical for neutrophil attachment to ICAM-1, showed no difference in APAP-induced liver injury compared wild type mice [62]. In contrast, another study showed that while TLR9-deficient mice were protected from liver injury, transferring wild type neutrophils into TLR9-deficient mice reversed this protection [63]. Furthermore, this study showed that neutrophils up-regulated TLR9 in response to APAP-induced injury and activated NF-κB pathways in response to stimulation with liver DNA *in vitro* [63].

A role for TLR9 in APAP-induced injury is also supported by studies from Imaeda et al. in which DNA released from apoptotic hepatocytes signaled via TLR9 located on LSECs to potentiate inflammation [64]. Furthermore, they showed that the binding of DNA to TLR9 up-regulated the levels of pro-IL-1β and pro-IL-18 transcript, the first signal required for the secretion of these cytokines following NLRP3 inflammasome activation [64]. They went on to show that mice deficient for components of the NLRP3 inflammasome are protected from liver injury [64]. The role of IL-1β and the NLRP3 inflammasome, however, is controversial. Jaeschke and colleagues presented two studies that showed no role for either IL-1β or the NLRP3 inflammasome in APAP-induced liver injury [65, 66].

TLR4 also contributes to inflammation due to APAP hepatotoxicity [67, 68]. A TLR4 inhibitor reduced KC activation, circulating monocytes and neutrophils, and necrosis in the liver [68]. The role of TLR4 signaling is further supported by studies using gadolinium-chloride and clodronate-depletion of KCs which suggest that TLR4 signaling occurs by the activation of KCs and production of mRNA for IL-6, TNF-α, and IL-1β [69].

The importance of TLR4 suggests that LPS could aggravate the inflammation produced following APAP overdose. While a 2010 study showed the amelioration of APAP-induced hepatotoxicity by blockade of LPS, a recent study used germ-free mice to show that the presence or lack of gut microbiota did not reduce hepatocyte necrosis, leaving the contribution of non-pathogenic bacteria undetermined [70, 71].

Studies of APAP hepatotoxicity reveal that monocyte and neutrophil infiltrate is a key component of inflammation following hepatocyte death. Importantly, APAP-mediated mouse injury models also highlight the pivotal role played by CCL2 and the inflammatory cytokines, IL-6, TNF-α, and IL1-β, in response to hepatocyte death. Though TLR4-mediated pathways are critical for the inflammatory response, the contribution of MyD88-dependent and TRIF-dependent signaling pathways remains unclear.

Ischemia-reperfusion injury

Another type of non-infectious injury characterized by hepatocyte death is IR injury. Ischemia, or a lack of blood flow to the organ, is the first stage of IR-induced liver injury. The lack of blood flow results in metabolic stress on cells and the release of DAMPs including HMGB1, DNA, ATP, and urate [32]. Reperfusion, the second stage, reintroduces blood, and therefore oxygen, to the tissue and results in hepatocyte necrosis due to signaling by DAMPs and the generation of ROS by KCs, LSECs, and hepatocytes [32, 72]. Hepatocyte death is also caused by neutrophils, which are recruited by chemokines and adhesion molecules, particularly ICAM-1 on LSECs, induced downstream of TNF-α production [32, 73].

As with APAP hepatotoxicity, TLR4 and TLR9 are major players in the inflammatory response to IR injury. Inhibition of TLR9 signaling resulted in reduction in liver damage, as well as a reduction in ROS, IL-6, and TNF-α [73]. *In vitro* results suggest that DNA from necrotic hepatocytes served as the DAMP binding to TLR9 [73].

Histones also propagate IR injury through TLR9 and MyD88 signaling [74]. Along with DNA and histones, HMGB1 has been identified as an important DAMP in IR injury. One hour after the start of reperfusion, HMGB1 levels were increased and remained elevated through 24 hours [39]. Furthermore, blockade of HMGB1 binding resulted in the reduction of *Tnf* and *Il6* mRNA [39]. The same group further demonstrated that anti-HMGB1 antibody did not prevent IR-induced injury in TLR4-defective mice, but did prevent damage in wild type mice [39].

In addition to HMGB1-directed induction of TLR4-dependent pathways in IR-induced inflammation, the downstream TLR4-dependent signaling cascade has also been elucidated. Zhai, et al. identified this pathway to occur via an IRF3-dependent, MyD88-independent route [72]. In a mouse transplant model, mice receiving livers from TLR4-deficient donors were protected against IR injury compared to mice receiving wild type livers and showed a reduction in neutrophils, CXCL10, ICAM-1, TNF-α, IL-1β, IL-2, and IFN-γ concomitantly with increased IL-4 and IL-10 expression [8]. Corroborating results were obtained in the transplant of Type I IFN receptor (IFNAR)-deficient livers to wild type recipients [75].

As with APAP-mediated injury, IR-mediated injury induces inflammation through both TLR4 and TLR9. The role of downstream signaling is complicated, with studies implicating both MyD88-dependent and MyD88-independent pathways. The involvement of IRF3 and IFNAR in the inflammatory response suggests that the TRIF-dependent pathway is utilized during IR-induced inflammation. Though not shown in the liver, a study using a mouse model of ischemia-reperfusion in the brain did; however, show that HMGB1 signals via TLR4-dependent, TRIF-independent route to mediate injury; [76].

Non-alcoholic liver disease and non-alcoholic steatohepatitis

APAP- and IR-driven liver inflammation are both acute responses with inflammation either resolving or resulting in death and organ rejection, respectively. There are also chronic modes of non-infectious liver injury, such as the NAFLD and ALD spectrums. NAFLD is characterized by steatosis, or the accumulation of more than 5% fat in hepatocytes, in the absence of other causes, such as chronic alcohol consumption [77, 78]. Most patients with NAFLD have simple steatosis; however, 10-30% of those with NAFLD actually have the more-advanced NASH, or inflammation and hepatocyte death on top of fatty liver [79]. Originally, the “two-hit hypothesis” was used to explain why only a small percentage of patients progress from simple steatosis to NASH [80]. In this model, a “first hit” (hepatic steatosis linked to the risk factors obesity, insulin resistance, or metabolic syndrome) sensitizes the liver, and in particular hepatocytes, to damage by a “second hit”. The “second hit” can be any of a number of stressors including oxidative stress, pro-inflammatory cytokines, or endogenous LPS [35, 80, 81]. More recently, a “multiple hit” hypothesis has been proposed which posits that many “hits”—such as genetic factors, obesity and other metabolic disorders, the intestinal microbiota, and diet—acting in concert are necessary for the development of NASH [77, 82].

Much research is being done to determine how diet, alcohol, and the host microbiota contribute to the progression to NASH. Studies using the methionine-choline-deficient (MCD) diet, a common mouse model of NASH, showed that signaling via TLR4 and TLR9, but not TLR2, contributed to the pathogenesis of NASH [83, 84]. Supporting these findings, Li et al. reported that the infusion of free fatty acids (a “hit”) resulted in TLR4- and MyD88-dependent signaling in hepatocytes [85]. The subsequent release of HMGB1 from damaged hepatocytes activated TLR4 in the hepatocytes themselves, resulting in increased IL-6 and TNF-α production [85]. Gut-derived LPS has also been

implicated in in the pathogenesis of NASH. In particular, leptin-deficient (*ob/ob)* obese mice were more sensitive to low doses of LPS than wild type mice and studies using probiotics in *ob/ob* mice suggest that altering the gut microbiota affects inflammation in NASH [34, 35]. Though pathways to inflammation have been identified, much remains to be elucidated regarding the contribution of additional PRRs and their adaptors in the pathogenesis of NAFLD.

Alcoholic liver disease and alcoholic steatohepatitis

Like NAFLD, alcoholic liver disease is characterized by initial steatosis of the liver. Also like NAFLD/NASH, development of inflammation precipitates the transition to ASH. The same “two-hit” model for the development of steatosis into steatohepatitis has been proposed for ALD as well as an additional, though similar, “sensitization and prime” theory which posits that ethanol exposure sensitizes the liver, increasing its susceptibility to subsequent risk factors [86]. The “sensitization and prime” theory fits well with the observation that the major pathology in ALD is due to increased gut permeability and translocation of bacteria and bacterial products into the liver via the portal vein, which sensitizes KCs to LPS. The resulting constant stimulation of TLR4 on KCs induces the production of the inflammatory cytokines TNF-α, IL1-β, IL-12, and IL-18, the recruitment of neutrophils, and finally, hepatocyte injury [87]. Supporting this role of liver injury, mice deficient for TLR4 and CD14, components required for the recognition of LPS, are protected from injury resulting from chronic ethanol exposure [16, 88].

An extensive body of literature has detailed the TRIF-dependent pathway involved in ALD/ASH pathogenesis. In 2001, Uesugi et al. reported that while mice lacking a functional TLR4 had increased LPS in the portal vein when compared to wild type mice, they were protected from alcohol-induced injury and show decreased levels of *Tnf* transcript [16]. Subsequently, a key study found that the TLR4-driven pathway

was MyD88-independent [89] and an additional study demonstrated that TRIF-deficient mice were protected from ethanol-induced liver injury [90]. The latter study also showed that TNF-α production by macrophages was induced by signaling through TRIF and IRF3 [90]. Additional studies have implicated a role for IRF3 in the signaling cascade inducing hepatocyte apoptosis following ethanol-induced endoplasmic reticulum stress [91].

Alcohol-mediated liver injury does not solely rely on signaling through TLR4. Recently, TLR2 and TLR9 were demonstrated to signal via the MyD88-dependent pathway to control the influx of neutrophils into the liver in a model of chronic-binge ethanol-feeding [92]. Additionally, Roh et al. showed that hepatocytes and HSCs, and not KCs, were responsible for the production of CXCL1 that recruited neutrophils to the liver [92]. Finally, crosstalk between TLRs has been demonstrated to play a protective role in ethanol-mediated injury via TLR3-dependent induction of IL-10 in KCs and HSCs, which resulted in a reduction of infiltrating monocytes and levels of *Tnf*, *Ccl2*, and *Il6* transcript [93].

While NASH and ASH are separate forms of liver injury, they share many commonalities; the foremost being fatty liver. NASH and ASH also share the use of TLR4 as an important mediator of the chronic inflammation seen in these diseases. The TLR4 signaling pathway and the role of LPS in the induction of inflammation has been well-characterized for ASH; however, the role for LPS-initiated TLR4 signaling in NASH is less defined. Additionally, TRIF is central to the response in ASH, while reports indicate that MyD88-dependent responses are central to NASH. Additional research into these areas is needed to clarify the similarities and differences between these pathologies.

Dissertation Aims

The unifying theme throughout the introduction has been the innate immune response to liver injury. TLR4 and TLR9, in particular, are identified as major contributors to the inflammation caused by liver injury. In some cases, this inflammation is MyD88-dependent, while in other cases, it is TRIF-dependent, though much remains to be elucidated on this topic. To expand on innate immune mechanisms in liver injury, this dissertation will describe the use of two models—diphtheria toxin-mediated killing of hepatocytes and diet- and ethanol-induced liver injury—to define immunological pathways downstream of hepatocyte injury. Chapter 2 describes the materials and methods used in Chapters 3 and 4. Chapter 3 describes the role of the TRIF pathway in the response to hepatocyte death. Chapter 4 describes the effect of high-glucose diets in conjunction with alcohol on immunity within the liver. Finally, Chapter 5 of this dissertation presents a synthesis of the earlier chapters, focusing on the important role hepatocytes play in the preceding models, while weaving the results into the greater landscape of liver immunology.

CHAPTER 2: MATERIALS AND METHODS

This chapter presents a section on methods used in both Chapters 3 and 4 (Shared Methods), a section for methods specific to Chapter 3, and a section for methods specific to Chapter 4.

Shared Methods

Liver perfusion

Livers were perfused as described in the publication presented in the Appendix, with only slight modifications, which will be noted here. Briefly, mice were anesthetized with Avertin, the portal vein cut, up to 500 µL of blood collected for serum analysis of ALT and protein, and ~2/3 of the right posterior lobe cut off, with a piece for RNA put into TRIzol and a piece for histology put into either 4% paraformaldehyde in 1X PBS or 10% neutral-buffered formalin and fixed for approximately 24 hours. Perfusion solution followed by approximately 8 mL of 0.8 mg/mL collagenase solution was pumped through the liver, the liver cut out, and gently mashed in Wash Buffer (1X PBS + 4% FBS; heat-inactivated, Gibco and Corning) to form a single cell suspension. The hepatocyte pellet was washed two times with Wash Buffer and 50 µL taken into TRIzol for RNA analysis. The non-parenchymal cells contained in the supernatant were isolated on a 20% iodixonal layer and resuspended in Flow Buffer (1X PBS + 2% FBS + 1 mM EDTA) for staining.

Flow cytometry and cell sorting

Non-parenchymal cells were stained with a panel of antibodies designed for isolating specific cell populations found within the liver: liver sinusoidal endothelial cells (LSECs), Kupffer cells (KCs), hepatic stellate cells (HSCs), neutrophils, and Ly6C(+) and Ly6C(-) monocytes. The specific antibody panels and dilutions used in Chapters 3 and 4

are presented in the section-specific methods, below. Cells were isolated by fluorescence-activated cell sorting on a BD Aria III (BD Biosciences). Analysis of cell populations was performed using FlowJo software, version 9.8.5 (Tree Star Inc.).

Cell purity

Cell purity was determined by the enrichment of cell-specific genes by quantitative real-time PCR as described in the publication presented in the Appendix, with the exception that gene expression was normalized to *Hprt*. Total liver, hepatocyte, LSEC, and KC populations in the Chapter 3 and 4 studies were evaluated by this method (Chapter 3, Figure 2-1; Chapter 4, Figure 2-2).

Measurement of liver enzymes

Levels of alanine aminotransferase (ALT) and aspartate aminotransferase (AST) were quantified from serum. Blood collected from the portal vein was allowed to clot at room temperature for a minimum of 30 min, centrifuged at 6000 rpm for 10 min, and the supernatant collected. When necessary, the supernatant was clarified for an additional 4 min at 6000 rpm. ALT levels were quantified using the Alanine Aminotransferase-SL Kit and AST levels were quantified using the Aspartate Aminotransferase (AST/SGOT)-SL Kit (Sekisui Diagnostics LLC).

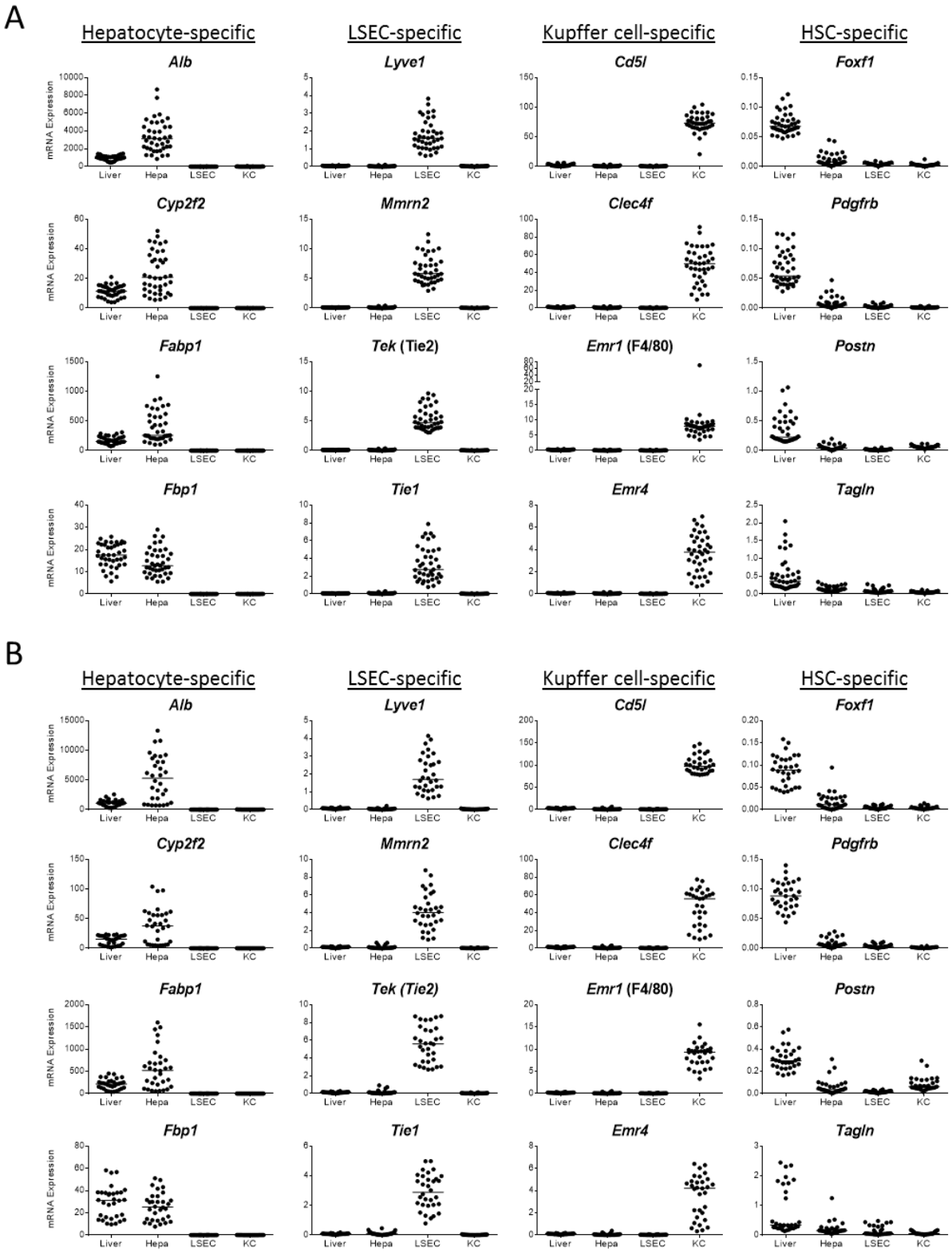
A
Hepatocyte-specific
LSEC-specific
Kupffer cell-specific
HSC-specific
Alb
Lyve1
Cd5l
Foxf1
Cyp2f2
Mmrn2
Clec4f
Pdgfrb
Fabp1
Tek (Tie2)
Emr1 (F4/80)
Postn
Fbp1
Tie1
Emr4
Tagln
mRNA Expression
Liver
Hepa
LSEC
KC
B
Hepatocyte-specific
LSEC-specific
Kupffer cell-specific
HSC-specific
Alb
Lyve1
Cd5l
Foxf1
Cyp2f2
Mmrn2
Clec4f
Pdgfrb
Fabp1
Tek (Tie2)
Emr1 (F4/80)
Postn
Fbp1
Tie1
Emr4
Tagln
mRNA Expression
Liver
Hepa
LSEC
KC

Figure 2-1. Enrichment of cell-specific genes in total liver, hepatocyte, LSEC, and KC populations for Chapter 3. Genes specific for hepatocytes, LSECs, KCs, and HSCs were measured in total liver, hepatocyte, LSEC, and KC RNA samples by qRT-PCR and expressed relative to *Hprt*. (A) Data combined from the two C57BL/6J time course experiments. All time points combined into one group per population. Each data point represents an individual mouse (n = 40, total liver, hepatocytes, LSEC; n = 39, KC), bars represent the median. (B) Data combined from 2 of 3 of the experiments performed in C57BL/6J and TRIF$^{-/-}$ mice. All four treatment groups combined into one group per population, each data point represents an individual mouse (n = 32, total liver, hepatocytes, and LSECs; KCs, n = 31), bars represent the median.

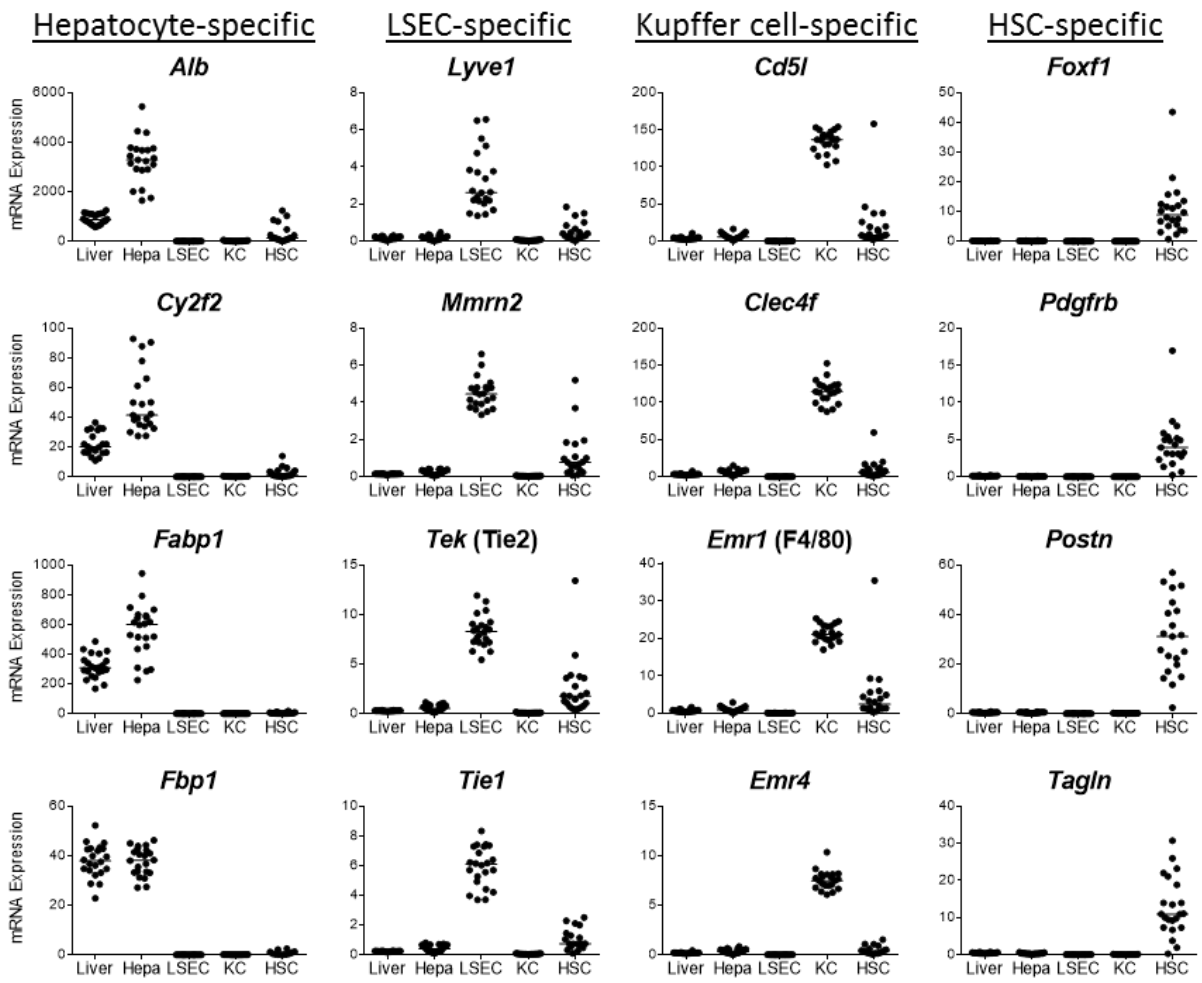

Figure 2-2. Enrichment of cell-specific genes in total liver, hepatocyte, LSEC, KC, and HSC populations for Chapter 4. Genes specific for hepatocytes, LSECs, KCs, and HSCs were measured in total liver, hepatocyte, LSEC, KC, and HSC RNA samples by qRT-PCR and expressed relative to *Hprt.* Data are for the Round 3, Week 8 samples. All four treatment groups combined into one group per population, data are from one experiment. Each data point represents an individual mouse. Median value is represented by a bar.

Quantitative real-time PCR (qRT-PCR) expression analysis

Liver tissue, hepatocytes, LSECs, KCs, and HSCs were stored in TRIzol at -80°C until processing. Liver samples were homogenized and hepatocyte samples were sheared by passage through a 27G1/2 needle 3-5 times. All samples were treated with proteinase K (Qiagen) for 20 min at 56°C. RNA was isolated using the Direct-zol RNA

Miniprep Kit (Zymo Research Corporation) for Chapter 3 studies and chloroform for Chapter 4 studies. Complementary DNA was generated using the QuantiTect Reverse Transcription Kit (Qiagen), preamplified using BIO-X-ACT Short Mix (Bioline USA Inc.) and the TaqMan assays of interest (Applied Biosciences), and diluted 1:5 for analysis. Microfluidic qRT-PCR was performed on a BioMark HD microfluidics system (Fluidigm). The Fluidigm Gene Expression software was used to calculate Ct thresholds and Microsoft Excel used to calculate relative expression levels and fold change values using the $2^{-\Delta Ct}$ and $2^{-\Delta\Delta Ct}$ methods, respectively. Relative expression was calculated relative to *Gapdh* or *Hprt*. Fold change was calculated as the ratio between individual mice compared to the median of the control group mice. For Chapter 3, except in the time course experiment where raw Ct values from two experiments were combined and analyzed together, fold change values were calculated per experiment and graphed in sum. qRT-PCR was also performed on a MJ Research DNA Engine Opticon 2 (BioRad Laboratories). The Opticon Monitor software, version 2 (BioRad Laboratories) was used to calculate Ct thresholds and Microsoft Excel used to calculate relative expression levels using the $2^{-\Delta Ct}$ method.

Histology

Liver pieces were fixed in either 4% paraformaldehyde in 1X PBS or 10% neutral-buffered formalin for approximately 24 hours (up to 72 hours for Chapter 4 studies) and then stored in 1X PBS. Samples were either paraffin-embedded, sectioned, and stained with hematoxylin and eosin; or OCT-embedded, cyro-sectioned, and stained with DAPI. All images were taken on a Nikon Eclipse T*i*-E inverted microscope with a Nikon Digital Sight DS-Ri1 camera using NIS-Elements, version 4.50, Advanced Research software (Nikon), at room temperature. Both the 10X objective (0.30 NA) for a total 100X magnification and the 20X objective (0.45 NA) for a total of 200X

magnification were used. Fluorescent image acquisition was conducted with consistent exposures per channel to facilitate cross-image conformity. Fluorescent images are the merge of 3 channels: FITC for hepatocyte auto-fluorescence false-colored green, PETR for mCherry fluorescence false-colored red, and UV for DAPI nuclear staining false-colored blue. Image processing was performed in NIS-Elements, version 4.3 software (Nikon). All embedding, sectioning, and staining was performed by the University of Washington Histology Imaging Core.

Materials and Methods for Chapter 3

To induce hepatocyte death, we used recombinant adeno-associated virus (rAAV) vectors as a tool for delivering the sequence encoding the human diphtheria toxin receptor (hDTR) to hepatocytes. These vectors utilize the AAV serotype-8 capsid proteins to preferentially target to the liver and use both the mouse alpha-fetoprotein enhancer and albumin promoter (pAlb) for hepatocyte-specific expression of transgenes. We allowed two weeks for stable expression of transgenes after intravenous injection of AAV into mice and then injected mice intraperitoneally with diphtheria toxin (DT) to induce sterile inflammation in the liver via hepatocyte death.

Originally, we used rAAV8.pAlb.OVA.hDTR (OVA = ovalbumin) to induce sterile inflammation in the liver. It was through the use of this vector that we refined many methods related to these studies, including: rAAV quantification, intravenous injection of rAAV into mice, intraperitoneal injection of DT, and antibody panels for flow cytometry and cell sorting. A limited amount of this data is presented as supporting data for Chapter 3, in which we used the optimized methods developed using the rAAV8.pAlb.OVA.hDTR vector in concert with the rAAV8.pAlb.mCherry.hDTR vector.

Plasmids for rAAV vectors

We constructed two replication-defective rAAV8 vectors, rAAV8.pAlb.OVA.hDTR and rAAV8.pAlb.mCherry.hDTR. The transgene-encoding plasmid, either pAAV.pAlb.OVA.T2A.hDTR or pAAV.pAlb.mCherry.T2A.hDTR, was constructed by inserting either DNA encoding mCherry (no stop) or DNA encoding OVA (no stop) into the SalI and BamHI sites, a T2A peptide linker sequence (provided by Mike Certo, University of Washington) into the BamHI and SacII sites, and DNA encoding the hDTR (provided by Richard Palmiter, University of Washington) into the SacII and XhoI sites of the pAAV.pAlb base plasmid. The pAAV.pAlb base plasmid was constructed by inserting AAV serotype-2 inverted terminal repeats (ITRs) into the BglII and NdeI restriction sites of the pLIVE plasmid (Mirus Bio), which has a multiple cloning site under the control of the minimal mouse albumin promoter.

The pDG2/8 helper plasmid, used in combination with both of the transgene-encoding plasmids during transfection, contains AVV serotype-2 replication components and AAV serotype-8 capsid protein (pDG base plasmid provided by Dr. Jurgen Kleinschmidt, Deutsches Krebsforschungszentrum Stiftung des offentlichen Rechts and serotype-8 capsid DNA provided by Dr. James Wilson, University of Pennsylvania). All construction of the pDG2/8 helper plasmid and construction of the pAAV.pAlb base plasmid with ITRs was performed by Dr. Isaac Mohar (University of Washington).

rAAV production and purification

rAAVs were produced using a two-plasmid calcium phosphate transfection system in HEK 293 cells. HEK 293s were grown in DMEM (high glucose, + L-glutamine; Gibco) + 10% CCS (Hyclone) + 1% Penicillin/Streptomycin (Gibco), transfected with 10 µg pDG2/8 plasmid to either 2.36 ug pAAV.pAlb.mCherry.T2A.hDTR or 2.56 ug pAAV.pAlb.OVA.T2A.hDTR , and grown at 37°C, 5-7.5% CO_2. Media was replaced the

following day with DMEM (high glucose, + L-glutamine) + 1% Penicillin/Streptomycin/Glutamine (Gibco). After 72 hours, the HEK 293s were lysed by 3 freeze-thaw cycles, incubated with 10 U/µL DNAse, pelleted, the supernatant purified by an iodixonal gradient (Optiprep; Sigma-Aldrich), and desalted using an Amicon Ultra-15 100K centrifugal filter device (EMD Millipore) with 1X PBS. The AAV was stored in 5% glycerol at -80°C.

Mice

rAAV8.OVA.hDTR Preliminary Experiments

Experiments generally used male mice, although female mice were used on occasion, aged approximately 8-20 weeks at the time of rAAV injection. C57BL/6J and C57BL/6NJ mice were purchased from the Jackson Laboratory. TRIF$^{-/-}$and TLR4$^{-/-}$ breeders were gifts from Dr. Alan Aderem (University of Washington/Center for Infectious Disease Research) and bred in-house at the Center for Infectious Disease Research and the University of Washington. IFNAR1$^{-/-}$ (gifts from Dr. Alan Aderem and Dr. Michael Gale, Jr., University of Washington) and TLR3$^{-/-}$ (gift from Dr. Michael Gale, Jr.) mice were bred in-house at the University of Washington. MyD88$^{-/-}$ mice were a gift from Dr. David Sherman (University of Washington/Center for Infectious Disease Research) and RIPK3$^{-/-}$ mice were a gift from Dr. Andrew Oberst (University of Washington). All mouse experiments described in this study were performed under Institutional Animal Care and Use Committee approval (Center for Infectious Disease Research, protocol NC-01 and University of Washington, protocol 4308-01). They were housed in a specific pathogen-free environment, provided with *ad libitum* food and water, and monitored daily.

rAAV8.mCherry.hDTR Chapter 3 Experiments

Experiments used male mice, aged 8-12 weeks. C57BL/6J, C57BL/6NJ, TLR3$^{-/-}$, TLR4$^{-/-}$, and MyD88$^{-/-}$ mice were purchased from the Jackson Laboratory. IFNAR1$^{-/-}$ and TRIF$^{-/-}$ breeders were a gift from Dr. Alan Aderem (University of Washington/Center for Infectious Disease Research) and used to breed experimental mice in-house at the University of Washington. All mouse experiments described in this study were performed under Institutional Animal Care and Use Committee approval (University of Washington, protocol #4308-01). They were housed in a specific pathogen-free environment, provided with *ad libitum* food and water, and monitored daily.

Quantification of rAAV

rAAV8.OVA.hDTR Preliminary Experiments

Vector was quantified by qRT-PCR. Initially, OVA-specific primers and a previously-quantified rAAV were used. Over time, we found that this led to inaccurate vector titers due to drift in the quantification. To correct this issue, we made multiple aliquots of a standard curve using pAAV.pLIVE.OVA.T2A.hDTR plasmid (clone c4-12A) and diluted it in 10 µM Tris, pH 8.5, to dilutions of 10^2 through 10^8 plasmid copies/µl. Aliquots were stored at -20°C for future use. Quantification was performed using albumin-specific primers.

rAAV8.mCherry.hDTR Chapter 3 Experiments

Quantification was done using the QuickTiter AAV Quantitation Kit (Cell Biolabs).

Model of hepatocyte-specific death

rAAV8.OVA.hDTR Preliminary Experiments

Male mice aged 8-20 weeks were intravenously injected via the tail vein with $2.5x10^9$ DNAse-resistant genomes (DRGs) rAAV8.OVA.T2A.hDTR. After allowing two weeks for vector expression, mice were injected intraperitoneally with 20 ng DT (Sigma-Aldrich) in 200 µL 1X PBS or with 200 µL 1X PBS alone. Mice were anesthetized with Avertin for liver perfusion at approximately 6, 12, 24, 28, 72, and 96 hours post-DT injection.

rAAV8.mCherry.hDTR Chapter 3 Experiments

Male mice aged 8-12 weeks were intravenously injected via retro-orbital injection with $5x10^9$ DRGs rAAV8.mCherry.T2A.hDTR. After allowing two weeks for vector expression, mice were injected intraperitoneally with either 20 ng DT (Sigma-Aldrich) in 200 µL 1X PBS or with 200 µL 1X PBS alone. Mice were anesthetized with Avertin for liver perfusion at approximately 6, 12, 24, 28, 72, and 96 hours post-DT injection.

Measurement of protein

Levels of CCL-2 (MCP-1), IL-1β, IL-6, CXCL1, IL-10, and TNF-α were quantified using the Mouse MCP-1 Ultra-Sensitive Kit and a Custom Mouse Cytokine V-PLEX Kit, according to the manufacturer's instructions (Meso Scale Diagnostics, LLC). Analysis was performed using the Discovery Workbench 3.0 software (Meso Scale Diagnostics, LLC).

Western blot analysis

50 µL of hepatocyte pellet was suspended in 500 µL RIPA Buffer (Thermo Fisher Scientific) supplemented with 120 µL Halt Protease Cocktail and 120 µL EDTA (Thermo

Fisher Scientific). Quantification of protein was performed using the BioRad DC Protein Assay (BioRad Laboratories). 1 µg/1 µL loading samples were prepared in 4X Laemmli Sample Buffer (BioRad Laboratories), boiled for 10 min, and 20 µg of total protein run on a 12% SDS-PAGE gel. Gels were transferred to PVDF membranes for 1 hour at 100 volts. Blocking was performed for 1 hour at room temperature in 0.1% PBS-Tween 20 (PBST) with 10% milk. Incubation with anti-hHB-EGF primary antibody (R&D Systems, AF-259-NA, 1:50 final dilution) was performed overnight at 4°C in 0.1% PBST with 10% milk. Incubation with donkey anti-goat HRP secondary antibody (Santa Cruz Biotechnology, SC-2020, 1:5000 final dilution) was performed for 2 hours at room temperature in 0.1% PBST. All washing used 0.1% PBST. Blots were developed using the Western Lighting Plus-ECL Reagent (PerkinElmer) and exposed to film for 1 minute.

Statistical analysis

Graphs present aggregate data from 2-3 independent experiments, exact numbers and repetitions are noted in figure legends. For all experiments except the C57BL/6J time course, mice in the + DT groups that expressed *hDTR* levels comparable to those in the + PBS groups at the 48 hour collection point—indicating failure of DT to reach the liver—were eliminated from the analysis (Figure 2-1).

Due to the range of responses seen in mice, data cannot be assumed to be normal, therefore, nonparametric statistical analyses were performed. For time course data, significance was determined by a Kruskal-Wallis test, followed by pairwise comparisons to the control group using Dunn's post-test. For data comparing wild type (WT) and knock-out (KO), control (+ PBS) and treated (+ DT) groups, initial p-values were calculated using a pairwise Mann-Whitney test for four comparisons (WT + PBS versus WT + DT, KO + PBS versus KO + DT, WT + PBS versus KO + PBS, and WT + DT versus KO + DT) and then adjusted p-values calculated using the Holm-Bonferroni

method to correct for multiple comparisons. Correlation plots were evaluated by Goodness of Fit and the R^2 value and significance level provided on the graph. All other data were analyzed using pairwise Mann-Whitney tests. Significant p-values are represented by asterisks at the following levels: *, $P \leq 0.05$; **, $P \leq 0.01$; ***, $P \leq 0.001$; and ****, $P \leq 0.0001$; while ns = not significant ($P > 0.05$). In general, if a test was non-significant it was not represented on figures. All statistical analysis was performed in either GraphPad Prism 6 or Microsoft Excel.

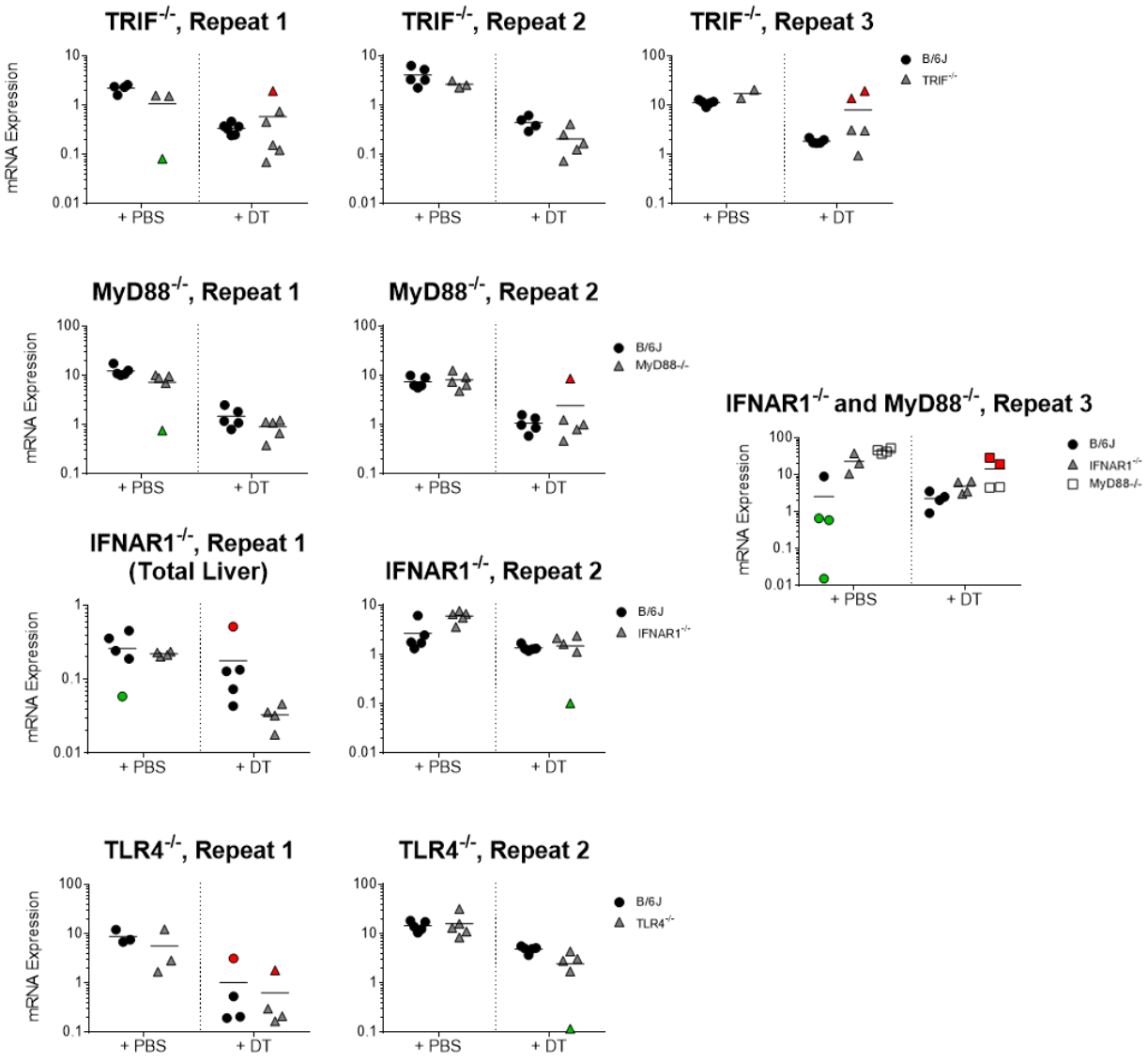

Figure 2-3. Expression of *hDTR* as a criteria to eliminate mice from the analyses for Chapter 3. Two weeks following rAAV injection, mice received PBS or DT and were sacrificed 48 hours later. The expression of *hDTR* relative to *Hprt* was measured for all mice across 10 independent experiments to assess if vector had been successfully eliminated in + DT groups. If the level of *hDTR* vector expression in the + DT group was comparable to that in the + PBS group, that mouse was eliminated from the analysis on the basis that vector had not been reduced by DT treatment and therefore, hepatocyte death not induced (represented by red symbols). Some mice also had lower expression of *hDTR* (represented by green symbols), however, these mice were not eliminated from the study as the relevance of this could not be objectively determined.

Materials and Methods for Chapter 4

As three independent experiments were performed with slightly altered methods, they are referred to as Round 1 (5 weeks), Round 2 (12 weeks), and Round 3 (8 weeks) throughout the description of materials and methods. When no distinction is made, the method was the same for all three experiments.

Mice

Experiments used male C57BL/6J mice, at least 10 weeks of age, purchased from the Jackson Laboratory. All mouse experiments described in this study were performed under Institutional Animal Care and Use Committee approval (University of Washington, protocol 4308-02). For Round 1, mice were housed individually; for Round 2, mice were housed in pairs; and for Round 3, mice were housed in trios. Mice were housed in a specific pathogen-free environment and provided food and water as described below.

Description of diets

Mice received standard vivarium chow (LabDiet) or one of four liquid Lieber-DeCarli diets (Bio-Serv). The composition of the diets is described in Table 2-1. Based on the amount of dietary fat in the diets, we refer to the Lieber-DeCarli ’82 control and ethanol diets as “mid-fat” and to the Low Fat, Lieber-DeCarli ’83, ’89 control and ethanol diets as “low-fat”. Amounts of ethanol are measured as percent volume/volume (v/v) or as percent ethanol-derived calories. For Round 1 and the first 2 weeks of Round 2, we used 6.7% v/v ethanol, equivalent to 35.5% ethanol-derived calories. This percentage was reduced to 5.0% v/v ethanol, equivalent to 27.6% ethanol-derived calories, for the remaining 10 weeks of Round 2 and for all of Round 3.

			Caloric Profile (%)			
	Diet Name	Cat No	Protein	Fat	Carb.	Ethanol
Chow	PicoLab Rodent Diet 20 EXT IRR, 5053	0007688	24.5	13.1	62.4	0
Mid-Fat Control	Lieber-DeCarli '82 (Control)	F1259SP	15.1	35.9	49	0
Mid-Fat Ethanol	Lieber-DeCarli'82, Ethanol	F1258SP	15.1	35.9	13.5/21.4	35.5/27.6
Low-Fat Control	Low Fat, Lieber-DeCarli '83, '89 (Control)	F1340SP	15	12.5	72.5	0
Low-Fat Ethanol	Low Fat, Lieber-DeCarli '83, '89, Ethanol	F1341SP	15	12.5	44.9	27.6

Table 2-1. Caloric profile for diets used in Chapter 4 experiments.

Preparation of diets

Diets were prepared under sterile conditions in a biosafety cabinet each day before feeding. Control and ethanol dry mix was weighed out into autoclaved 500 mL or 1 L glass bottles. Water provided by the vivarium was added to the mixtures and 200 proof ethanol (Decon Laboratories) was added to the ethanol diet. Diets were shook vigorously until resuspended.

Administration of diets

Mice for Rounds 1, 2, and 3 received the diets as outlined in Table 2-2. Standard vivarium chow was provided *ad libitum* for Round 3. When water was provided, it was provided *ad libitum*. Mice receiving liquid diets were fed every morning at approximately the same time throughout the length of the experiment. Liquid diets were provided in specialized feeding tubes (Bio-Serv, Product #9019).

	Collection Time (weeks)	Ethanol percentage (vol/vol)	Group 1	Group 2	Group 3	Group 4	Water
Round 1	5	6.7%, decreased to 5.0%	Mid-Fat Control	Mid-Fat Ethanol	N/A	N/A	No
Round 2	4, 8, 12	5.0%	Mid-Fat Control	Mid-Fat Ethanol	N/A	N/A	Yes
Round 3	4, 6, 8	5.0%	Mid-Fat Control	Low-Fat Control	Low-Fat Ethanol	Vivarium Chow	Yes

Table 2-2. Experimental design for Chapter 4 experiments.

We used an acclimation period during which the mice initially received liquid diets, vivarium chow, and water. The chow and water were taken away during the acclimation period, before the start of the study. The acclimation period for Round 1 was 4 days and for Round 2 was 7 days and all mice were fed the control liquid diet. Following the acclimation period, control group mice continued to receive the control diet and ethanol group mice were switched to the ethanol diet with 6.7% v/v ethanol. Due to unexpected mouse mortality, we decreased the ethanol percentage to 5.0% v/v after 10 days of feeding the ethanol diet in Round 2. In the acclimation period for Round 3, mice received their respective control or ethanol liquid diets with the calories from ethanol replaced by maltose dextrin (Bio-Serv) in the ethanol diet. After two days, ethanol was added to the ethanol liquid diet and increased using the following scheme: 1.0% v/v for 1 day, 2.0% v/v for 2 days, and 4.0% v/v for 2 days. Following the acclimation week, the ethanol diet group received 5.0% v/v ethanol for the remainder of the study.

For the acclimation period, mice initially received the liquid diets *ad libitum*, but were transitioned to paired feeding during the week. Paired feeding continued for the remainder of the experiment. We paired a control liquid diet cage with an ethanol liquid diet cage. On the first day of paired feeding, both cages received liquid diet *ad libitum*. We measured the combined weight of the feeder tube and the diet before placing it in the cage. The following morning, we weighed the feeder tube from the ethanol liquid diet cage and calculated the amount of liquid diet consumed, in grams, the previous day. We then added this amount of liquid control diet to the matched control cage for consumption that day. This pattern continued until the end of the studies. For Round 3 feeding, both the mid-fat and low-fat control liquid diet groups received the same amount (grams) as the low-fat ethanol liquid diet group ate on the previous day.

Measurement of mouse weight

Mice were weighed every day by placement into a plastic beaker on scale.

Statistical methods

Nonparametric statistical analyses were performed. Pairwise comparisons were made using the Mann-Whitney test. All other data was assessed for significance by a Kruskal-Wallis test, followed by pairwise comparisons to the control group using Dunn's post-test. Significant p-values are represented by asterisks at the following levels: *, $P \leq 0.05$; **, $P \leq 0.01$; ***, $P \leq 0.001$; and ****, $P \leq 0.0001$; while ns = not significant ($P > 0.05$). In general, if a test was non-significant it was not represented on figures. All statistical analysis was performed in GraphPad Prism 6.

CHAPTER 3: HEPATOCYTE-SPECIFIC DEATH AS A MODEL OF ACUTE, STERILE LIVER INJURY

Abstract

In addition to conserved motifs displayed by pathogens, the innate immune system also responds to tissue damage in the absence of pathogens, termed sterile injury. Several key pathways that drive the sterile inflammatory response in the liver have been described; however, it is unclear how the type of cells injured or the mechanism of injury activate these pathways. Here, we use a model of selective hepatocyte death to investigate sterile liver injury. In this model, the TIR-domain-containing adapter-inducing interferon-β (TRIF) was a central mediator of the resulting intrahepatic inflammatory response that was independent of both upstream Toll-like receptor 4 (TLR4) signaling and downstream Type I interferon (IFN) signaling. TRIF was required for the induction of IL-10, IL-6, and IL-1β cytokines. Conversely, TRIF was not required for the induction of CCL2 or CXCL1 protein, nor was it required for the up-regulation of chemokine (*Ccl2*, *Ccl7, Cxcl1*, *Cxcl2*, and *Cxcl10*) and cell adhesion (*Icam1* and *Vcam1*) genes involved in myeloid-cell recruitment. Furthermore, we found that hepatocytes themselves were the main responders to hepatocyte death, increasing transcription of genes involved in myeloid-cell recruitment more than either liver sinusoidal endothelial cells or Kupffer cells. In summary, our studies define a TRIF-dependent, TLR4- and Type I IFN-independent pathway of sterile liver injury in which hepatocytes are both the targets of damage and the principal responding cell type.

Introduction

Tissue damage generally induces a robust sterile inflammatory response comprised of increased production of inflammatory mediators and recruitment of neutrophils and monocytes to the site of injury [13]. When the sterile inflammatory response is short-lived, the tissue recovers; however, the response may also produce persistent inflammation, which in the liver, can lead to fibrosis, cirrhosis, and hepatocellular carcinoma (HCC) [94, 95]. Drug-induced damage (acetaminophen (APAP) hepatotoxicity), alcoholic liver steatohepatitis (ASH), diet-induced damage (non-alcoholic steatohepatitis (NASH)), and mechanically-induced damage (ischemia-reperfusion injury), all promote cell death within the liver.

Damage-associated molecular patterns (DAMPs) released from dying cells signal through the same pattern recognition receptors (PRRs) that recognize pathogen-associated molecular patterns to initiate the inflammatory response [13]. While there are multiple families of PRRs that bind DAMPs, Toll-like receptors (TLRs) are an important class of PRR in the sensing of sterile liver injury. Multiple mouse models of sterile inflammation have shown a central role for signaling through TLRs and their downstream effectors Toll/IL-1 receptor domain-containing adapter protein inducing IFN-β (TRIF) and myeloid differentiation primary-response protein 88 (MyD88).

Models of sterile inflammation in the liver have provided key insights about the inflammatory pathways involved in the response to liver damage. There exists, however, a knowledge gap concerning the sterile inflammatory response to the death of each specific cell type. Models of toxic liver injury result in complexity that is challenging to analyze. For example, in APAP-mediated toxicity, injury to liver sinusoidal endothelial cells (LSECs) and disruption of the microvasculature precedes necrosis of hepatocytes, occurring as early as 30 min after drug administration [96-98]. In the mouse model of concanavalin A (Con A)-induced hepatitis, LSECs are eliminated early in the pathology

by CD4+ T cells, destroying the lining and exposing hepatocytes to activated T cells [99]. Additionally, the Con A model of hepatitis relies on components of the adaptive immune system, activated T cells, to induce hepatic damage, further complicating efforts to study the response of the innate immune system [100, 101]. Models of ischemia-reperfusion injury produce no clearer results as the death of both LSECs and hepatocytes occurs [102].

Inflammation in response to cell death is critically important in the liver not only in situations of drug-, diet-, and mechanically-induced damage, but also in the context of infection, where inflammation is complicated by responses to host cell death and pathogen. Separating the different pathways of inflammation—those against pathogen versus those against host cell death—may prove essential to address inflammatory liver disease. In particular, the response to hepatocyte death is critical to understand as it is a central component of both damage induced by infectious and non-infectious insults.

We have, therefore, developed a mouse model of sterile liver inflammation initiated by hepatocyte-specific death. We find that TRIF, independent of TLR4 and type I IFN, plays a key role in the initiation of sterile inflammation, of which hepatocytes themselves are major regulators. Furthermore, we identify separate arms of the response distinguished by their requirement for TRIF-pathway signaling.

Results

Model of hepatocyte-specific death

To identify pathways of sterile inflammation in the liver we developed a mouse model of hepatocyte-specific death. We designed a recombinant adeno-associated virus (rAAV) vector encoding the fluorescent reporter protein mCherry and the human diphtheria toxin receptor (hDTR, also known as the heparin-binding EGF-like growth

factor, or HB-EGF), rAAV8.pAlb.mCherry.hDTR (Figure 3-1A). This vector utilizes the AAV serotype-8 capsid proteins to preferentially target to the liver (Figure 3-1B) and the mouse alpha-fetoprotein enhancer (AFP^E) in combination with the albumin promoter (Alb^P) for hepatocyte-specific expression of transgenes (Figure 3-1C). Mice received $5x10^9$ DNase-resistant genomes (DRGs) of vector by retro-orbital injection. After allowing two weeks for vector expression to stabilize within the mouse, we induced hepatocyte death by injection of diphtheria toxin (DT). Liver damage, measured by alanine aminotransferase (ALT) levels, peaked at 48 hours (Figure 3-1D). Preliminary data using the rAAV8.pAlb.OVA.hDTR vector produced the same result (Figure 3-2A).

Histological examination showed rounded eosinophilic cells with condensed or fragmented nuclei by 24 hours, indicative of cell death (Figure 3-1E). By 48 hours, a cellular infiltrate was present as well as extensive hepatocyte necrosis indicated by widespread eosinophilia and both condensed and dissolving nuclei (Figure 3-1E). Hepatocytes undergoing mitosis, indicative of tissue repair, began to appear by 48 hours (arrow, Figure 3-1E). By 72 hours, the infiltrate had increased and there were increased numbers of mitotic hepatocytes, indicating further tissue repair, though there still remained evidence of dying hepatocytes (Figure 3-1E).

Immunofluorescence showed strong, diffuse mCherry expression limited to the cytoplasm of hepatocytes in the control group (Figure 3-1F). By 24 hours and continuing to 48 hours, the mCherry signal was consolidating into round vacuoles largely within the cytoplasm of hepatocytes but also within cells in the sinusoids, indicative of phagocytosis of dying cells by hepatocytes and other non-parenchymal cells (NPCs) within the liver (Figure 3-1F). By 72 hours, large vacuoles of mCherry signal were less concentrated in hepatocytes, with smaller puncta of mCherry signal appearing throughout the cytoplasm of hepatocytes and within cells in the sinusoids (Figure 3-1F).

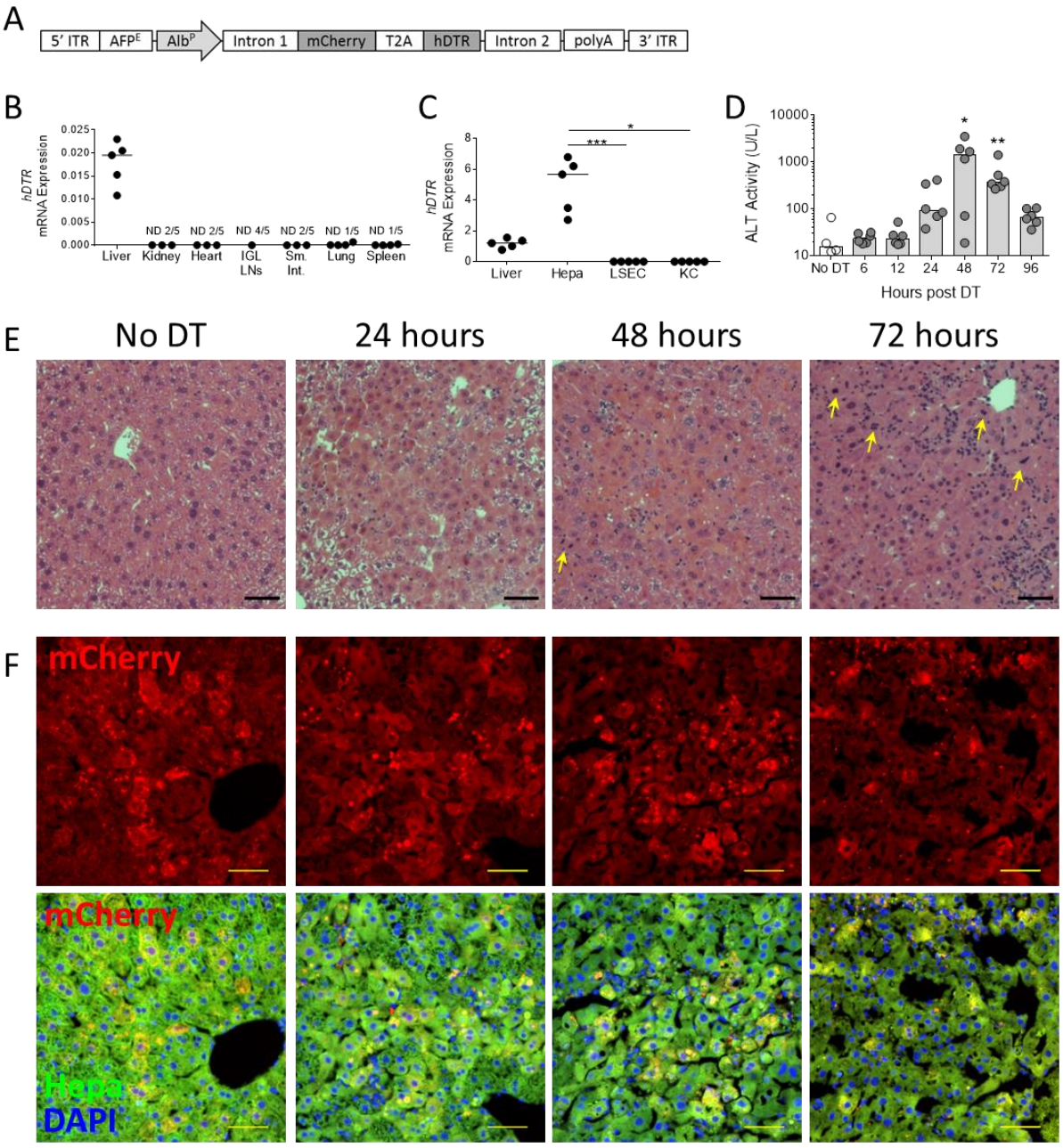

Figure 3-1. Hepatocyte-specific expression of rAAV8.pAlb.mCherry.hDTR results in peak liver damage 48 hours following diphtheria toxin injection. (A) rAAV8.pAlb.mCherry.hDTR vector encoding the mouse AFP^{E} and Alb^{P}; mCherry and the hDTR linked by a T2A linker sequence; and AAV serotype-2 5' and 3' ITRs. Two weeks following rAAV injection, mice received either no injection, 1X PBS (control), or DT and were sacrificed 6, 12, 24, 48, 72, or 96 hours later. *hDTR* mRNA levels, relative to (B) *Gapdh* in organs and (C) *Hprt* in total liver and liver cell populations of C57BL/6NJ mice that received 1X PBS, n=5, each data point represents an individual mouse. (D) ALT levels from C57BL/6J mice that received no DT or DT. Each data point represents an individual mouse, bars represent the median. (E) Paraffin-embedded sections stained for

(Figure Legend 3-1, continued)
hematoxylin and eosin, 100X. Bar, 50 µm. Arrow, mitotic hepatocytes. (F) Cryo-preserved sections with mCherry (top) or the merge of mCherry fluorescence (red), hepatocyte autofluorescence (green), and DAPI to distinguish nuclei (blue) (bottom). Bar, 50 µm. (D-F) are combined from two experiments (n = 4, No DT group; n = 6, all other time points). Representative images chosen from one mouse at each time point for (E) and (F), based on median ALT levels. AFP^{E}, alpha-fetoprotein enhancer; Alb^{P}, albumin promoter; hDTR, human diphtheria toxin receptor; ITR, inverted terminal repeats; IGL, inguinal lymph nodes; Sm. Int., small intestine; and ND, non-detect. Significance determined by a Kruskal-Wallis test followed by Dunn's post-test of (C) Liver, LSEC, and KC to hepatocytes and (D) of each time point to the No DT group. * represents significance compared to No DT group; *, P ≤ 0.05; **, P ≤ 0.01; ***, P ≤ 0.001; non-significance represented by absence of bar or asterisk.

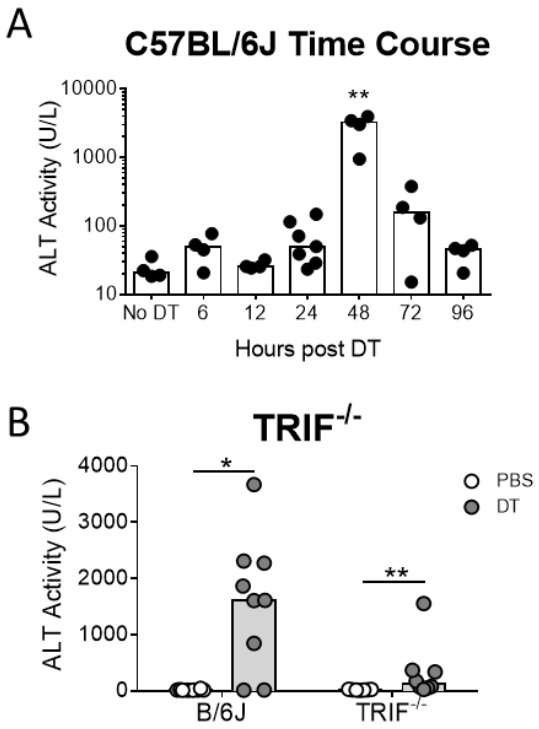

Figure 3-2. Preliminary experiments using rAAV8.pAlb.OVA.hDTR support findings from rAAV8.pAlb.mCherry.hDTR experiments. Two weeks following rAAV8.pAlb.OVA.hDTR injection C57BL/6J and $TRIF^{-/-}$ mice received no injection, 1X PBs (control), or DT and were sacrificed 6, 12, 24, 48, 72, or 96 hours later. (A) Serum ALT levels in (A) C57BL/6J mice and (B) in C57BL/6J and $TRIF^{-/-}$ at 48 hours. (A, B) Data are combined from two individual experiments. Each data point represents an individual mouse, bars represent the median. For (A) n = 4 for all time points except 24 hours where n = 6 and for (B) n = 8, B6 + PBS, $TRIF^{-/-}$ + DT; n = 9, B6 + DT; n = 7, $TRIF^{-/-}$ + PBS. Significance determined by (A) a Kruskal-Wallis test followed by Dunn's post-test of each time point to the No DT group and (B) four pairwise Mann-Whitney tests and the p-values adjusted for multiple comparisons using the Holm-Bonferroni method as described in the methods. *, P ≤ 0.05; **, P ≤ 0.01; non-significance represented by absence of bar.

Neutrophils and monocytes are recruited to the liver following hepatocyte death

Sterile inflammation is characterized by a neutrophil and monocyte infiltrate [17, 18]. To identify which cells play a role in the inflammatory response to tissue injury linked to hepatocyte death, we used flow cytometry to assess the populations present in the liver in control mice and at 6, 12, 24, 48, 72, and 96 hours after injection of DT. Following doublet exclusion and size gating (Figure 3-3), we gated for LSECs, Kupffer cells (KCs), neutrophils, eosinophils, and a CD11b(+) Ly6G(-) F4/80(-) population we term monocytes, further split into Ly6C(+) and Ly6C(-) populations, and further characterized by their expression of CD11c and MHC-II (I-A/I-E) (Figure 3-4A, control; and 3-4B, 48 hours). Neutrophils began infiltrating the liver 12 hours following DT injection and peaked between 24-48 hours while monocytes began infiltrating the liver by 24 hours and peaked between 48-72 hours (Figure 3-4C). Within the monocyte population, the proportion of Ly6C(+) monocytes began to increase by 24 hours while the proportion of Ly6C(-) monocytes began to increase by 48 hours (Figure 3-4C). A complete characterization of the infiltrating monocyte population confirms the dominance of Ly6C(+) monocytes at earlier time points and dominance of Ly6C(-) monocytes at later time points (Figure 3-5)

The presence of neutrophils and monocytes caused us to ask whether chemokines and adhesion molecules involved in myeloid cell recruitment were induced as a component of the inflammatory response against hepatocyte death. To examine this, we looked at the expression of chemokine genes in total liver, hepatocytes, LSECs, and KCs 6, 12, 24, 48, 72, and 96 hours following DT administration. Genes for monocyte-recruiting chemokines (*Ccl2*, *Ccl5, Ccl7*, *Cxcl10*), neutrophil-recruiting chemokines (*Cxcl1*, *Cxcl2*), and adhesion molecules (*Icam1*, *Vcam1*) were strongly induced across all populations (Figure 3-6A). For *Ccl7* expression in hepatocytes, levels of transcript were not detectable in 3 of 4 control mice, making a fold-change calculation

not possible; however, *Ccl7* transcript levels were induced by 12 hours and increased by 24 hours (Figure 3-6B). Induction was greatest in the hepatocytes for almost all genes measured and peaked at 24 hours (Figure 3-6B). Examination of the relative expression levels between hepatocytes, LSECs, and KCs revealed that KCs generally expressed the highest levels of transcript in control mice, with the notable exception that hepatocytes expressed the most *Cxcl1* (Figure 3-6B). Upon hepatocyte death, however, the level of gene expression for *Ccl2*, *Cxcl2*, *Cxcl10*, and *Icam1* increased in hepatocytes so that it surpassed that of LSECs and KCs, further suggesting that hepatocytes are the central responding cell (Figure 3-6B).

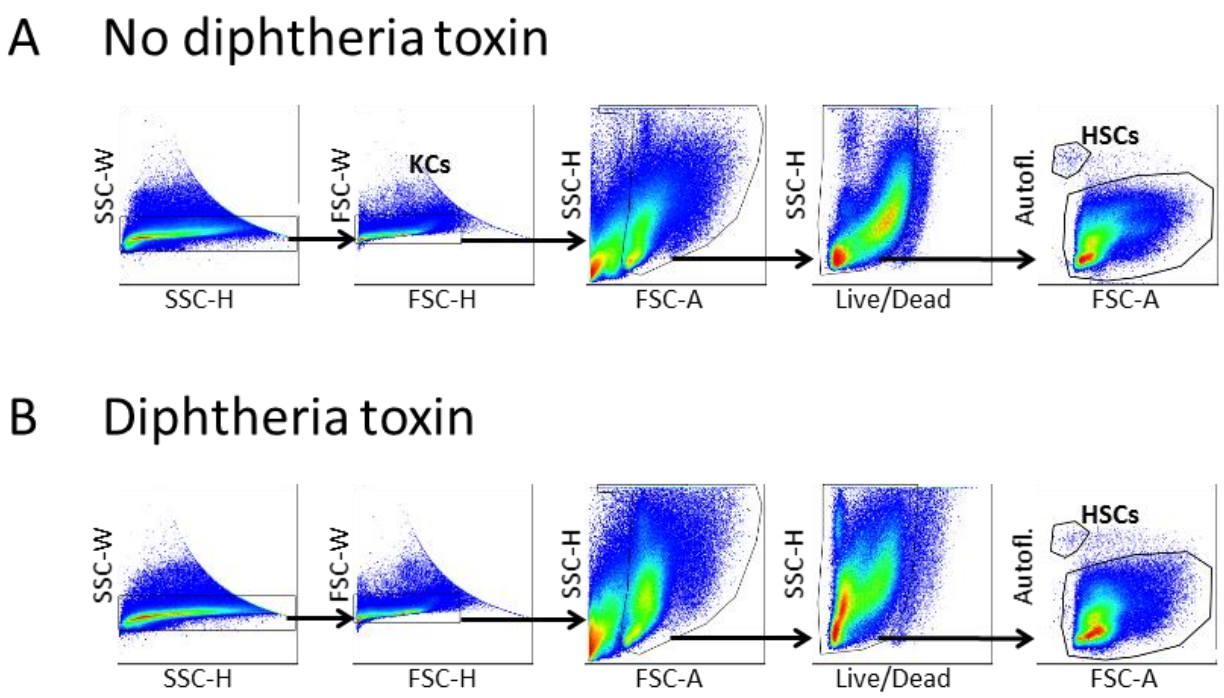

Figure 3-3. Preliminary gating strategy. Preliminary gating strategy used for the isolation of LSECs and KCs and the identification of HSCs, neutrophils, eosinophils, and monocytes. Two weeks following rAAV injection, C57BL/6J mice received DT and were sacrificed 6, 12, 24, 48, 72, or 96 hours later. Representative gating scheme to identify and characterize cell populations within the liver of (A) control mice and (B) DT-treated mice 48 hours after DT injection. (A, B) Data are representative of two combined experiments (n = 4, No DT group; n = 6, 48 hours).

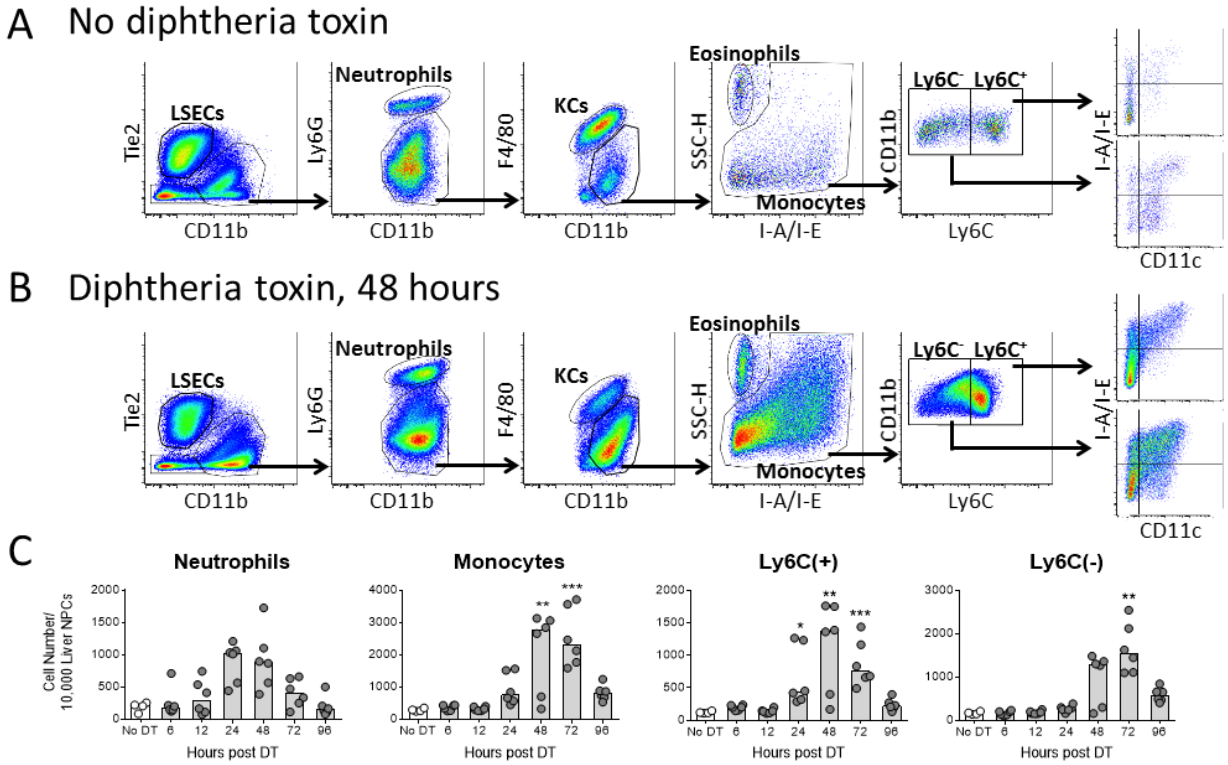

Figure 3-4. Hepatocyte death promotes the infiltration of neutrophils and monocytes. Two weeks following rAAV injection, C57BL/6J mice received DT and were sacrificed 6, 12, 24, 48, 72, or 96 hours later. Representative gating scheme to identify and characterize cell populations within the liver of (A) control mice and (B) DT-treated mice 48 hours after DT injection. (C) Neutrophil, monocyte, Ly6C(+) monocyte, and Ly6C(-) monocyte cell numbers per 10,000 liver non-parenchymal cells. (A-C) Data are combined from two experiments, each data point represents an individual mouse (n = 4, No DT group; n=6, all other time points), bars represent the median. (C) Significance determined by a Kruskal-Wallis test followed by Dunn's post-test of each time point to the No DT group. * represents significance compared to No DT group; *, $P \leq 0.05$; **, $P \leq 0.01$; ***, $P \leq 0.001$; non-significance represented by absence of asterisk.

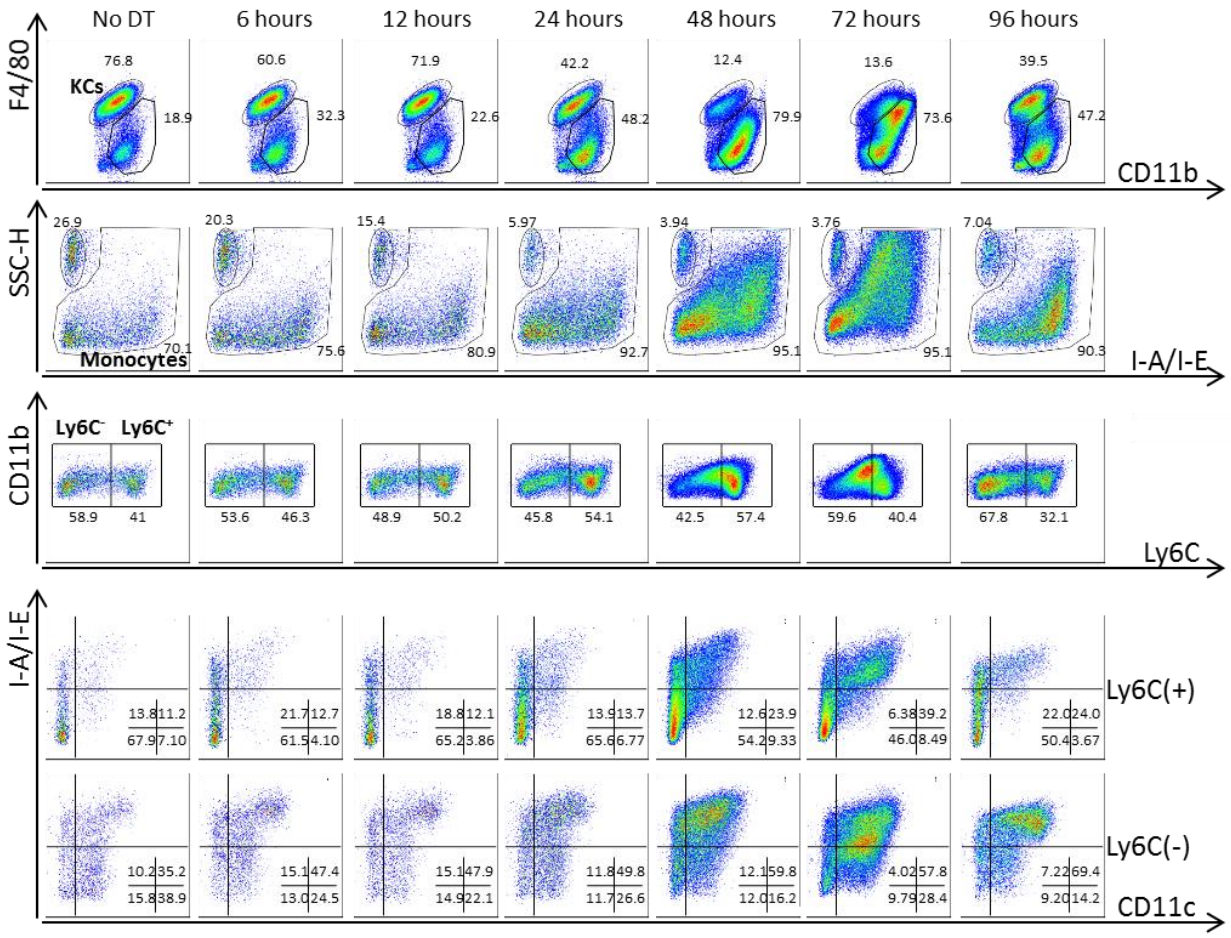

Figure 3-5. Ly6C(+) monocytes are the predominant monocyte population in the liver at 24 hours but by 48 hours Ly6C(-) monocytes dominate. Two weeks following rAAV injection, C57BL/6J mice received DT and were sacrificed 6, 12, 24, 48, 72, or 96 hours later. Figure shows representative flow plots at each time point for the KCs, total monocytes, the proportion of Ly6C(+) versus Ly6C(-) monocytes, and the expression of MHC-II (I-A/I-E) and CD11c on Ly6C(+) and Ly6C(-) monocytes. Representative flow plots for monocyte infiltrate chosen based on median ALT value for the group. Data are representative of two combined experiments (n = 4, No DT group; n = 6 all other time points).

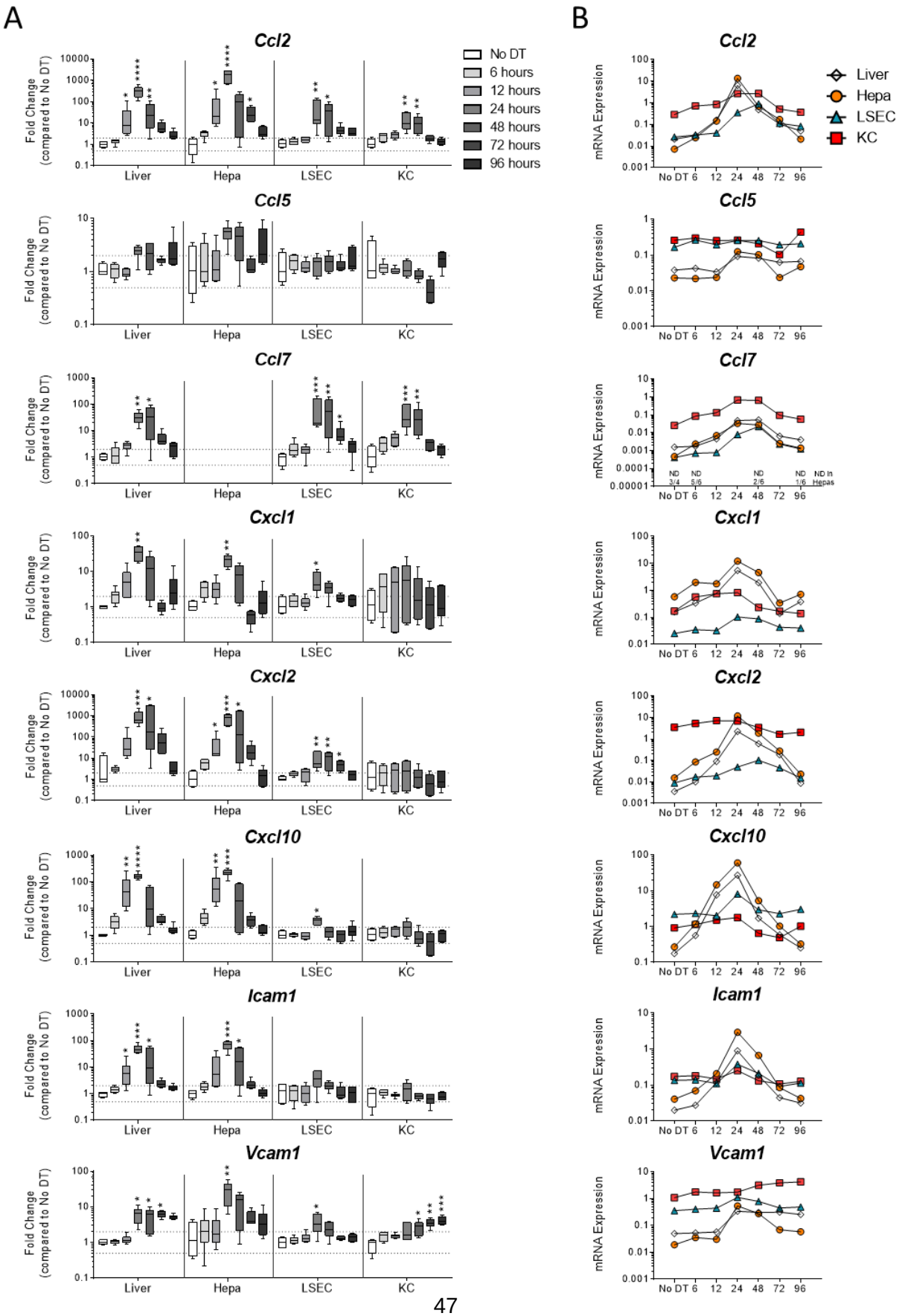
A
B
Ccl2
Ccl5
Ccl7
Cxcl1
Cxcl2
Cxcl10
Icam1
Vcam1
Fold Change (compared to No DT)
mRNA Expression
Liver
Hepa
LSEC
KC
No DT
6 hours
12 hours
24 hours
48 hours
72 hours
96 hours
No DT 6 12 24 48 72 96
ND 3/4
ND 5/6
ND 2/6
ND 1/6
ND in Hepas

Figure 3-6. Hepatocyte death up-regulates genes associated with myeloid cell-recruitment, predominantly in hepatocytes. Two weeks following rAAV injection, C57BL/6J mice received DT and were sacrificed 6, 12, 24, 48, 72, or 96 hours later. (A) Fold change gene expression in total liver, hepatocytes, LSECs, and KCs compared to the No DT group median, *Hprt* used as reference gene. Data are median and range. (B) mRNA expression relative to *Hprt* in total liver, hepatocytes, LSECs, and KCs. Median values only represented. For *Ccl7*, non-detect values represented on graph are for hepatocyte population only. (A, B) Data are combined from two experiments, each data point represents an individual mouse (n = 4, No DT group; n = 6, all other time points for all populations except n = 5, KC at 96 hours). ND, non-detect. (A) Significance determined by a Kruskal-Wallis test followed by Dunn's post-test of each time point to the No DT group. * represents significance compared to No DT group; *, $P \leq 0.05$; **, $P \leq 0.01$; ***, $P \leq 0.001$; ****, $P \leq 0.0001$; non-significance represented by absence of asterisk.

Type I interferon expression is increased following hepatocyte death

In mouse models of inflammation, *Ccl2* and *Ccl7* production occurs downstream of type I IFNs [103-106]. In turn, the type I IFNs, IFN-α and IFN-β, are primarily driven by signaling through the TRIF pathway [107]. We hypothesized, then, that the inflammation following hepatocyte death resulted in the production of TRIF-dependent chemokines. To examine this, we measured the expression of *Ifn-beta* (*Ifnb1*), the main downstream effector of TRIF, as well as cytokines driven by the MyD88-dependent pathway: *Tnf*, *Il1-alpha* (*Il1a*), *Il1-beta* (*Il1b*), *Il-6* (*Il6*), and *Il12-beta* (*Il2b*). *Ifnb1* transcript, though not statistically significant due to non-detects, went from low or non-detectable expression to approximately 100-fold greater expression levels by 24 hours, when compared to the detectable transcript at 6 hours (Figure 3-7A). *Tnf* was up-regulated by 24 hours and *Il12b* modestly up-regulated by 48 hours, but the remaining MyD88-driven cytokines showed no significant up-regulation in total liver (Figure 3-7A). Relative expression levels and induction of *Ifnb1* were greater in hepatocytes compared to either LSECs or KCs (Figure 3-7B).

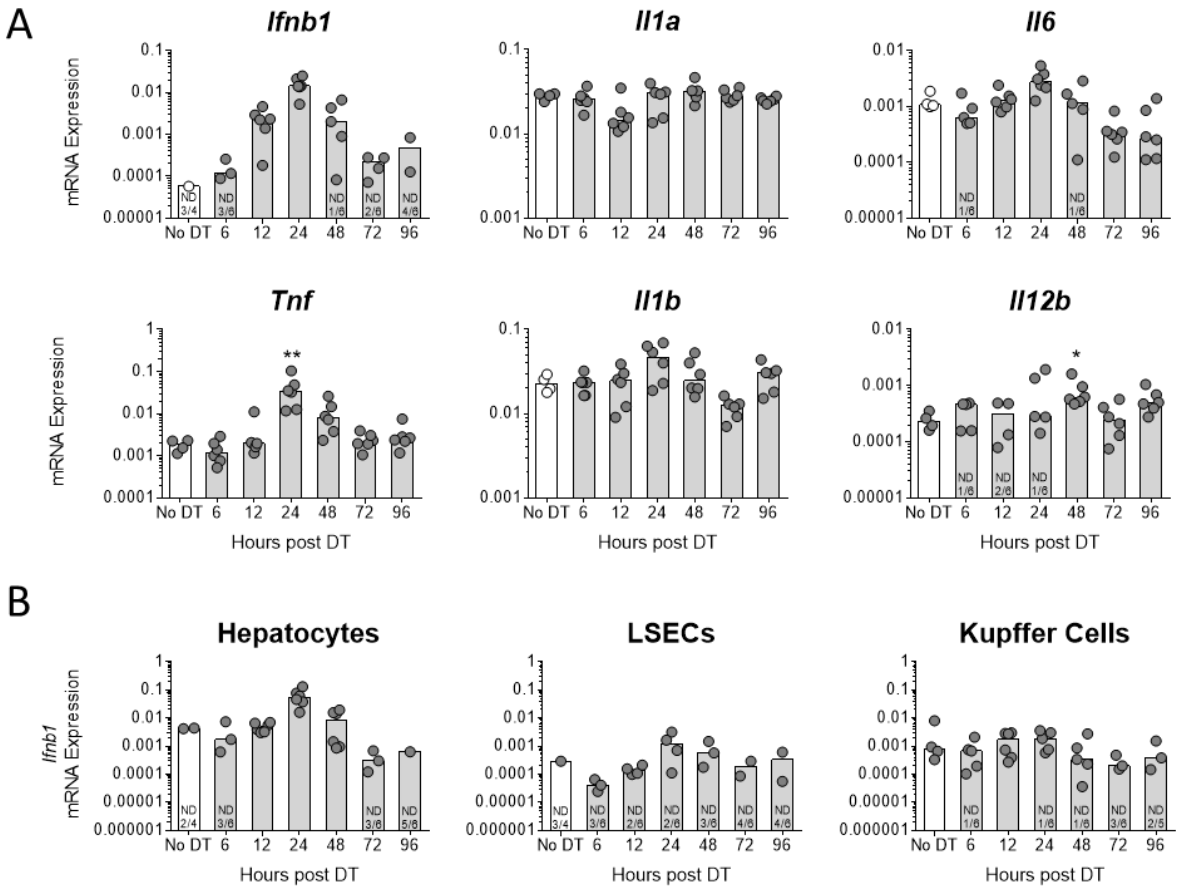

Figure 3-7. Hepatocyte death induces expression of the TRIF-pathway cytokine IFN-β, predominantly in hepatocytes, and only minimally induces expression of MyD88-pathway cytokines. Two weeks following rAAV injection, C57BL/6J mice received DT and were sacrificed 6, 12, 24, 48, 72, or 96 hours later. mRNA expression relative to *Hprt* in (A) total liver for *Ifnb1*, *Tnf*, *Il6*, *Il1a*, *Il1b*, and *Il12b* and in (B) hepatocytes, LSECs, and KCs for *Ifnb1*. Data are combined from two experiments, each data point represents an individual mouse (n = 4, No DT; n = 6 for all other time points for all populations except n = 5, KC at 96 hours), bars represent the median. ND, non-detect. Significance (A) determined by a Kruskal-Wallis test followed by Dunn's post-test of each time point to the No DT group and (B) not determined due to the presence of non-detects. * represents significance compared to No DT group; *, P ≤ 0.05; **, P ≤ 0.01; non-significance represented by absence of asterisk.

TRIF plays a larger role than MyD88 in the inflammatory response to hepatocyte death

The preferential induction of *Ifnb1* over MyD88-driven cytokines indicated that the inflammation could be controlled by TRIF-dependent signaling. To address this, we induced hepatocyte death in TRIF-deficient ($TRIF^{-/-}$) and MyD88-deficient ($MyD88^{-/-}$) mice and measured the response at 48 hours, the time point when ALT levels peaked in the time course. Both $TRIF^{-/-}$ and $MyD88^{-/-}$ mice showed significantly reduced elevation in ALT and neutrophil infiltrate compared to wild type mice; however, only $TRIF^{-/-}$ mice showed a significant reduction in the influx of monocytes (Figure 3-8). While we found that the influx of neutrophils required MyD88, $MyD88^{-/-}$ mice were only partially protected from liver damage, suggesting that neutrophils do not play a role in liver damage. Overall, the magnitude of the effects on the ALT and monocyte levels was more dramatic in the case of $TRIF^{-/-}$ mice. Data using the rAAV8.pAlb.OVA.hDTR vector produced the same result in $TRIF^{-/-}$ mice (Figure 3-2B).

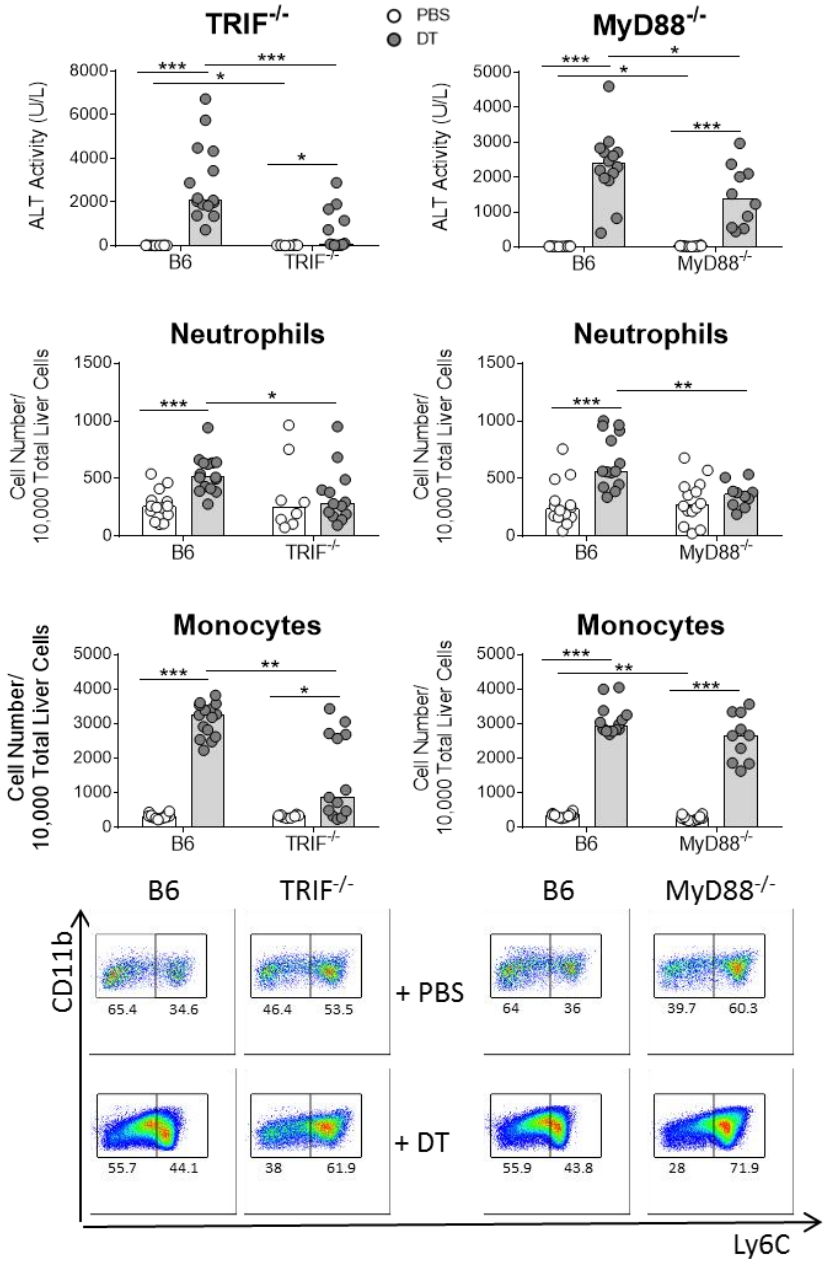

Figure 3-8. TRIF$^{-/-}$ mice exhibit less inflammation than MyD88$^{-/-}$ mice following hepatocyte death. Two weeks following rAAV injection, C57BL/6J, TRIF$^{-/-}$, and MyD88$^{-/-}$ mice received 1X PBS (control) or DT and were sacrificed 48 hours later. Serum ALT and neutrophil and monocyte cell numbers per 10,000 liver non-parenchymal cells were measured. Data are combined for 3 individual TRIF$^{-/-}$ experiments and 3 individual MyD88$^{-/-}$ experiments. Each data point represents an individual mouse (TRIF$^{-/-}$: n = 14, B6 + PBS; n = 15, B6 + DT; n = 8, TRIF$^{-/-}$ + PBS; n = 13, TRIF$^{-/-}$ + DT and MyD88$^{-/-}$: n = 14, B6 + PBS, B6 + DT, MyD88$^{-/-}$ + PBS; n = 10, MyD88$^{-/-}$ + DT), bars represent the median. Significance determined by four pairwise Mann-Whitney tests and the p-values adjusted for multiple comparisons using the Holm-Bonferroni method as described in the methods. *, P ≤ 0.05; **, P ≤ 0.01; ***, P ≤ 0.001; non-significance represented by absence of bar.

TRIF is not required for increased expression of myeloid cell-recruiting chemokines or cell-adhesion molecules, nor for increased production of CCL2 and CXCL1 protein

Since TRIF$^{-/-}$ mice exhibited reduced monocyte and neutrophil infiltrate, we next asked if the up-regulation of monocyte- and neutrophil-recruiting genes was also impaired in TRIF$^{-/-}$ mice. At 48 hours following injection of DT, TRIF$^{-/-}$ mice showed less induction of *Ccl2*, *Ccl5*, *Ccl7*, *Cxcl1*, *Cxcl2*, *Cxcl10*, *Icam1*, and *Vcam1* transcripts in total liver when compared to wild type mice (Figure 3-9A). Due to the presence of non-detects in hepatocytes and LSECs, *Ccl7* transcript levels were evaluated based on relative expression, rather than fold change. Hepatocytes produced *Ccl7* in all wild type mice but only a portion of the TRIF$^{-/-}$ mice, while expression of *Ccl7* in LSECs was lower in TRIF$^{-/-}$ mice when compared to wild type mice (Figure 3-9C). Examination of serum for CCL2 and CXCL1 protein revealed that both chemokines were significantly reduced in TRIF$^{-/-}$ mice compared to wild type mice (Figure 3-9E). Direct comparison of *Ifnb1* was complicated by a number of non-detects; however, hepatocytes from TRIF$^{-/-}$ mice produced more non-detects and the expression in LSECs from TRIF$^{-/-}$ mice was marginally lower, when compared to hepatocytes from wild type mice (Figure 3-9D).

While TRIF-deficiency resulted in reduced liver injury and inflammation as measured by ALT levels, cellular infiltrate, mRNA levels, and protein levels, TRIF-deficiency did not abolish the production of these mediators entirely. Specifically, the upper range of ALT, mRNA, and protein levels in TRIF$^{-/-}$ mice treated with DT overlapped with the range in wild type mice treated with DT. We hypothesized that *Ccl2*, *Ccl5*, *Ccl7*, *Cxcl1*, *Cxcl2*, *Cxcl10*, *Icam1*, and *Vcam1* mRNA levels and CCL2 and CXCL2 protein levels would increase with increasing liver injury in the TRIF$^{-/-}$ mice. To test this hypothesis, we correlated cellular infiltrate, total liver mRNA, and protein levels with serum ALT levels in DT-treated TRIF$^{-/-}$ and wild type mice. In all cases except for *Ccl5* in wild type mice, mRNA level and protein level was significantly correlated with

ALT and often the correlation was stronger in TRIF$^{-/-}$ than in wild type mice (Figures 3-9B and 3-9F). Monocyte infiltrate correlated with increasing ALT, however, neutrophil infiltrate was not significantly correlated with increasing ALT levels (Figure 3-9G). The lack of neutrophil correlation with ALT level could be a result of measuring at 48 hours rather than an earlier time point, as we found neutrophils to begin infiltrating the liver earlier than monocytes (Figure 3-4).

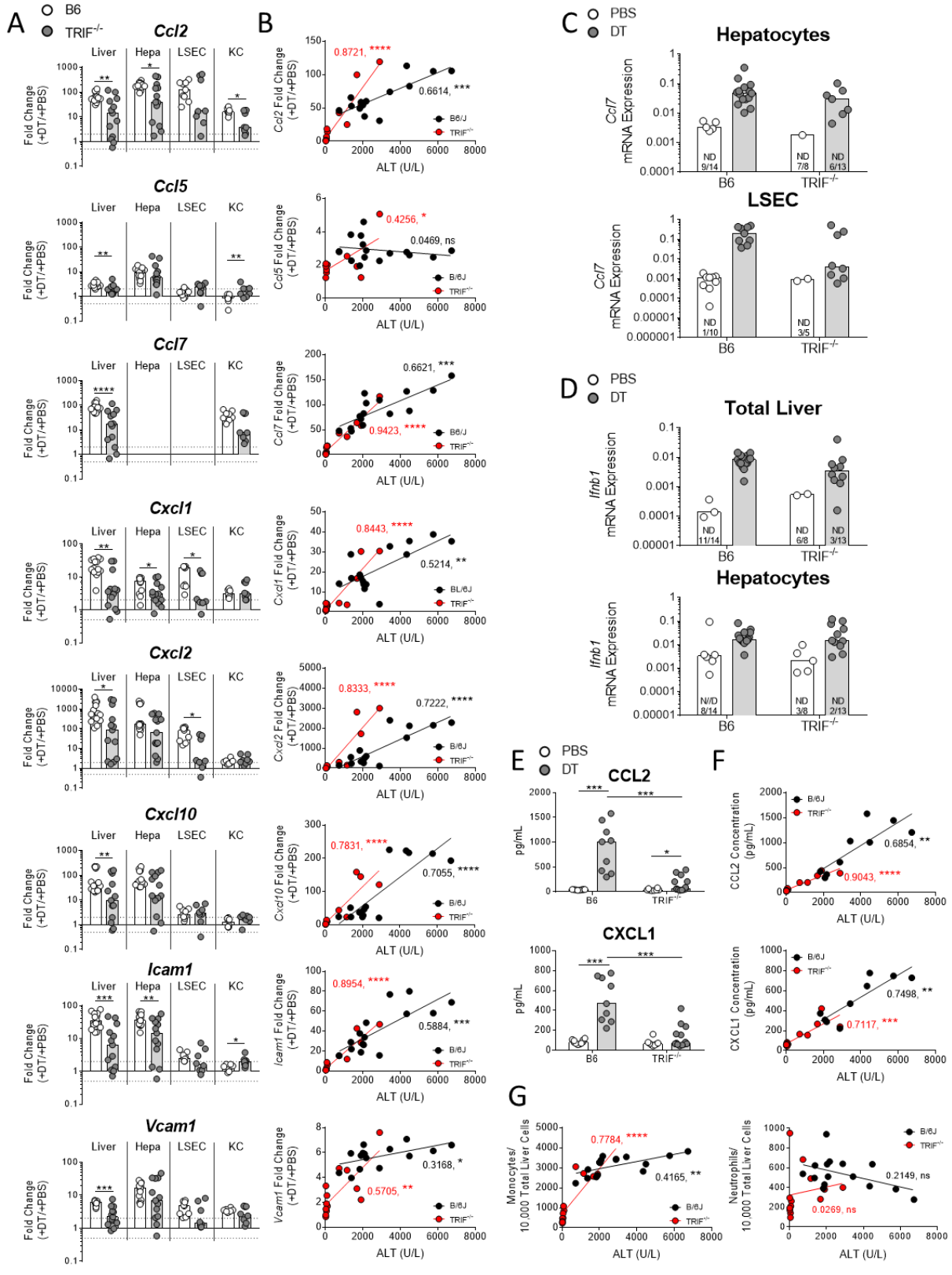
A
B6
TRIF-/-
Ccl2
Ccl5
Ccl7
Cxcl1
Cxcl2
Cxcl10
Icam1
Vcam1
Liver
Hepa
LSEC
KC
Fold Change (+DT/+PBS)
B
ALT (U/L)
0.8721, ****
0.6614, ***
0.4256, *
0.0469, ns
0.6621, ***
0.9423, ****
0.8443, ****
0.5214, **
0.8333, ****
0.7222, ****
0.7831, ****
0.7055, ****
0.8954, ****
0.5884, ***
0.3168, *
0.5705, **
B/6J
BL/6J
C
PBS
DT
Hepatocytes
LSEC
Ccl7 mRNA Expression
ND 9/14
ND 7/8
ND 6/13
ND 1/10
ND 3/5
D
Total Liver
Hepatocytes
Ifnb1 mRNA Expression
ND 11/14
ND 6/8
ND 3/13
N/D 8/14
ND 3/8
ND 2/13
E
CCL2
CXCL1
pg/mL
F
CCL2 Concentration (pg/mL)
0.6854, **
0.9043, ****
CXCL1 Concentration (pg/mL)
0.7498, **
0.7117, ***
G
Monocytes/ 10,000 Total Liver Cells
0.7784, ****
0.4165, **
Neutrophils/ 10,000 Total Liver Cells
0.2149, ns
0.0269, ns

Figure 3-9. TRIF is dispensable for increased expression of myeloid cell-recruiting chemokines and cell-adhesion molecules, as well as increased production of CCL2 and CXCL1 protein. Two weeks following rAAV injection, C57BL/6J and TRIF$^{-/-}$ mice received PBS or DT and were sacrificed 48 hours later. (A) Fold change gene expression in total liver, hepatocytes, LSECs, and KCs, + PBS group and + DT group compared to the + PBS group median, *Hprt* used as reference gene. (B) Correlation of serum ALT levels and gene expression fold change levels for B6 + DT (black) and TRIF$^{-/-}$ + DT (red) groups. mRNA expression relative to *Hprt* for (C) *Ccl7* in hepatocytes and LSECs and (D) *Ifnb1* in total liver and hepatocytes. (E) Serum protein levels for CCL2 and CXCL1. (F) Correlation of serum ALT levels and serum chemokine levels for B6 + DT (black) and TRIF$^{-/-}$ + DT (red) groups. (G) Correlation of serum ALT levels and monocyte and neutrophil infiltrate for B6 + DT (black) and TRIF$^{-/-}$ + DT (red). (A-G) Data are combined for 2-3 experiments. Each data point represents an individual mouse, bars represent the median. For (A-D, G) total liver and hepatocytes: n = 14, B6 + PBS; n = 15 B6 + DT; n = 8, TRIF$^{-/-}$ + PBS; n = 13 TRIF$^{-/-}$ + DT; for LSECs; n = 10, B6 + PBS; n = 9, B6 + DT; n = 5, TRIF$^{-/-}$ + PBS; n = 8, TRIF$^{-/-}$ + DT; and, for KCs: n = 10, B6 + PBS; n = 8, B6 + DT; n = 5, TRIF$^{-/-}$ + PBS; n = 8, TRIF$^{-/-}$ + DT. For (E, F) serum: n = 10, B6 + PBS; n = 9, B6 + DT; n = 8, TRIF$^{-/-}$ + PBS; n = 13, TRIF$^{-/-}$ + DT. ND = non-detect. (A) *Ccl2* has one non-detect value in each + PBS group not noted on the graph. Significance determined by (A) an individual Mann-Whitney test per population, (B, F, G) Goodness of Fit, with R^2 and p-value reported on the graph, and (C-E) by four pairwise Mann-Whitney tests and the p-values adjusted for multiple comparisons using the Holm-Bonferroni method as described in the methods. *, $P \leq 0.05$; **, $P \leq 0.01$; ***, $P \leq 0.001$; ****, $P \leq 0.0001$; non-significance represented by absence of bar.

TRIF is required for increased production of IL-1β, IL-10, and IL-6

The inflammatory cytokines TNF-α, IL-1β, and IL-6 and the anti-inflammatory cytokine IL-10, are commonly produced in response to acute liver injury [17]. We evaluated the levels of these cytokines in serum from wild type mice and TRIF$^{-/-}$ mice 48 hours following DT injection. The production of IL-10, IL-6, IL-1β, and TNF-α was reduced in TRIF$^{-/-}$ mice compared to wild type mice 48 hours following DT injection (Figure 3-10A). Correlation analysis of serum cytokine levels with serum ALT levels from DT-treated mice demonstrated that levels of IL-10, IL-6, and IL-1β did not correlate with increasing liver injury in TRIF$^{-/-}$ mice, while TNF-α levels moderately correlated with increasing liver injury in TRIF$^{-/-}$ mice (Figure 3-10B). This suggests that the production of IL-10, IL-6, and IL-1β following hepatocyte death requires TRIF, while TNF-α may result from liver injury by a different mechanism.

To ask which cell type might be producing these cytokines, we examined the relative expression of *Il10*, *Il6*, *Il1b*, and *Tnf* in wild type mice 6, 12, 24, 48, 72, and 96 hours following DT administration. At all time points, KCs expressed the highest level of transcripts for all four cytokines, and furthermore, expressed levels ~100-fold higher than hepatocytes and LSECs for *Il10*, *Il6*, and *Il1b* (Figure 3-11A). While KCs also expressed the highest levels of *Tnf*, the effect was not as dramatic and the largest induction of *Tnf* was seen in hepatocytes at 24 hours (Figure 3-11A). In KCs, *Il10*, *Il6*, and *Il1b* transcript either remained unchanged or increased slightly from 6-24 hours but began decreasing by 48 hours and continued to decrease through 72 hours (Figure 3-11B). *Tnf* transcript also increased through 24 hours, but didn't begin decreasing until 72 hours (Figure 3-11B). We hypothesized that the gene regulation seen at 48 hours in KCs for *Il10*, *Il6*, *Il1b*, and *Tnf* would be reduced in TRIF$^{-/-}$ mice. We examined the fold-induction of these cytokines in KCs 48 hours following DT injection in wild type and TRIF$^{-/-}$ mice. The down-regulation *Il10*, *Il6,* and *Il1b* seen in wild type mice was absent in TRIF$^{-/-}$ mice (Figure 3-

12). Additionally, at 48 hours the up-regulation of *Tnf* seen in wild type mice was modestly reduced in TRIF$^{-/-}$ mice (Figure 3-12). This suggests that KCs are responsible for the production of IL-10, IL-6, and IL-1β, but not TNF-α, and furthermore, that the production of IL-10, IL-6, and IL-1β following hepatocyte death is dependent upon TRIF-pathway signaling.

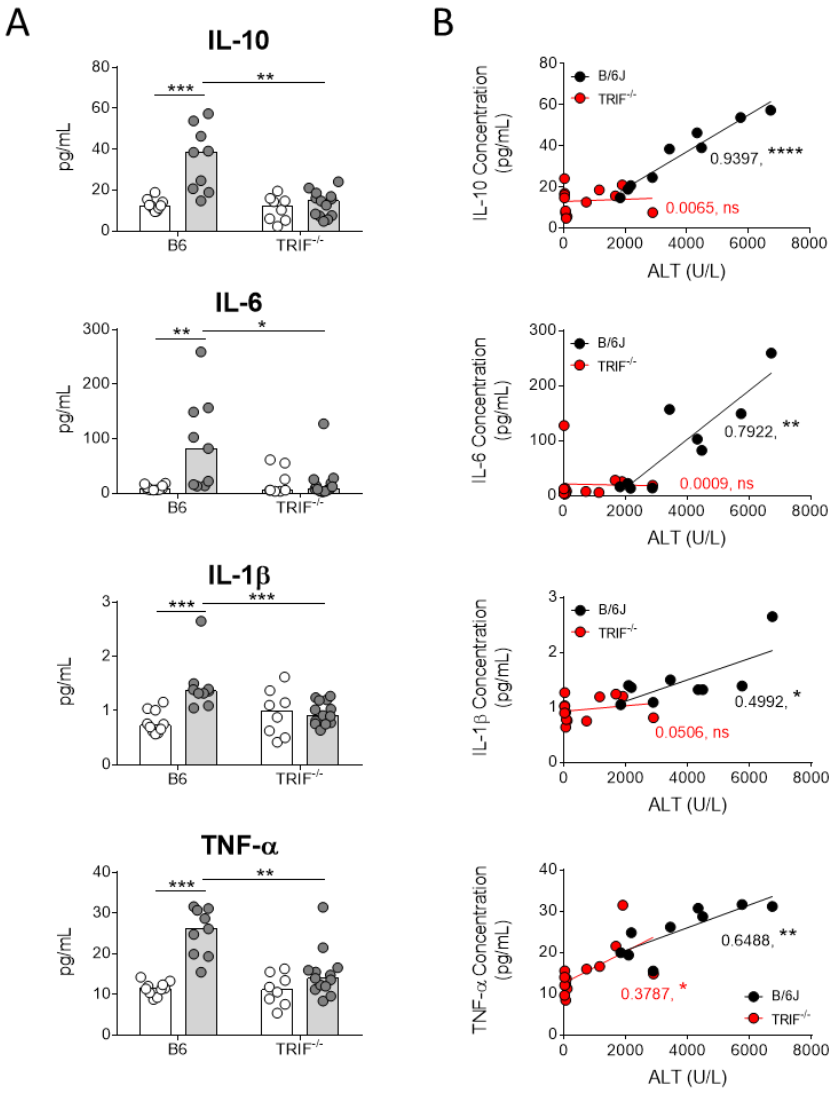

Figure 3-10. The increased production of IL-10, IL-6, and IL-1β depends on TRIF. Two weeks following rAAV injection, C57BL/6J and TRIF$^{-/-}$ mice received PBS or DT and were sacrificed 48 hours later. (A) Serum chemokine levels were measured. (B) Correlation of serum ALT levels and gene expression fold change levels for B6 + DT (black) and TRIF$^{-/-}$ + DT (red) groups. Data are combined for 2-3 individual experiments. Each data point represents an individual mouse (n = 10, B6 + PBS; n = 9, B6 + DT; n = 8, TRIF$^{-/-}$ + PBS; n = 13, TRIF$^{-/-}$ + DT), bars represent the median. Significance determined by (A) four pairwise Mann-Whitney tests and the p-values adjusted for multiple comparisons using the Holm-Bonferroni method as described in the methods and (B) Goodness of Fit, with R^2 and p-value reported on the graph. *, P ≤ 0.05; **, P ≤ 0.01; ***, P ≤ 0. 001; ****, P ≤ 0.0001; non-significance represented by absence of bar.

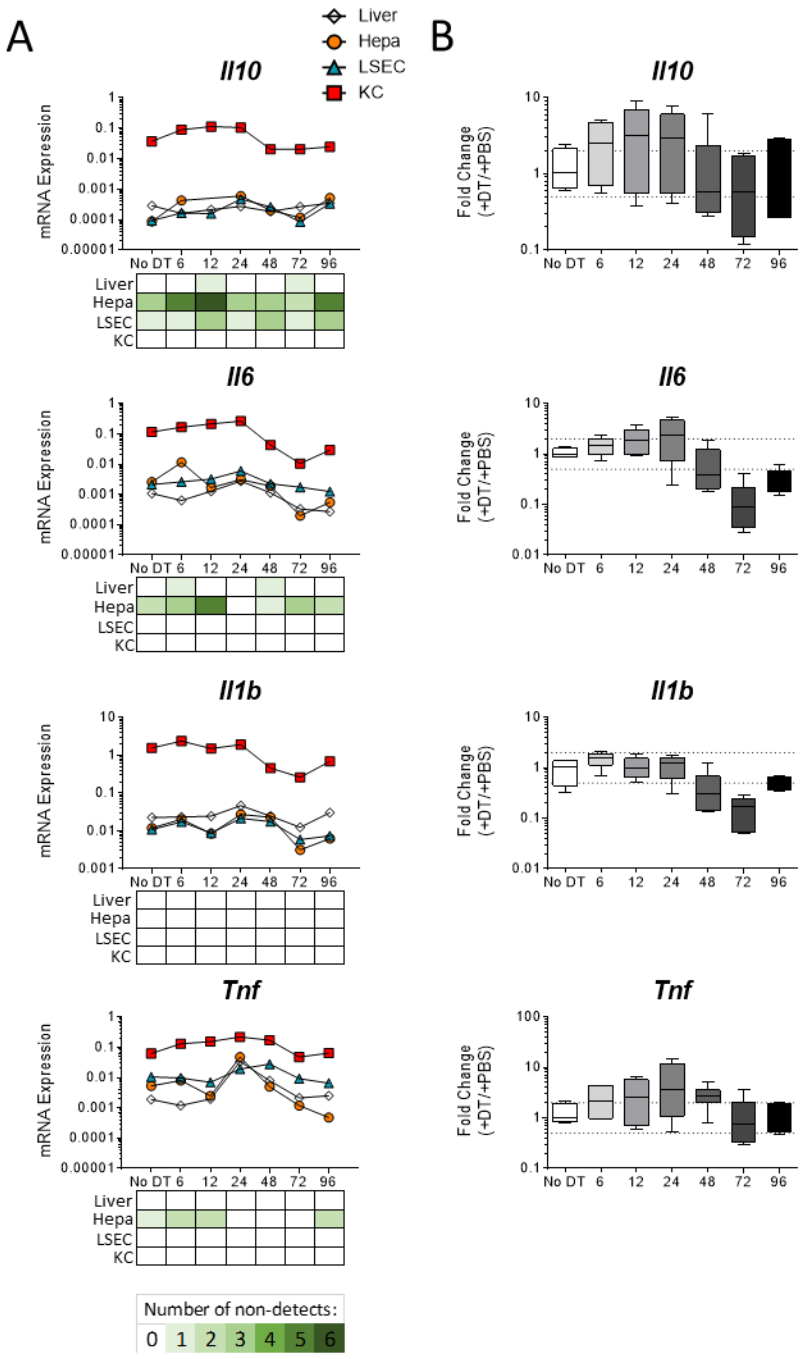

Figure 3-11. *Il10*, *Il6*, *Il1b*, and *Tnf* are expressed most highly by Kupffer cells and levels decrease 48-72 hours following diphtheria toxin injection. Two weeks following rAAV injection, C57BL/6J mice received DT and were sacrificed 6, 12, 24, 48, 72, or 96 hours later. (A) mRNA expression relative to *Hprt* in total liver, hepatocytes, LSECs, and KCs. Median values only represented. The number of non-detects are represented by a green color scale below each graph. (B) Fold change gene expression in KCs compared to the No DT group median. Data are median and range. (A, B) Data are combined from two experiments (n = 4, No DT group; n=6, all other time points for all

(Figure Legend 3-11, continued)
populations except n =5, KC at 96 hours). (B) Significance determined by a Kruskal-Wallis test followed by Dunn's post-test of each time point to the No DT group. Kruskal-Wallis determined *Il6* and *Il1b* to be significant (***), however, the individual post-tests were found to be non-significant. *Tnf* and *Il10* were determined to be non-significant by the Kruskal-Wallis test.

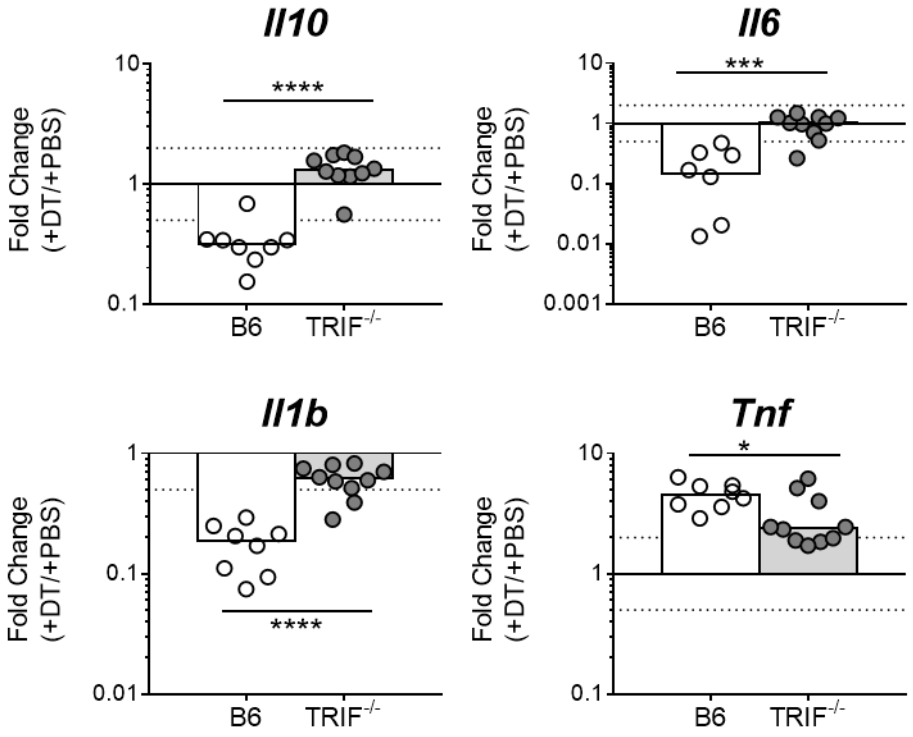

Figure 3-12. TRIF is required for the down-regulation of *Il10*, *Il6*, and *Il1b* in Kupffer cells. Two weeks following rAAV injection, C57BL/6J and TRIF$^{-/-}$ mice received PBS or DT and were sacrificed 48 hours later. Fold change gene expression in KCs: + PBS group and + DT group compared to + PBS group median, *Hprt* used as reference gene. Each data point represent an individual mouse (n = 10, B6 + PBS; n = 8, B6 + DT; n = 5, TRIF$^{-/-}$ + PBS; n = 8, TRIF$^{-/-}$ + DT), bars represent the median. Significance determined by four pairwise Mann-Whitney tests and the p-values adjusted for multiple comparisons using the Holm-Bonferroni method as described in the methods. *, P ≤ 0.05; ***, P ≤ 0.001; ****, P ≤ 0.0001; non-significance represented by absence of a bar.

Type I IFN signaling does not mediate the inflammation that follows hepatocyte death

The literature indicates that signaling via TRIF activates interferon regulatory factor 3 (IRF3) which drives expression of type I IFN, and particularly of IFN-β [43, 108]. Our results indicated that *Ifnb1* expression may be uncoupled from TRIF in this model of inflammation. To test if type I IFNs played a role in the observed TRIF-driven inflammation, we induced hepatocyte death in IFN (α and β) receptor 1 (IFNAR1)-deficient (IFNAR1$^{-/-}$) mice and looked at the response 48 hours after DT administration. IFNAR1$^{-/-}$ mice responded to hepatocyte death with the same increases in ALT, neutrophil infiltrate, and monocyte infiltrate as wild type mice (Figure 3-13), suggesting that the production of type I IFN following hepatocyte death does not contribute to propagating liver damage.

TLR4 does not mediate the inflammation that follows hepatocyte death

TRIF is the common signaling adapter for TLR3 and TLR4 [42]. To ask which receptor was responsible for initiating the inflammation to hepatocyte death, we examined the response to hepatocyte death in TLR4-deficient (TLR4$^{-/-}$) and TLR3-deficient (TLR3$^{-/-}$) mice at 48 hours following DT administration. ALT levels, neutrophil infiltrate, and monocyte infiltrate were induced to comparable levels in wild type and TLR4$^{-/-}$ mice (Figure 3-14). The TLR3$^{-/-}$ mice were not transduced to equal levels by the rAAV8.pAlb.mCherry.hDTR vector and so while we obtained very low ALT in DT-treated, vector-transduced TLR3$^{-/-}$ mice, the results could not be interpreted (Figure 3-15).

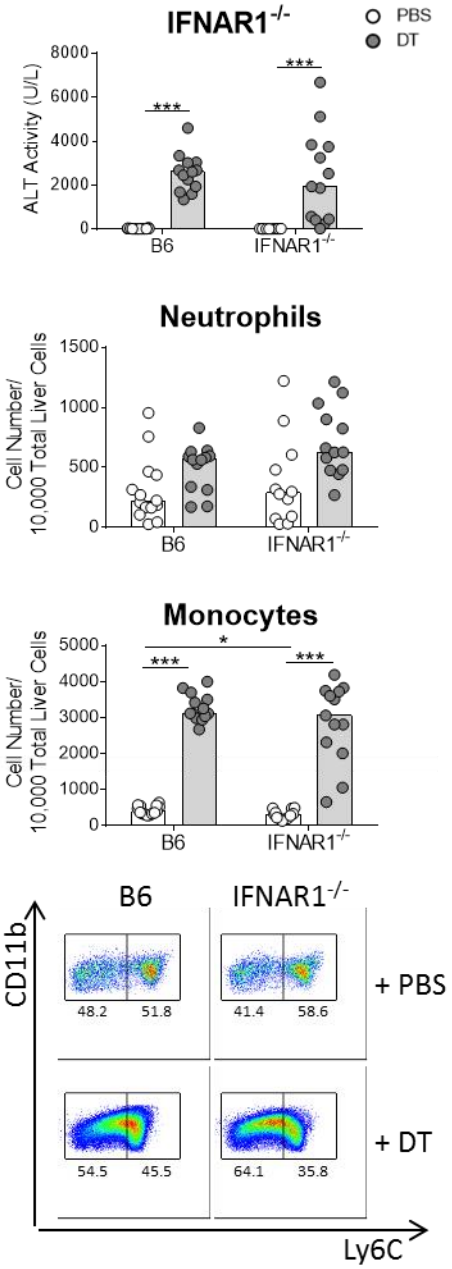

Figure 3-13. Type I IFN does not contribute to the inflammation induced by hepatocyte death. Two weeks following rAAV injection, C57BL/6J and IFNAR1$^{-/-}$ mice received PBS or DT and were sacrificed 48 hours later. Serum ALT and neutrophil and monocyte cell numbers per 10,000 liver non-parenchymal cells were measured. Data are combined for 3 individual experiments. The B6 mice used in the third repetition of this experiment were also used for the 3rd repetition of the MyD88$^{-/-}$ experiments in Figure 5, so the data appears twice (n = 4, B6 + PBS and B6 + DT). Each data point represents an individual mouse (n = 14, B6 + PBS; n = 13, B6 + DT, IFNAR1$^{-/-}$ + PBS, IFNAR1$^{-/-}$ + DT), bars represent the median. Significance determined by four pairwise Mann-Whitney tests and the p-values adjusted for multiple comparisons using the Holm-Bonferroni method as described in the methods. *, $P \leq 0.05$; ***, $P \leq 0.001$; non-significance represented by absence of bar.

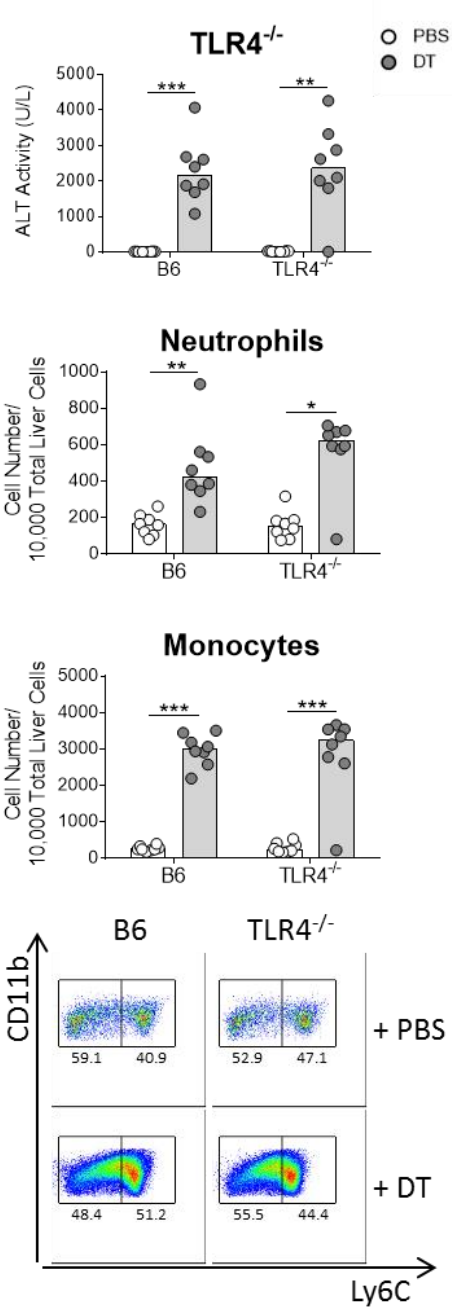

Figure 3-14. TLR4 signaling is not required for the inflammation induced by hepatocyte death. Two weeks following rAAV injection, C57BL/6J and TLR4$^{-/-}$ mice received PBS or DT and were sacrificed 48 hours later. Serum ALT and neutrophil and monocyte cell numbers per 10,000 liver non-parenchymal cells were measured. Data are combined for 2 individual experiments. Each data point represents an individual mouse (n = 8 for all groups), bars represent the median. Significance determined by four pairwise Mann-Whitney tests and the p-values adjusted for multiple comparisons using the Holm-Bonferroni method as described in the methods. *, $P \leq 0.05$; **, $P \leq 0.01$; ***, $P \leq 0.001$; non-significance represented by absence of bar.

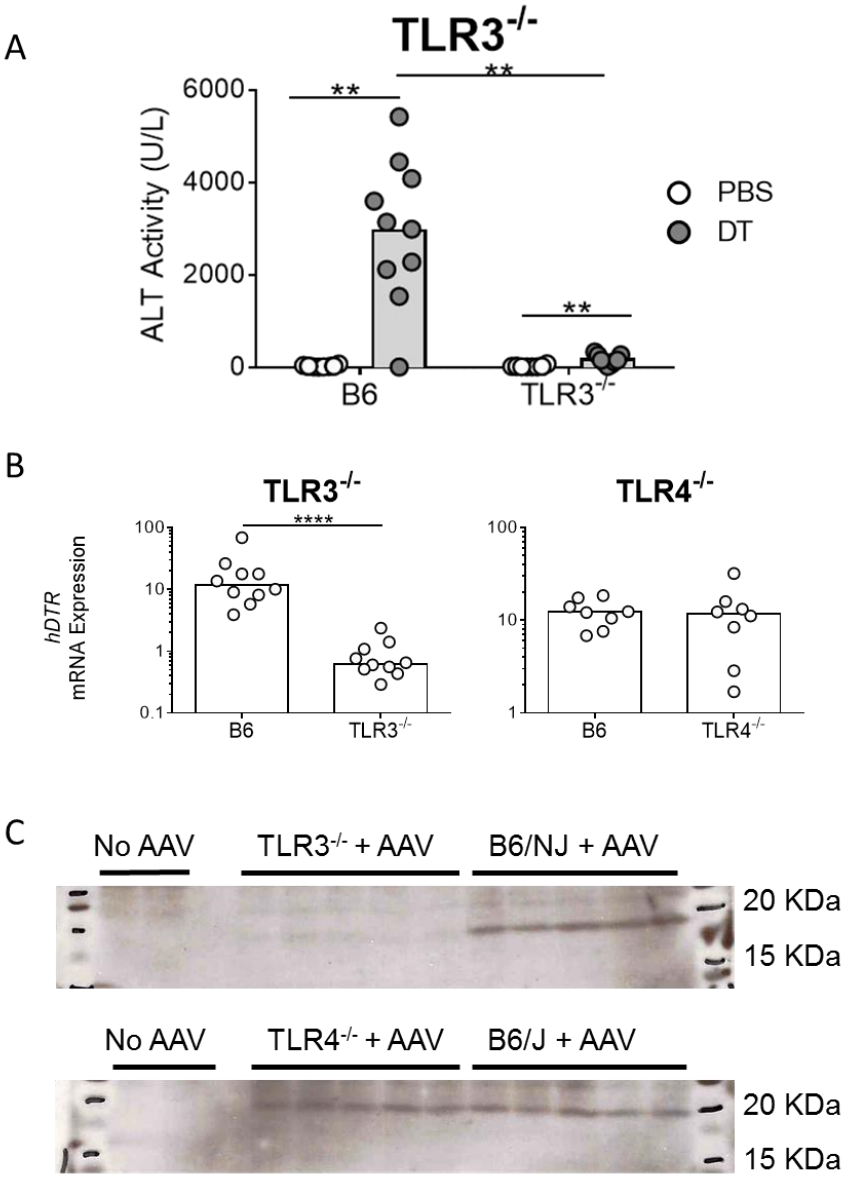

Figure 3-15. Reduced transduction of TLR3$^{-/-}$ hepatocytes by rAAV. Two weeks following rAAV injection, C57BL/6J and TLR4$^{-/-}$, or C57BL6/NJ and TLR3$^{-/-}$ mice received PBS or DT and were sacrificed 48 hours later. (A) Serum ALT for C57BL/6NJ and TLR3$^{-/-}$ mice was measured. (B) Expression of *hDTR* relative to *Hprt* in hepatocytes from + PBS groups. (C) Levels of hDTR protein in B6/NJ, TLR3$^{-/-}$, B/6J, and TLR4$^{-/-}$ mice. No AAV lanes represents B/6J mice that had not received vector, the same mice used for both blots. (A-C) Data are combined for 2 individual TLR3$^{-/-}$ and 2 individual TLR4$^{-/-}$ experiments. Each data point represents an individual mouse (for TLR3$^{-/-}$ experiments: n = 10, B6/NJ + PBS, B6/NJ + DT, TLR3$^{-/-}$ + PBS; n = 9, TLR3$^{-/-}$ + DT and for TLR4$^{-/-}$ experiments: n = 8, B/6J + PBS, TLR4$^{-/-}$ + PBS), bars represent the median. Significance determined by (A) four pairwise Mann-Whitney tests and the p-values adjusted for multiple comparisons using the Holm-Bonferroni method as described in the methods and (B) by a single pairwise Mann-Whitney test. **, $P \leq 0.01$; ****, $P \leq 0.0001$; non-significance represented by absence of bar.

Discussion

Hepatocyte death is a key component of both pathogen- and sterile-induced pathologies, and contributes to the development of chronic liver disease. The inflammatory circuits that respond to host death and pathogen insult overlap extensively and models of sterile inflammation help to isolate the signaling pathways involved by removing the responses to pathogen. Though there are many mouse models of sterile liver injury, there is a lack of models to identify pathways unique to the response initiated by DAMPs released from dying hepatocytes.

We have developed a mouse model of hepatocyte-specific death using a rAAV8 vector to target the hDTR construct to hepatocytes for expression. rAAV8 vectors, containing AAV2 serotype DNA and AAV8 serotype capsid proteins, are optimized for delivery of transgenes to hepatocytes. Unlike rAAV2 vectors which achieve transduction of only ~10% of hepatocytes even at high doses, rAAV8 is more efficient at transducing hepatocytes and can transduce up to 100% of hepatocytes [109, 110]. Examination of the expression pattern of *hDTR* mRNA confirmed that our rAAV8 vector provided liver- and hepatocyte-specific expression. In stark contrast to adenoviral vectors, the immune response to single-stranded AAV vectors is transient and mild, resolving within 6 hours following AAV injection [111]. The response is driven by TLR9- and MyD88-dependent signaling and results in a short-term increase of infiltrating neutrophils and CD11b(+) cells and an increase in mRNA for *Tnf*, *Ccl2*, *Ccl4*, *Ccl5*, *Cxcl2*, and *Cxcl10* [111]. To assure that the initial immune response to AAV was no longer present and that transgene expression was stable, we allowed for 2 weeks between AAV injection and injection of DT.

Hepatocyte death, induced by injection of DT, resulted in maximal liver damage 48 hours following DT injection and was accompanied by an increase in neutrophil and monocyte numbers in the liver. This response was largely dependent on TRIF and, to a

lesser extent, also dependent on MyD88. Perhaps the most-studied liver injury driven by TRIF-dependent signaling is chronic alcohol abuse, where increased translocation of endotoxin from gut microbiota into the liver via the portal vein results in signaling via TLR4 in a MyD88-independent, TRIF-dependent manner [14-16, 89, 90]. The role for TRIF signaling in acute liver injury is less clear. In APAP-induced injury, TLR4 and TLR9 have been identified as key receptors involved in the recruitment of infiltrating monocytes and neutrophils and the production of IL-6, TNF-α, and IL-1β; however, the downstream signaling pathways need to be elucidated [64, 67-69]. The similarities in the inflammation profile between our model and the APAP model suggest that TRIF signaling could be important for the induction of inflammation in APAP hepatotoxicity. Lastly, in a model of ischemia-reperfusion injury, TLR4$^{-/-}$ mice were protected from injury, producing less *Cxcl10*, *Icam1*, *Tnf*, *Il1b*, and *Ifng* [8]. Furthermore, a study by Zhai et al. showed that the DAMP high mobility group box 1 (HMGB1) signaled via a MyD88-independent, IRF3-dependent route to propagate inflammation in ischemia-reperfusion injury [72]. Both of these studies suggest that TRIF may be the adaptor mediating the inflammatory responses. It should be noted that signaling via TRIF generally results in production of type I IFNs [43, 108]. In sterile inflammation resulting from ischemia-reperfusion injury, IFNAR1-deficient mice were protected from liver damage and produced less transcript for *Tnf*, *Il1b*, *Il6*, *Ccl2*, *Cxcl10*, and *Icam1*, as well as had fewer infiltrating neutrophils and macrophages [75]. While we observed the induction of *Ifnb1*, liver damage in an IFNAR1$^{-/-}$ mouse was not significantly different that seen in wild type mice, eliminating a role for type I IFN signaling in the pathology to hepatocyte-specific death.

Interestingly, while the aforementioned models are heavily dependent upon signaling through TLR4, we find that the TRIF-dependent response to hepatocyte death is independent of TLR4. In the absence of upstream signaling through TLR4, TRIF

signaling is initiated via TLR3. The role of TLR3 in sterile liver injury remains relatively unknown, though it has been found to contribute to liver damage in models of APAP hepatotoxicity and Con A-induced hepatitis [112, 113]. As we observed ~30-fold less transduction of hepatocytes by rAAV8.pAlb.mCherry.hDTR in TLR3$^{-/-}$ mice when compared to their wild type C57BL/6NJ controls, we could not evaluate the role of TLR3 signaling in this model. A study by Jayandharan et al. demonstrated that the alternative nuclear factor kB (NF-kB) pathway was necessary for expression of AAV transgene [114]. It is therefore possible that the lack of functional TLR3 in TLR3$^{-/-}$ mice either directly affects the alternative NF-κB pathway, or affects the ability of AAV to use the alternative NF-κB for transgene expression. The TLR4-independent inflammation produced following hepatocyte death suggests that TLR3 is the receptor that is responding to cell death. This is an attractive option and supported by *in vitro* studies using dendritic cells which show that mRNA from necrotic cells signals via a TLR3- and TRIF-dependent pathway [115].

The role hepatocytes play in sterile liver inflammation, and particularly in the response to hepatocyte death, is relatively unknown. Though there is limited data available concerning the role of hepatocytes as drivers of an inflammatory response, *in vitro* studies have produced some provocative results. Primary mouse hepatocytes secrete IL-6 in response to free fatty acids (FFAs) and IL-17 [116], and IL-6 and TNF-α in response to FFAs alone [85]. In mouse models of chronic liver injury induced by carbon tetrachloride (CCl_4), CCL20 was detected in hepatocytes by immunohistochemistry [117] and secreted by murine primary hepatocytes in culture in response to CCl_4 [118]. Additionally, hepatocytes isolated from ethanol-treated mice expressed more *Cxcl1* than those from the control mice [92]. In our model of hepatocyte-specific death, the up-regulation of *Ccl2*, *Ccl5*, *Ccl7*, *Cxcl1*, *Cxcl2*, *Cxcl10*, *Icam1*, *Vcam1*, *Ifnb1*, and *Tnf* transcripts was greater in hepatocytes than in either LSECs or

KCs, highlighting hepatocytes as key players in the sterile inflammatory response to hepatocyte death.

A number of studies have shown that cells undergoing apoptosis, necrosis, or necroptosis maintain the capacity to up-regulate transcription and protein production [119-123]. IL-6 has been found to be secreted by necrotic cells [121]; IL-6, CCL2, and CXCL1 secreted by apoptotic cells [122]; and most recently, necroptotic cells showed increased transcription of many genes, including *Cxcl1*, *Cxcl10*, *Ccl2*, C*cl7*, and *Il6* [123]. Given the transcript repertoire we detected in our studies it is possible that dying hepatocytes are producing chemokines in our model. Alternatively, or in parallel, live hepatocytes sensing and responding to death may also be responsible for the up-regulation of these transcripts. This latter possibility is supported by our observation that many of these transcripts are also up-regulated in KCs and LSECs 6 hours following DT injection, indicating the induction of an innate immune response in neighboring cells. Additionally, in preliminary studies we found that RIPK3$^{-/-}$ mice, which are incapable of necroptotic death, were not protected from liver injury (data not shown). Finally, sensing and response by live hepatocytes is also supported by *in vitro* findings in which primary mouse hepatocytes, independent of death, increased expression for a number of inflammatory proteins including: *Cxcl1*, *Cxcl2*, *Cxcl10*, *Ccl2*, *Ccl7*, *Ccl20*, *Icam1*, *Vcam1*, *Il1b*, and *Il10* in response to bile acids [124]. The results of our *in vivo* study of hepatocyte death combined with this *in vitro* study provide compelling evidence for a common inflammatory pathway induced in hepatocytes in response to insult, in these cases, DAMPs released from other dying hepatocytes or bile acids.

Interestingly, while we found that TRIF regulates inflammation overall, we still observed inflammation in a subset of TRIF$^{-/-}$ mice. This provides insights as to what arm of the inflammation is directly influenced by TRIF and what arm is indirectly influenced by TRIF. Up-regulation of *Ccl2, Ccl7, Cxcl1, Cxcl2, Cxcl10*, *Icam1,* and *Vcam1* in total

liver and CCL2 and CXCL1 in serum directly correlated with increasing liver injury in TRIF$^{-/-}$ mice, and therefore, did not require TRIF-mediated signaling. In contrast, IL-6, IL-10, and IL-1β levels in the serum were not correlated with liver injury in TRIF$^{-/-}$ mice as they were in wild type mice, and therefore, their induction following hepatocyte death required TRIF-mediated signaling. Furthermore, consistent with the literature on acute liver injury, our data suggest that KCs may be the main producers of IL-6, IL-10, and IL-1β as these genes are not down-regulated at 48 hours in TRIF$^{-/-}$ mice. We speculate that the arm of the inflammatory response not dependent upon TRIF—the up-regulation of chemokines and cell adhesion molecules—signals through a TLR4-, TRIF-, and Type I IFN-independent pathway, potentially driven by a MyD88-dependent pathway. In addition, we speculate that the arm of the inflammatory response dependent on TRIF—the production of IL-6, IL-10, and IL-1β—amplifies the effects of hepatocyte death and results in increased inflammation. Therefore, in mice lacking TRIF, less amplification of the inflammatory response occurs, resulting in reduced or absent liver injury.

In summary, we have identified TRIF as a central mediator in the response to hepatocyte-specific death. Hepatocytes themselves produce the most robust response to hepatocyte death through the up-regulation of genes for myeloid cell-recruiting factors. In serum as a whole, we see an increase in IL-6, IL-1β, and IL-10, which is absent in TRIF$^{-/-}$ mice, indicating a direct role for TRIF in the production of these inflammatory cytokines. Conversely, TRIF is not required for the increased expression of chemokine and cell adhesion genes and proteins associated with the myeloid cell-recruiting response. Finally, we find the TRIF-driven response to hepatocyte death to be independent of TLR4 and Type I IFN.

CHAPTER 4: DIET- AND ALCOHOL-INDUCED DAMAGE AS A MODEL OF CHRONIC LIVER INJURY

Abstract

Steatosis, or fatty liver, the dominant indication in the nonalcoholic fatty liver disease and alcoholic liver disease spectrums is a serious health concern in developed nations, affecting up to 30% of adults in the United States and other Western nations. Untreated, steatosis can progress to steatohepatitis characterized by inflammation and hepatocyte death. Ultimately, a subset of persons with steatohepatitis progress to cirrhosis and eventually hepatocellular carcinoma. Steatosis in mice is most commonly induced by methionine/choline-deficient or high-fat diets, though studies are emerging which show an important role for high-fructose diets in the induction of steatosis and steatohepatitis. Research suggests that moderate alcohol consumption may exert protective effects in non-alcoholic fatty liver disease. Using low-fat and mid-fat Lieber-DeCarli diets in mice, we showed that increasing liver inflammation, monocyte infiltrate, and histological damage correlated with increasing amounts of dietary carbohydrate, specifically glucose and longer chain carbohydrates composed of glucose, rather than increasing amounts of dietary fat. In contrast to the classically-dominant role of Kupffer cells, our studies found that hepatocytes up-regulated more myeloid cell-recruiting (*Ccl2*, *Ccl5*, *Cxcl9*, *Cxcl10*), cell adhesion (*Vcam1*), and fibrosis (*Mmp9*, *Mmp12*, *Pdgfra*, and *Tgfb1*) genes than either liver sinusoidal endothelial cells or Kupffer cells after 8 weeks on either the mid-fat or low-fat diet. Lastly, we showed that ethanol may play conflicting roles by reducing overall pathology and expression of *Tgfb1* in hepatocytes, but by increasing neutrophilic infiltrate.

Introduction

The spectrum of fatty liver (steatosis) diseases includes both the diet- and alcohol-induced liver injuries, non-alcoholic fatty liver disease (NAFLD) and alcoholic liver disease (ALD). Only a portion (10-30%) of those with simple steatosis progress to the more severe forms of disease, non-alcoholic steatohepatitis (NASH) and alcoholic steatohepatitis (ASH), respectively, characterized by inflammation and hepatocyte death; however, the mechanisms driving this selective progression of pathology are obscure. Attempts to define the factors involved in progression have resulted in the proposition of both the “two hit” and “multiple hit” hypotheses [80, 82]. These models share the common theme that no one event is sufficient for the progression from steatosis to steatohepatitis, though they differ in the necessity for two, or more than two rounds of insult. Accordingly, the “two hit” model proposes that a “first hit” sensitizes the liver to a “second hit” that drives more severe pathologies, while the “multiple hit” hypotheses proposes that various “hits” work in parallel to promote pathogenesis.

The development of NAFLD is linked to obesity and insulin resistance, and particularly a disruption in the metabolism of lipids [125]. Steatosis develops when the fatty acid balance is disrupted in the liver and more fatty acids are imported or synthesized by hepatocytes than are exported or catabolized [125, 126]. Diets high in fat and carbohydrates, and particularly fructose, are correlated with an increased risk for developing NAFLD [127]. In recent years, the effects of high fructose on the induction of fatty liver have garnered attention as a model for the Western diet which is high in carbohydrates and high in fat. Two pivotal studies showed that consumption of soft drinks, which contain high amounts of fructose and glucose, correlated with the development of NAFLD in the absence of risk factors such as the metabolic syndrome [128, 129].

In attempts to define what dietary factors contribute to the development of fatty liver, multiple rodent models of diet-induced steatosis have been developed. The most commonly used diet, the methionine choline-deficient (MCD) diet, contains 40% sucrose and 10-20% fat, but lacks methionine and choline so that β-oxidation is inhibited, resulting in fatty acid accumulation within hepatocytes [125, 130]. While the MCD diet causes the most severe liver pathology compared to other mouse models of NAFLD, its drawback is that is does not reproduce the human conditions of NASH [130]. High-fat diets (composed of anywhere from 60% to greater than 85% fat), on the other hand, do replicate the human conditions of NASH, including weight gain, increased fat, and development of insulin resistance [131]. The limitation of high-fat models is that they produce variable results dependent on the mouse strain, length of study, type of fat, and amount of fat in the diet [125]. Finally, high-fructose models, designed to mimic the high-fat, high-fructose nature of the "Western diet", are still being developed and range from 10% fructose in drinking water up to 70% fructose in solid diets [132-137].

Alcohol consumption presents an additional complication in the spectrum of fatty liver disease. Whether alcohol consumption has a protective role for the development and progression of NAFLD/NASH is still under debate. Recent studies indicate that moderate alcohol consumption is associated with both lower prevalence of and lower disease severity of NAFLD [138-141]. In contrast, consumption of alcohol was found to increase the risk of disease progression for those patients with established NAFLD [142, 143]. Thus, as with other multi-factorial disease indications, context and timing are likely critical for our understanding of the contribution of alcohol to fatty liver disease, and controlled mouse models to address these questions are a high priority.

We set out to first establish a model of chronic alcohol exposure using the Lieber-DeCarli mid-fat control and ethanol (6.7% v/v) diets. After observing early and unexpected mouse mortality, we reduced the alcohol percentage to 5.0% v/v.

Surprisingly, ethanol concentrations of 5.0% v/v resulted in less liver damage and immune activation in the ethanol group when compared to the control group. We hypothesized that the high amount of fat in the diet (35.9% calories from fat versus the 13.2% of vivarium chow) was responsible for the increased damage in the control group and might be obscuring any effects of ethanol.

To address this hypothesis, we tested different diets that varied in fat, carbohydrate, and ethanol content: vivarium chow, Lieber-DeCarli mid-fat control diet, Lieber-DeCarli low-fat control diet, and the Lieber-DeCarli low-fat ethanol diet. Histological examination showed increased amounts of fat, lobular inflammation, and hepatocyte ballooning in the mice fed the mid-fat and low-fat control diets compared to the mice fed the chow diet. In addition, mice fed the low-fat diet had increased pathology compared to the mice fed the mid-fat diet. Mice fed both the low-fat and mid-fat control diets showed extensive gene up-regulation in the hepatocytes, and relatively less so in liver sinusoidal endothelial cells (LSECs) and Kupffer cells (KCs). When compared to the low-fat control diet, the low-fat ethanol diet caused neutrophil infiltration and increased expression of *Ccl2* and *Cxcl1* but down-regulation of *Tgfb1* in hepatocytes. Additionally, mice fed the low-fat ethanol diet showed less liver injury by histological analysis than those mice fed the low-fat control diet.

In the spectrum of human disease and in animal models of steatosis and steatohepatitis a consistent observation is that an imbalance in caloric load leads to liver damage. We demonstrate that the increased amount of carbohydrates in a low-fat diet compared to a mid-fat diet increases liver damage. Additionally, we conclude that while ethanol mediates the recruitment of neutrophils, it may also act to suppress fibrosis in hepatocytes through the down-regulation of *Tgfb1*. While the exact causal role of the caloric distribution between carbohydrates versus fat remains unclear, these studies give clues to mechanisms of liver pathologies, including the previously-underappreciated role

of the hepatocyte as active drivers of inflammation in non-alcoholic and alcoholic fatty liver diseases.

Results

6.7% vol/vol ethanol resulted in early, unexpected mouse mortality

To establish a model of chronic ethanol exposure in mice, we used the Lieber-DeCarli mid-fat control and ethanol diets. Mice were individually caged and pair-fed and received all of their caloric intake from the mid-fat control or ethanol diet. Unexpected mouse mortality beginning 2 weeks into feeding of the diets forced termination of the experiment after only 37 days (Figure 4-1A). Only 4 of 12 ethanol-fed mice survived until the collection date. Another two ethanol-fed mice (mice #113 and #129) had to be removed from the study on day 33; however, we obtained blood for serum analysis and had a necropsy performed by the University of Washington, Department of Comparative Medicine, Vet Services.

At day 37, the 4 surviving ethanol-fed mice, along with the 4 pair-fed control mice, were anesthetized and livers perfused. Serum alanine aminotransferase (ALT) was moderately elevated in ethanol-fed mice over the control-fed mice (Figure 4-1B). Additionally, the serum ALT levels in the two mice collected at day 33 were elevated compared to 3 of 4 of the ethanol-fed mice collected at day 37 (Figure 4-1B). Mice #113 and #129 were diagnosed by Vet Services with generalized hepatic lipidosis in zones 2 and 3, moderate to severe in Mouse #113 and severe in #Mouse 129 (Figure 4-1C). Of the mice collected at day 37, the mice receiving the ethanol diet had more neutrophils than those receiving the control diet, and additionally, trended towards increased Ly6C(+) monocytes while the Ly6C(-) monocyte population was not altered (Figure 4-1D).

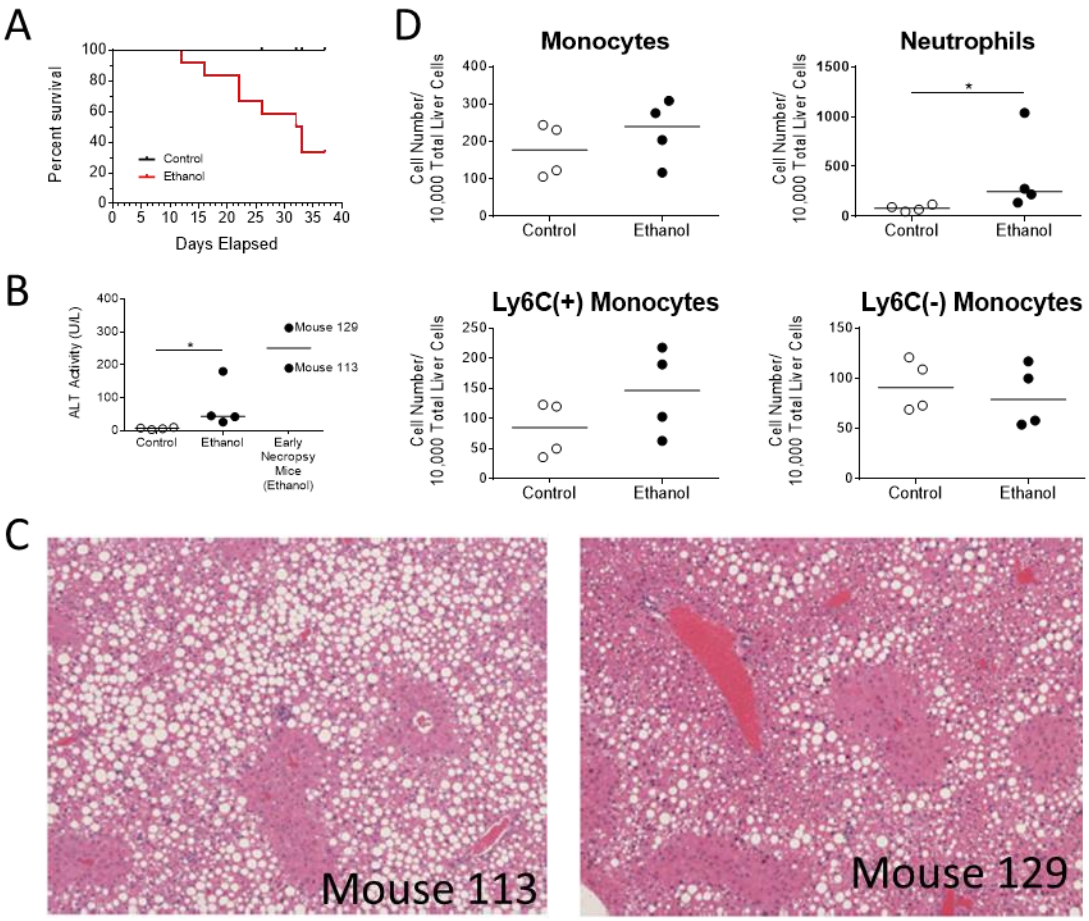

Figure 4-1. A 6.7% vol/vol ethanol diet caused early mouse mortality. Mice were fed the mid-fat control or mid-fat ethanol Lieber-DeCarli diets. (A) Survival curve (control diet, black; ethanol diet, red) shows ethanol mice began dying by day 12. For the ethanol-fed group, starting n = 12 and final n = 4. For the control-fed group, n = 12. Mice that survived to day 37 were collected and analyzed for: (B) serum ALT levels and (D) neutrophil, total monocyte, Ly6C(+) monocyte, and Ly6C(-) monocyte cell numbers per 10,000 total liver cells. (C) Hematoxylin and eosin-stained sections for Mice #113 and #129, euthanized at day 32. (B, D) Data from one experiment. Each data point represents an individual mouse (final n = 4 for control- and ethanol-fed groups). Significance determined by a pairwise Mann-Whitney test. *, $P \leq 0.05$; non-significance represented by the absence of a bar.

5.0% vol/vol ethanol prevented unexpected mouse mortality

Following the mortality seen during our first attempt to establish a mouse model of chronic alcohol exposure, we modified certain conditions with the aim of reducing mouse mortality. These modifications were: adjusting the vivarium temperature set-point to 74°C [personal correspondence with Dr. Bin Gao], providing water in addition to the liquid diets, and group-housing mice in cages of 5. The mid-fat control and ethanol diets were not modified; however, we added a build-up period to the final concentration of ethanol, as follows: we began with 2.23% v/v ethanol for 2 days, followed by 4.46% v/v for 2 days, and then 6.7% v/v. Eleven days after the start of the 6.7% v/v ethanol diet, 2 mice had to be euthanized and 1 mouse was found dead. We were able to collect blood from the 2 euthanized ethanol group mice (mice #1848 and #1853) as well as from 2 control group mice (#1864 and #1865). An exhaustive search of the literature suggested that other groups had experienced similar mouse mortality at 6.7% v/v ethanol and thus, we reduced the ethanol concentration 5.0% v/v. This successfully prevented any additional mouse mortalities.

Ethanol-fed mice had lower measures of liver damage than control-fed mice at 8 weeks

Analysis of serum for the liver enzymes ALT and aspartate aminotransferase (AST) paradoxically showed that ALT and AST levels were significantly higher in control-fed mice than in ethanol-fed mice at 8 weeks (Figure 4-2A). Furthermore, this elevation in AST persisted to 12 weeks (Figure 4-2A). While neutrophils trended towards increased numbers in control-fed mice compared to ethanol-fed mice at 4 and 8 weeks ($p= 0.0571$), by 12 weeks there was no difference in neutrophil numbers between the two groups (Figure 4-2B). At 12 weeks, however, the Ly6C(+) monocyte population trended towards increased numbers in control-fed mice ($p= 0.0571$) and the Ly6C(-)

monocyte population was significantly increased in the control-fed mice compared to the ethanol-fed mice (Figure 4-2B).

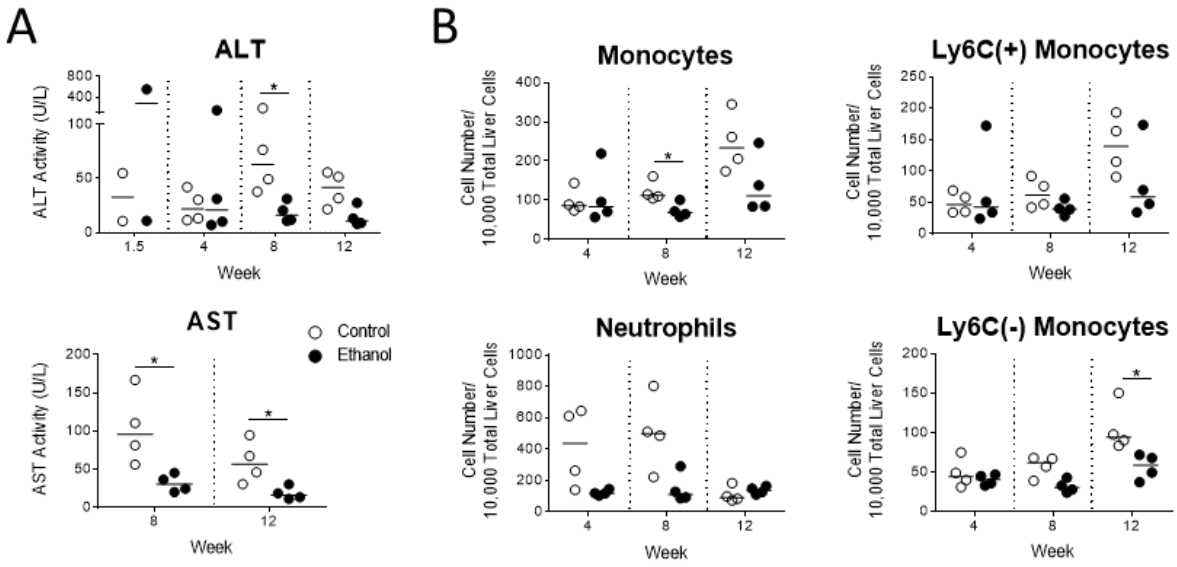

Figure 4-2. Ethanol-fed mice had lower levels of ALT, AST, and monocytes than control-fed mice. Mice were fed the mid-fat control or mid-fat ethanol Lieber-DeCarli diets. Collections occurred at 1.5 weeks (two ethanol group mice removed from study and their controls), 4, 8, and 12 weeks. (A) Serum ALT and AST levels. (B) Neutrophil, total monocyte, Ly6C(+) monocyte, and Ly6C(-) monocyte cell numbers per 10,000 total liver cells. Data from one experiment. Each data point represents an individual mouse (n = 4 per group). Significance determined by a pairwise Mann-Whitney test at each time point. *, $P \leq 0.05$; non-significance represented by the absence of a bar.

Low-fat diets increased ALT and AST serum levels in mice

The increased levels of ALT and AST as well as the trend towards more infiltrate in control-fed mice compared to ethanol-fed mice, prompted us to examine the levels of dietary fat in both diets compared to regular vivarium chow. In the vivarium chow diet, 13.1% of the calories came from fat, while in both the mid-fat control and ethanol diets, 35.9% of the calories came from fat (Table 2-1). This led us to hypothesize that higher levels of dietary fat in the Lieber-DeCarli diets were causing increased inflammation, and therefore, obscuring any additional effects of ethanol.

To test this hypothesis, we designed an experiment to compare mid-fat and low-fat Lieber-DeCarli control diets to standard vivarium chow. Additionally, we included a low-fat Lieber-DeCarli ethanol diet to assess if ethanol had any affects over the control diet when the amount of fat was lower. Mice were fed one of four diets: standard vivarium chow (13.1% calories from fat), mid-fat control Lieber-DeCarli diet (35.9% calories from fat), low-fat control Lieber-DeCarli diet (12.5% calories from fat), or low-fat ethanol Lieber-DeCarli diet (12.5% calories from fat) (Table 4-1). At 8 weeks, ALT levels in the low-fat control group were significantly higher than those in mid-fat control group, though the presence of an outlier in the chow group made all comparisons to the chow group not significant (Figure 4-3A). By 6 weeks, AST levels were significantly higher in the low-fat control group compared to the chow group and by 8 weeks, AST levels were significantly higher in both the low-fat control and ethanol groups when compared to the chow group (Figure 4-3B). While the levels of ALT trended upwards in the low-fat ethanol group, there was no significant difference in ALT at 8 weeks when compared to either the chow group or the low-fat control group (Figure 4-3A). Lastly, there was no difference in AST levels between the low-fat control and ethanol groups at 8 weeks Figure 4-3B). In sum, the results indicated that low-fat diets cause more liver damage than chow or mid-fat diets.

	Chow	Mid-Fat Control	Low-Fat Control	Low-Fat Ethanol
Caloric Profile (kcal/L)				
Protein	247	151	150	150
Fat	132	359	125	125
Carbohydrate	621	490	725	449*
Ethanol	0	0	0	276
Carbohydrates (g/L)				
Monosaccharides (glucose)	0.42 (0.19 glucose, 0.23 fructose)	18.3	30.1	14.5
Disaccharides	1.34 (lactose) 3.18 (sucrose)	18.0 (maltose) 3.5 (sucrose)	25.8 (maltose) 3.5 (sucrose)	14.3 (maltose) 3.5 (sucrose)
Polysaccharides (long chain glucose polymers)	33.9 (starch)	84.1	111.0	61.8
				+ 20.3 g/L maltose dextrin

*79 kcal/L from maltose dextrin

Table 4-1. Caloric profile and carbohydrate composition for diets.

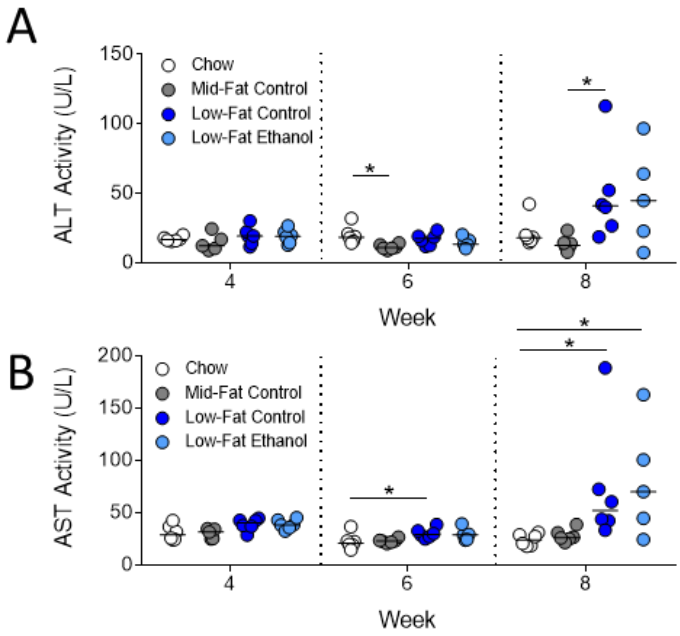

Figure 4-3. Low-fat control and ethanol diets induced more damage in mice than mid-fat control and chow diets. Mice were fed standard chow or the mid-fat control, low-fat control, or low-fat ethanol Lieber-DeCarli diets. Collections occurred at 4, 6, and 8 weeks. (A) Serum ALT levels. (B) Serum AST levels. Data from one experiment. Each data point represents an individual mouse (n = 6, all groups except: n = 5, mid-fat control at 4 weeks, low-fat ethanol at 6 and 8 weeks). At each time point, significance determined by a Kruskal-Wallis test followed by Dunn's post-test for each Lieber-DeCarli diet compared to the chow diet and for the low-fat ethanol diet compared to the low-fat control diet. *, $P \leq 0.05$; non-significance represented by the absence of a bar.

Low-fat diets increased monocyte and neutrophil infiltrate in mice

We next assessed the myeloid cell populations in the liver at 4 and 8 weeks. At 4 weeks, there were no significant differences in the monocyte and neutrophil populations in the liver (Figure 4-4). By 8 weeks, the proportion of total monocytes was significantly increased in the low-fat control and ethanol groups when compared to the chow group, as a result of increased Ly6C(+) monocytes (Figure 4-4). While not significant, the levels of monocytes trended towards an increase in the mid-fat control group compared to the chow group. There was no significant difference in the levels of monocytes between the low-fat control and ethanol group. In contrast, the low-fat ethanol group had significantly

more neutrophils at 8 weeks when compared to the low-fat control group (Figure 4-4). These results indicate that monocyte infiltrate occurs as a result of the Lieber-DeCarli diets, with the effect of ethanol undetermined, and that neutrophil infiltrate is a direct result of ethanol.

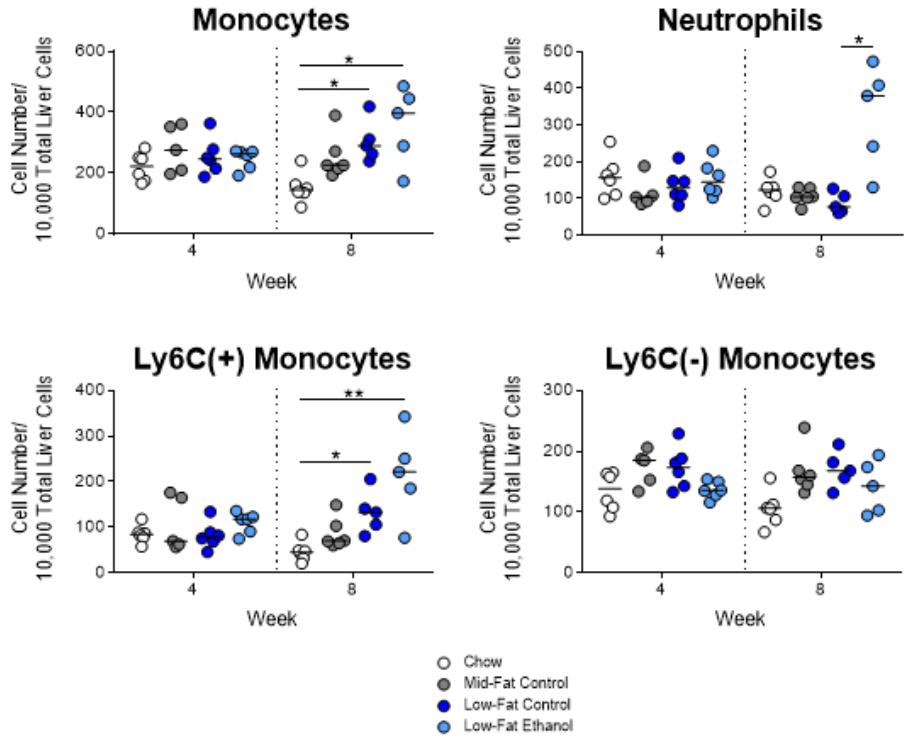

Figure 4-4. Low-fat diets induce greater monocyte and neutrophil infiltrate than mid-fat control and chow diets. Mice were fed standard chow or the mid-fat control, low-fat control, or low-fat ethanol Lieber-DeCarli diets. Data shown for 4 and 8 week collections. Neutrophil, total monocyte, Ly6C(+) monocyte, and Ly6C(-) monocyte cell numbers per 10,000 total liver cells. Data from one experiment. Each data point represents an individual mouse (n = 6, all groups except: n = 5, mid-fat control at 4 weeks, low-fat control at 8 weeks, low-fat ethanol at 8 weeks). At each time point, significance determined by a Kruskal-Wallis test followed by Dunn's post-test for each Lieber-DeCarli diet compared to the chow diet and for the low-fat ethanol diet compared to the low-fat control diet. *, $P \leq 0.05$; **, $P \leq 0.01$; non-significance represented by the absence of a bar.

Low-fat diets caused increased pathology in the liver

The necropsied mice from our first attempt to establish a model of chronic ethanol exposure showed extensive fatty livers. Additionally, fatty liver, or steatosis, is the main symptom of both NAFLD and ALD. So, liver pieces from mice fed chow, mid-fat control, low-fat control, and low-fat ethanol diets for 8 weeks was fixed in paraformaldehyde, paraffin-embedded, and stained with hematoxylin and eosin. The sections were blind-scored for fat, lobular inflammation, and hepatocyte ballooning and the scores tallied to provide the overall NAFLD activity score (NAS) (Table 4-2). Compared to the chow diet, all three Lieber-DeCarli diets had increased NAS scores. The low-fat control group had the highest median NAS score of 5.5, followed by the low-fat ethanol group (median NAS score of 4), and finally by the mid-fat control group (median NAS score of 2). The major contributing factor to the score was fat. Intriguingly, the low-fat control group scored highest for fat (median score of 3), followed by the low-fat ethanol group (median score of 2), and finally followed by the mid-fat control group (median score of 1.5). Compared to the low-fat control group, the low-fat ethanol group scored slightly lower for fat and slightly higher for hepatocyte ballooning, but both groups had equivalent scores for lobular inflammation. Finally, when observed, mice receiving a Lieber-DeCarli liquid diet had Zone 1 steatosis (located in the portal tracts) with mixed microvesicular and macrovesicular fat deposits (Figure 4-5).

	Mouse	ALT	Fat	Lobular Inflammation	Ballooning	NAS	Location of steatosis	Fat Droplet Type
Chow	1	18.4	0	1	0	1		
	2	14.6	0	1	0	1		
	3	16.0	0	0	0	0		
	4	18.0	0	0	0	0		
	5	42.5	0	0	0	0		
	6	20.0	0	0	0	0		
	Median	**18.2**	**0**	**0**	**0**	**0**		
Mid-Fat Control	1	11.5	0	0	0	0		
	2	23.6	2	2	1	5		Mixed large and small
	3	11.8	1	0	0	1	Zone 1	Predominantly large
	4	13.9	2	2	1	5	Zone 1	Mixed large and small
	5	8.0	0	1	0	1		
	6	14.4	2	1	0	3		Mixed large and small
	Median	**12.8**	**1.5**	**1**	**0**	**2**		
Low-Fat Control	1	52.3	3	2	2	7	Zone 1	Predominantly large
	2	42.1	3	1	1	5	Zone 1	Mixed large and small
	3	26.8	1	2	2	5		Mixed large and small
	4	40.2	3	2	1	6		Mixed large and small
	5	113.0	3	3	0	6		Predominantly large
	6	18.8	2	2	0	4	Zone 1	Predominantly large
	Median	**41.2**	**3**	**2**	**1**	**5.5**		
Low-Fat Ethanol	1	23.0	1	3	0	4	Zone 1	Mixed large and small
	2	96.8	3	3	0	6		Predominantly large
	3	45.0	2	2	0	4	Zone 1	Mixed large and small
	4	64.2	2	1	1	4	Zone 1	Predominantly large
	5	7.6	1	1	0	2	Zone 1	Predominantly large
	Median	**45.0**	**2**	**2**	**0**	**4**		

Table 4-2. Histological scores for hematoxylin and eosin stained sections, 8 weeks. NAS = NAFLD Activity Score.

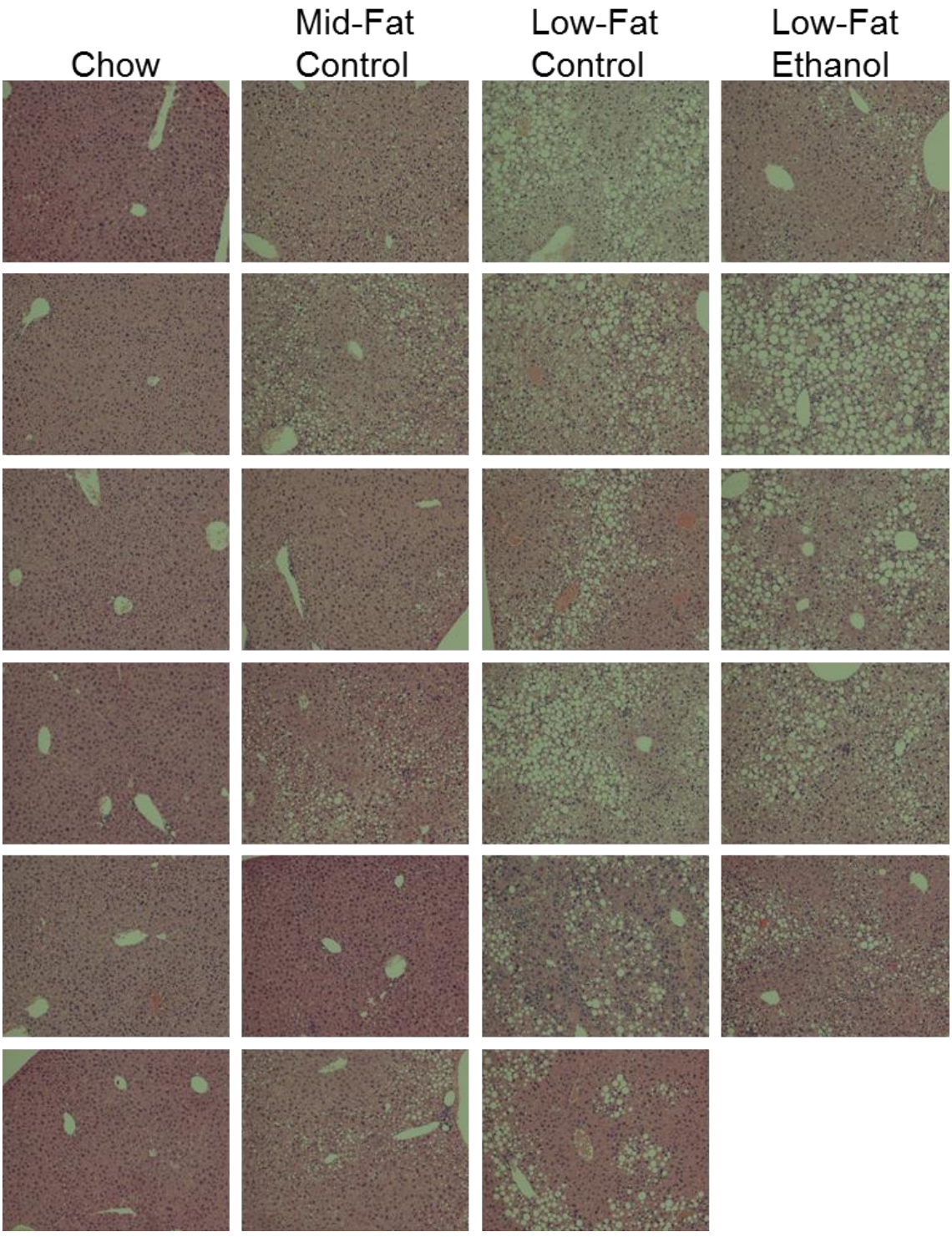

Figure 4-5. Hematoxylin and eosin-stained liver sections, 8 weeks. Mice were fed standard chow or the mid-fat control, low-fat control, or low-fat ethanol Lieber-DeCarli diets. Data from one experiment. Each image represents one mouse (n = 6, all groups except n = 5 for low-fat ethanol). Histology shown for 8 week collection. Sections were stained with hematoxylin and eosin. Magnification, 100X.

Mid-fat and low-fat diets caused up-regulation of inflammatory genes in hepatocytes

In NAFLD and ALD, KCs and hepatic stellate cells (HSCs) are the main mediators of inflammation and fibrosis. KCs produce TNF-α, IL-1β, and IL-6 as well a matrix metalloproteinases (MMPs) that degrade extracellular matrix components, while HSCs produce collagens and tissue inhibitors of metalloproteinases (TIMPs), the latter of which inhibit MMPs [144, 145]. We next asked if we saw the same activation of KCs and HSCs in our model of diet- and ethanol-induced damage. We selected a panel of genes covering antigen presentation, the inflammasome, recruitment of myeloid cells, general inflammation, oxidative stress, and fibrosis to measure by qRT-PCR. Due to many non-detect values that made the data difficult to analyze, the data from HSCs was excluded; however, we were able to compare the gene expression between total liver, hepatocytes, LSECs, and KCs.

To understand global gene expression profiles, we compared the median gene expression levels of the mid-fat and low-fat groups against the chow group. When compared to the chow group, *Ccl2*, *Ccl7*, *Lcn2*, *Nos2*, *Mmp12*, and *Timp1* in total liver from mice fed the mid-fat and low-fat diets were up-regulated (Figure 4-6). The low-fat control group also up-regulated additional genes for myeloid cell recruitment and fibrosis (Figure 4-6). The majority of gene regulation in mice fed the mid-fat and low-fat control diets occurred in hepatocytes rather than in either LSECs or KCs (Figure 4-6). In general, this up-regulation was modest (mostly 2-5 fold), however, a select number of genes (*Cd80*, *Ccl2*, *Ccl5*, *Vcam1*, *Tlr9*, and *Mmp12*) were induced to higher levels, particularly in the low-fat control group (Figure 4-6).

To better understand the global fold-change patterns seen in hepatocytes, we selected genes associated with myeloid cell recruitment, inflammation, and fibrosis to analyze for relative mRNA expression in chow, mid-fat control, and low-fat control groups. Many genes in the mid-fat and low-fat control groups trended towards up-

regulation, but few relationships were found to be significant. *Ccl2* was the only transcript significantly up-regulated by both the mid-fat and low-fat groups compared to the chow group (Figure 4-7). *Il1a*, *Il1b*, *Pdgfra*, and *Mmp9* were significantly up-regulated in the mid-fat control group compared to the chow group; while *Ccl5*, *Cxcl10*, *Vcam1*, *Mmp12*, and *Tgfb1* were significantly up-regulated in the low-fat control group compared to the chow group (Figure 4-7). No significant differences existed between the mid-fat and low-fat control groups (Figure 4-7). We conclude that the mid-fat and low-fat control diets induce expression of both inflammatory and fibrosis genes, potentially leading to the increased liver damage we observed.

Ethanol down-regulated chemokine and fibrosis gene expression in hepatocytes

To assess the effects of ethanol on global gene expression profiles, we compared median gene expression levels of the low-fat ethanol group against the low-fat control group. The low-fat ethanol group up-regulated expression of *Ccl2*, *Cxcl1*, *Il1b*, *Lcn2*, *Tlr7*, *Tnf*, *Nos2*, and *Mmp9* in total liver compared to the low-fat control group (Figure 4-8). Much of the regulation occurred in hepatocytes. Ethanol also induced down-regulation of genes in hepatocytes, predominantly antigen presentation and fibrosis genes, between 2-5 fold (Figure 4-8).

We were interested to follow-up on the global fold-change expression patterns of chemokines and fibrosis genes observed in hepatocytes. We evaluated the relative gene expression levels (Figure 4-9). While we observed overall trends of down-regulation in the low-fat ethanol group, only *Tgfb1* was significantly down-regulated compared to the low-fat control group (Figure 4-9C). The analysis of individual mice highlights the overlap seen between the two low-fat groups, as was evident in the histology, though suggests that ethanol exposure may be suppressing fibrosis genes.

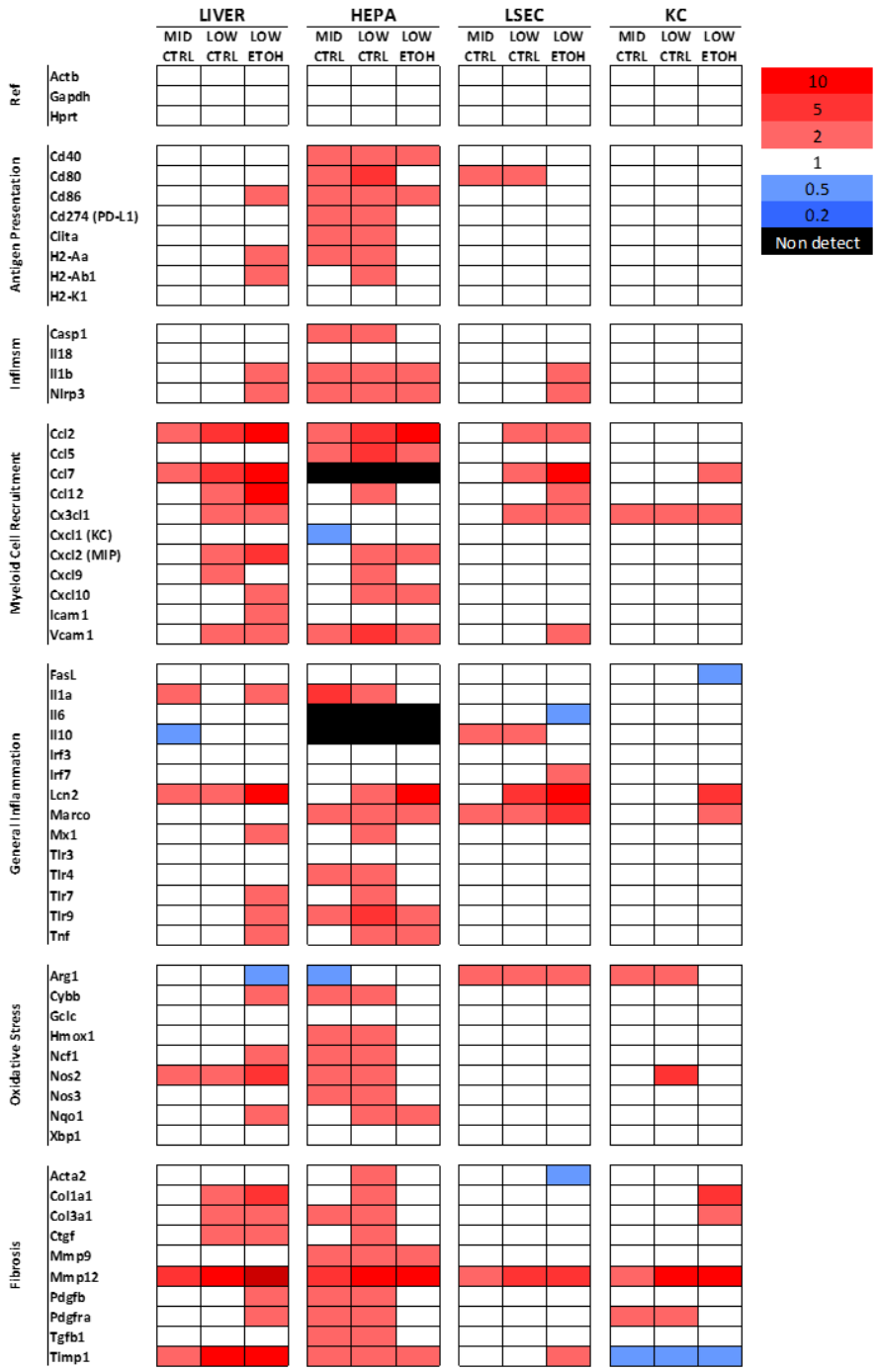

Figure 4-6. Mid-fat and low-fat Lieber-DeCarli control diets induce greater up-regulation of genes related to inflammation, oxidative stress, and fibrosis, predominantly in hepatocytes. Mice were fed standard chow or the mid-fat control, low-fat control, or low-fat ethanol Lieber-DeCarli diets. Data shown for 8 week collection. Fold change gene expression in total liver, hepatocytes, LSECs, and KCs of the median of the mid-fat control, low-fat control, and low-fat ethanol groups compared to the median of the chow group. *Hprt* used as the reference gene. Data from one experiment (n = 6, all groups except: n = 5, low-fat control for LSECs, low-fat ethanol for total liver, hepatocytes, LSECs, and KCs; n = 4 for low-fat control for KCs). Non-detects not

(Figure 4-6 legend, continued)
represented in this analysis. Fold change represented by blue to red scale, 1 = no change, red = induction, blue = reduction, and black = non-detect.

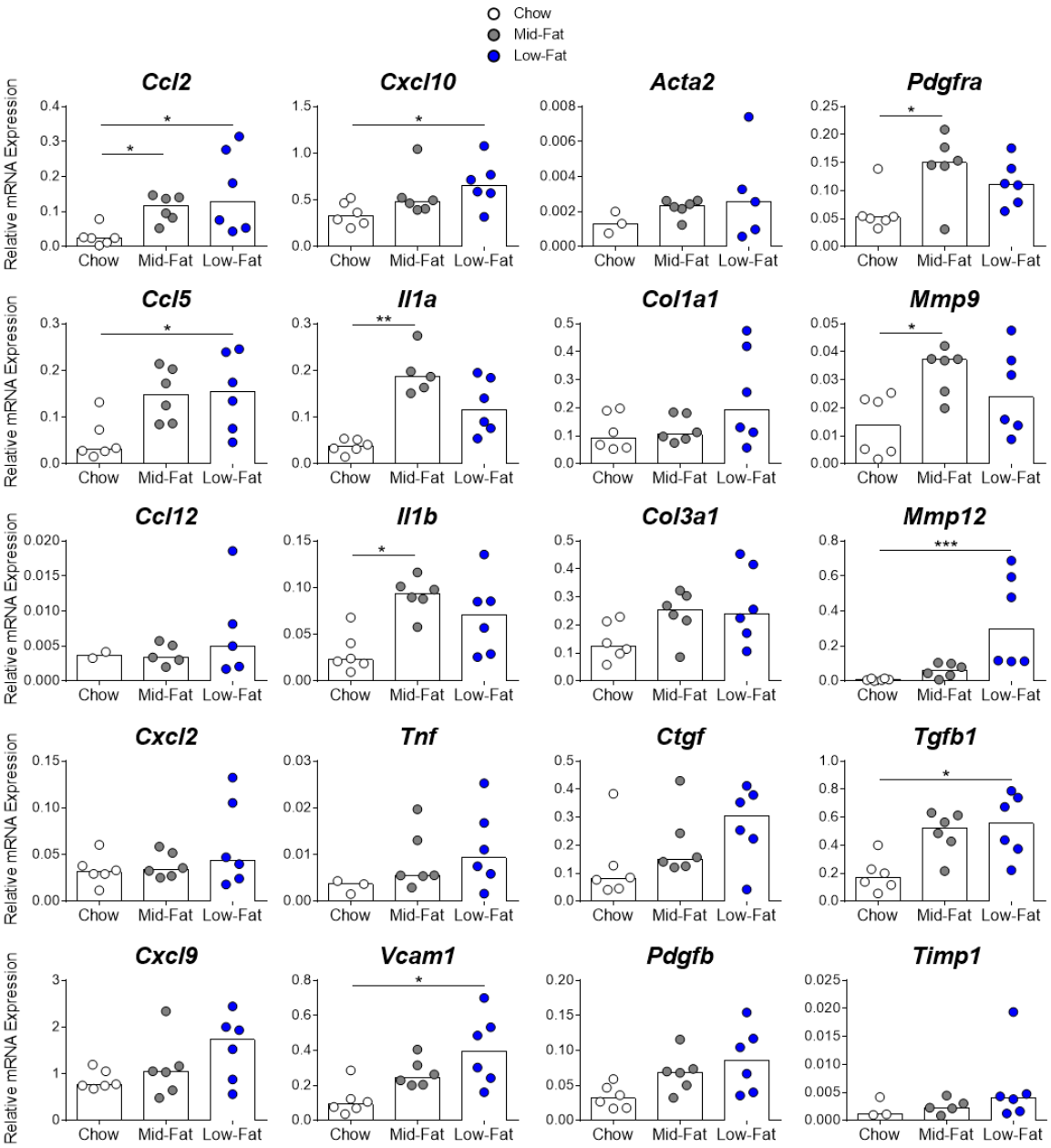

Figure 4-7. Mid-fat and low-fat Lieber-DeCarli diets cause up-regulation of inflammatory and fibrosis genes in hepatocytes. Mice were fed standard chow or the mid-fat control or low-fat control Lieber-DeCarli diets. Data shown for 8 week collection. mRNA expression in hepatocytes relative to *Hprt*. Data from one experiment (n = 6, all groups). Significance determined by a Kruskal-Wallis test followed by Dunn's post-test for each Lieber-DeCarli diet compared to the chow diet. *, P ≤ 0.05; **, P ≤ 0.01; non-significance represented by the absence of a bar.

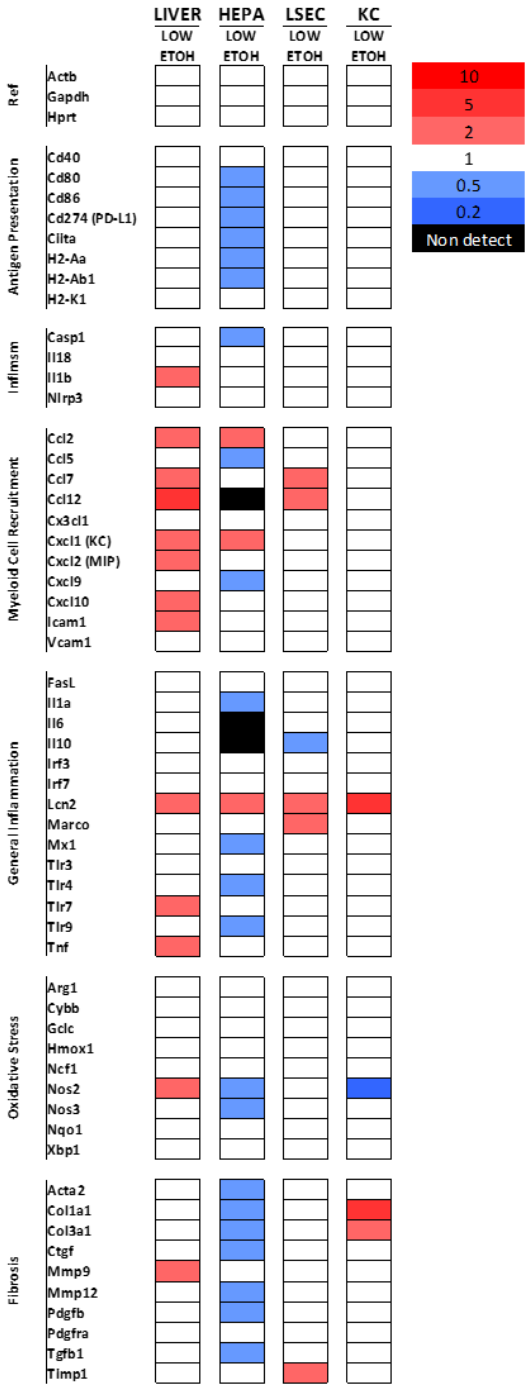

Figure 4-8. Ethanol suppresses gene expression in hepatocytes to a greater extent than in LSECs or KCs. Mice were fed low-fat control or low-fat ethanol Lieber-DeCarli diets. Data shown for 8 week collection. Fold change gene expression in total liver, hepatocytes, LSECs, and low-fat control group. *Hprt* used as the reference gene. Data from one experiment (n = 6, low-fat control for total liver, hepatocytes; n = 5, low-fat control LSECs, low-fat ethanol total liver, hepatocytes, LSECs, and KCs; n = 4, low-fat control KCs. Non-detects not represented in this analysis. Fold change represented by blue to red scale, 1 = no change, red = induction, blue = reduction, and black = non-detect.

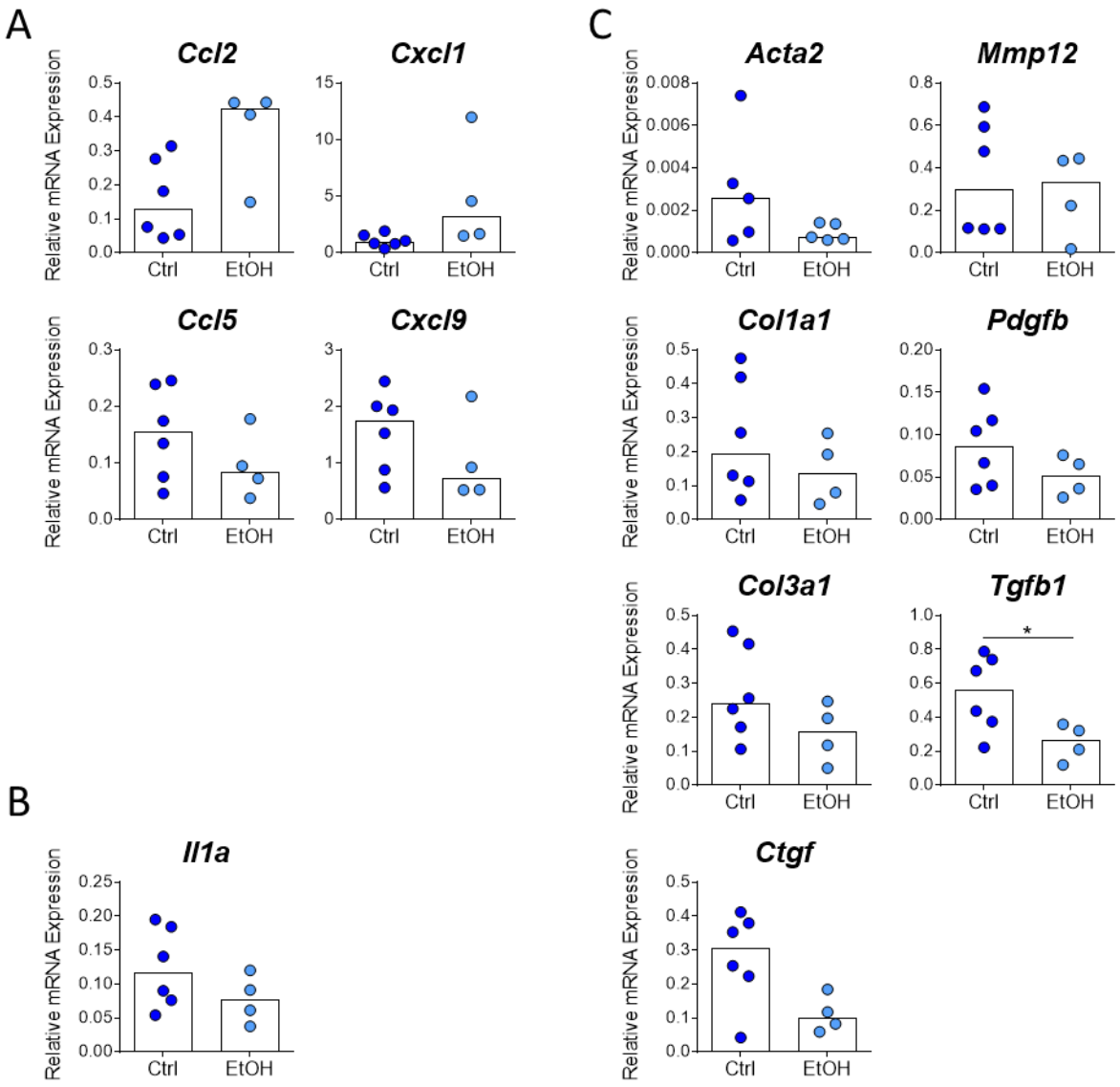

Figure 4-9. Ethanol suppresses *Tgfb1* expression in hepatocytes. Mice were fed low-fat control or low-fat ethanol Lieber-DeCarli diets. Data shown for 8 week collection. mRNA expression in hepatocytes relative to *Hprt*. Data from one experiment (n = 6, low-fat control; n = 4, low-fat ethanol). Significance determined by a pairwise Mann-Whitney test. *, P ≤ 0.05; non-significance represented by the absence of a bar.

Discussion

We set out to develop a mouse model of chronic ethanol exposure and discovered that Lieber-DeCarli control diets induced significant liver pathology themselves. Initial attempts to feed mice a chronic ethanol diet resulted in early mouse mortality. Three other studies have also reported mouse mortality with ethanol percentages over 29.2% of total calories and resolved the issue by gradually increasing the ethanol concentration in the diet as well as reducing the final ethanol percentage [146-148]. Reducing the percentage of ethanol from 6.7% v/v to 5.0% v/v (35.5% to 27.6% ethanol-derived calories) prevented mortality for the remainder of our studies.

Our studies found that hepatocytes, rather than either LSECs or KCs, were the most active cell population in the liver in regards to the regulation of a suite of inflammatory genes. While it is acknowledged that hepatocytes can produce TNF-α and IL-6 in response to injury [85, 116] and CCL2 and CXCL1 in response to alcohol-induced injury [92, 149, 150], relatively little else is known about the role hepatocytes play in the immune response to tissue injury. The responses of KCs and HSCs, on the other hand, have been well-characterized, particularly in ALD [151, 152]. HSCs are recognized as mediators of fibrosis through collagen deposition and production of TIMPs. Due to the presence of many non-detects in the gene expression data, we could not assess the role of HSCs in our model, but we observed that hepatocytes from mice in the mid-fat and low-fat control groups up-regulated expression of *Mmp9*, *Mmp12*, *Pdgfra*, and *Tgfb1*—genes linked to fibrosis. Ethanol had a suppressive effect on fibrosis genes overall and specifically caused the down-regulation of *Tgfb1*. This indicates that hepatocytes may play a more active role in the fibrotic response than previously recognized. Intriguingly, mice in the ethanol-fed group had increased numbers of neutrophils in the liver. This may indicate that ethanol is acting both to enhance inflammation through the recruitment of neutrophils but to suppress liver damage by suppressing the fibrotic response, as

supported by decreased *Tgfb1* expression in hepatocytes and the slightly reduced histological scores of mice fed the low-fat ethanol diet compared to the low-fat control diet. Preliminary histological data (not shown) indicated that fibrosis was not induced in mice fed any of the diets; however, the down-regulation of fibrosis-associated genes may indicate the mice were on the path to developing fibrosis.

Our preliminary studies indicated that the control Lieber-DeCarli diet induced greater liver damage than the ethanol diet. We hypothesized that the higher percentage of fat in the control diet was the driving factor behind the increased measures of liver injury. To test this, we evaluated the Lieber-DeCarli low-fat control diet against the mid-fat control diet. We found that the low-fat control diet induced more pathology than the mid-fat control diet. High-fat diets have been used in mice to induce hepatic steatosis with varying degrees of success. The original high-fat diet developed by Lieber et al., contained 71% calories from fat and induced steatosis in Sprague-Dawley rats after 3 weeks [153]. Interestingly, the “standard Lieber-DeCarli” diet used in their study (35% calories from fat) is the original version of our self-termed “mid-fat” control diet. As we observed, Lieber et al. also observed mild steatosis in the liver of rats fed the standard/mid-fat diet [153]. Unlike our observation that lower dietary fat correlated with increased liver damage, Lieber et al. observed significantly more steatosis and measures of NASH in the livers of mice fed the high-fat diet compared to the those fed the standard/mid-fat diet [153].

A possible explanation for this discrepancy could be due to the carbohydrate content of the low-fat and mid-fat control diets. In humans, excess carbohydrates can cause weight gain and hepatic steatosis in a relatively short time frame [127]. The composition of the diets (Table 4-1) shows that carbohydrates make up the calories not filled by fat, so that our diets could also aptly be named high-carbohydrate (low-fat) and mid-carbohydrate (mid-fat). The overall percentage of carbohydrates did not correlate

with the levels of damage we observed; however, analysis of the carbohydrate composition provided a compelling insight: increasing levels of monosaccharides, disaccharides, and polysaccharides correlated with increasing liver injury. The predominant simple sugar in the Lieber-DeCarli control diets is glucose: the monosaccharide category is composed of glucose, the disaccharide category is composed mainly of maltose, which in turn breaks down into two glucose molecules, and finally, the polysaccharide category is composed of long chain glucose polymers [personal correspondence with Jaime Lecker at Bio-Serv]. Thus, increasing pathology is associated with increasing amounts of glucose in the diets. Finally, we note that while the low-fat ethanol diet appears to have less monosaccharide and disaccharide than the mid-fat control and low-fat control groups, it is not directly comparable as an additional 20.3 gm/L of carbohydrate was provided as maltose dextrin, therefore affecting the true percentage of carbohydrate components.

Intriguingly, research suggests that while fructose can induce NAFLD/NASH, glucose does not. A study in C57BL/6J mice in which the effects of 30% glucose and 30% fructose in drinking water were assessed demonstrated that while the glucose-fed group gained weight, the fat localized to the abdomen and not the liver [137]. The fructose-fed group, however, developed hepatic steatosis and had increased expression of TNF-α [137]. Furthermore, fructose has been demonstrated to induce NAFLD/NASH through various mechanisms including its metabolism stimulating *de novo* lipogenesis and accumulation of intrahepatic lipid and production of reactive oxygen species (ROS) [127]. A direct comparison of the liquid low-fat control group used in our studies needs to be made with a comparable diet comprised mainly of fructose to explore the effects of glucose versus fructose; however, based on the results described here, we report a tractable model for the induction of fatty liver in mice through the excess intake of glucose. This model is appealing both as a counterpoint to traditional methods for

triggering metabolic disease and for informing our understanding of how excess glucose contributes to metabolic disorders.

CHAPTER 5: CONCLUSIONS AND FUTURE DIRECTIONS

Overview

The studies described in this dissertation used two models of non-infectious liver injury, one acute and one chronic, to elucidate pathways involved in the innate immune response to non-infectious liver injury, and more specifically to hepatocyte death. Chapter 3 described the development of a model of acute sterile inflammation induced by selective killing of hepatocytes. We found that the adaptor Toll/IL-1 receptor domain-containing adapter protein inducing IFN-β (TRIF) was a central mediator in the inflammatory response initiated against dying hepatocytes. Furthermore, we found that much of the inflammatory response, composed largely of the up-regulation of recruitment factors for, and the recruitment of, monocytes and neutrophils, was directed by hepatocytes themselves. To understand the role of hepatocyte death in a chronic setting, Chapter 4 detailed the use of a model of diet- and alcohol-induced liver injury to examine how dietary fat and carbohydrate content, with or without chronic alcohol exposure, provoke innate immune responses in the liver. We found that increasing liver injury correlated with increasing carbohydrate in the diet. Furthermore, as with the acute model of liver damage, we found that hepatocytes were the cell-type most active in responding both to diet-induced inflammation and the additional insult of ethanol, through the up-regulation of myeloid cell-recruiting chemokines (diet and ethanol) and the down-regulation of genes involved in fibrosis (ethanol). These studies broadly advance our understanding of how innate inflammatory pathways in the liver identify and respond to hepatocyte death, and particularly highlight the central role of hepatocytes in promoting inflammatory responses to non-infectious liver injury.

Discussion

Despite improvements in transplant technology, new vaccines and therapeutics for infections, and increased awareness through public health programs aimed to reduce drug and alcohol use, liver disease remains a global burden. The previously-undervalued role of hepatocytes in liver disease is two-pronged. Specifically, injury and death of hepatocytes is the defining feature of many liver diseases, and is the central reason for the resulting pathology; however, hepatocytes are also potent responders to cell death themselves and actively contribute to inflammation through the production of inflammatory mediators tuned to the nature of the insult. As discussed in Chapter 3, in the context of non-infectious injury the active role of hepatocytes in the recognition of tissue damage and the initiation of a response is an understudied area.

The role of hepatocytes as initiators of an immune response has been described in cases of pathogen infection. While there is not an expansive amount of literature on how the response of hepatocytes to infection shapes the overall immune response, it provides some insight into the type of signaling that can occur within hepatocytes following insult. For example, in hepatitis C virus (HCV) infection, both the Toll-like receptor (TLR) and RIG-I-like receptor (RLR) pathways are involved in the recognition of HCV within infected hepatocytes. Viral RNA is recognized by TLR3 within endosomes and by RIG-I and MDA-5 in the cytoplasm and both signaling pathways synergize to promote type I interferon (IFN) production [154, 155]. Interferon regulatory factor (IRF)3 is a critical downstream component in both of these pathways, with TLR3 signaling via TRIF and RIG-I signaling via MAVS (also known as IPS-1 and CARDIF) to activate IRF3, which then induces type I IFN [154, 155].

The role of hepatocytes as active responders and initiators of an immune response in the case of non-infectious injury is only just gaining traction. As such, the current dogma broadly relegates hepatocytes to “the producers of DAMPs” rather than

the producers of a productive inflammatory response, a role attributed mainly to Kupffer cells [151, 156, 157]. Our studies show that hepatocytes contribute significantly to the inflammatory response to tissue injury. In response to liver injury induced by our acute and chronic models, we observed hepatocyte up-regulation of multiple chemokines, cell adhesion molecules, and other inflammatory cytokines. One additional study corroborates this phenomenon that we have described [124]. Following *in vitro* stimulation by bile acids, a type of injury hypothesized to be involved in obstructive liver cholestasis, mouse primary hepatocytes up-regulated expression of a number of inflammatory genes including *Ccl2*, *Ccl3*, *Ccl5*, *Ccl7*, *Ccl20*, *Cxcl1*, *Cxcl2*, *Cxcl10*, *Icam1*, *Vcam1*, *Il1b*, and *Il10* [124]. It is intriguing to note the shared response between this model and our acute and chronic (diet- and alcohol-induced) models of liver injury. The induction of *Ccl2*, *Ccl5*, *Cxcl10*, and *Vcam1* in hepatocytes is conserved across all three models. There is additional overlap between subsets of the models, including *Ccl7*, *Cxcl1*, *Cxcl2*, and *Icam1* between the bile acids model and our acute model, and the induction of *Il1b* in the bile acids model and our diet- and alcohol-induced models of chronic injury. The synthesis of these models suggests that hepatocytes produce a conserved set of genes in response to a variety of stresses, and that rather than passive victims of pathogen-mediated and non-infectious injury these cells should be considered as first-responding mediators of the corresponding immune response.

This view of hepatocytes as responders to tissue injury, and particularly to hepatocyte injury, beg the questions: what are they responding to and by what mechanism? Hepatocyte death is documented to release many DAMPs that trigger immune responses driven by TLR-signaling in Kupffer cells (KCs) and hepatic stellate cells (HSCs) [156, 158]. High mobility group box 1 (HMGB1), cellular DNA, and ATP are examples of DAMPs that have been identified in various modes of liver injury [27]. Our observation that inflammation following diphtheria toxin (DT)-induced hepatocyte death

is driven by the TRIF adaptor protein suggests that one of two upstream TLRs, TLR3 or TLR4, are involved in the recognition of DAMPs and the initiation of the immune signaling cascade. Our studies ruled out TLR4 as the putative sensor; however, our results were inconclusive on the role of TLR3 due to significantly lower expression of hDTR transcript and protein in $TLR3^{-/-}$ mice. TLR3 has been found to contribute to inflammation in models of liver and intestinal inflammation [112, 113, 159, 160]. If TLR3 is in fact the pattern recognition receptor that is sensing hepatocyte injury, the likely DAMP is RNA released by the dying cells. An alternative explanation to our TLR4-independent, TRIF-driven response is the existence of a yet-undescribed receptor that also signals through TRIF. This has been proposed by Jeyaseelan et al. as a potential explanation for the TRIF-dependent, TLR3-independent, and *partially* TLR4-dependent, neutrophil-recruitment observed in the lung in during pneumonia induced by *Escherichia coli* [161]. If an unknown, alternate receptor is in fact signaling through TRIF, the DAMP that binds that receptor is also unknown. Lastly, we observed that myeloid differentiation primary response protein 88 (MyD88)-deficient mice were only partially protected from inflammation following hepatocyte death, suggesting that DAMP recognition and signaling could be occurring through a TLR4-independent but MyD88-dependent route. Studies in acetaminophen- and IR-induced liver injury suggest that HMGB1 and DNA can signal via TLR4 and TLR9 receptors to initiate a response. It is possible, then, that hepatocytes are responding to DNA in a TLR9-dependent manner. Additional studies in TLR9-deficient mice would be the first step to follow-up on this route of investigation.

Diet- and alcohol-induced chronic liver injury also results in the release of DAMPs from hepatocytes. In addition, another potential DAMP in these diseases is the free fatty acids (FFAs) produced in excess during metabolic dysregulation. FFAs have been suggested as a potential DAMP for TLR4 in adipocytes and macrophages, with many studies exhibiting FFA-induced signaling through TLR4 [162-165]. In contrast, two

studies posited that FFAs did not directly stimulate TLR4 [166, 167]. FFAs, however, have been reported to stimulate the release of HMGB1 from hepatocytes and then to induce production of IL-6 and TNF-α by these cells [85]. An additional source of inflammation in alcohol-induced liver injury is bacterial-derived endotoxin, a PAMP that induces inflammation through TLR4 signaling in alcoholic liver disease (ALD). The role that LPS may play in non-alcoholic fatty liver disease (NAFLD), however, is less clear. Intestinal bacteria have been suggested to contribute to inflammation in NAFLD by increasing production of ethanol and by LPS-driven production of cytokines [35]. A study using a fructose-induced model of NAFLD found that TLR4-mutant mice had reduced steatosis and markers of inflammation compared to wild type mice, though they had equivalent levels of portal endotoxin, suggesting a role for LPS activation of TLR4 in driving NAFLD pathology [133]. In contrast, epidemiological data show that endotoxin levels are elevated in patients with NAFLD; however, a recent study found that the elevated levels were not associated with fibrosis or non-alcoholic steatohepatitis (NASH) [168, 169]. It remains to be determined for our model of diet (glucose)-induced liver injury if endotoxin from the gut microbiota plays a role in the pathology of the disease. Use of this model in TLR4-deficient mice would help elucidate this outstanding question, both for glucose-induced liver injury and for diet-induced liver injury in general.

In our model of diet-induced liver injury, we found that increasing amounts of carbohydrate, and particularly glucose, was associated with increased amounts of steatosis, alanine aminotransferase (ALT), aspartate aminotransferase (AST), and the up-regulation of inflammatory genes. Intriguingly, the literature indicates that mice fed glucose develop only limited steatosis, with fructose determined to be the sugar molecule more important for the induction of fatty liver [137, 170]. Therefore, we may be inducing hepatic steatosis and liver inflammation through a previously undefined mechanism of chronic exposure to high levels of glucose. While we have no direct

evidence for the involvement of particular DAMPs in our model, clues from the gene expression in the mid-fat control, low-fat control, and low-fat ethanol group mice compared to the chow diet may provide a starting point to help determine the direction of future studies. We see induction of *Tnf* in the low-fat (high-carbohydrate) control and ethanol groups. This could be indicative of signaling through TLR4 as TNF-α is generally produced downstream of TLR4 activation in KCs in models of ALD/alcoholic steatohepatitis (ASH). We also see variable induction of *Tlr4*, *Tlr7*, and *Tlr9* across all the diet groups, potentially indicating activation of those TLRs. Interestingly, *Tlr4* is only up-regulated in the mid-fat and low-fat control groups and while *Tlr7* and *Tlr9* are up-regulated in all three groups, *Tlr7* is additionally up-regulated in the low-fat ethanol group, potentially suggesting a role for TLR7 signaling in the innate response to the effects of ethanol.

Finally, a related question is where does the hepatocyte come in contact with the inflammation-inducing DAMP? Our acute model of liver injury sheds some light on this question. Twenty-four hours following DT-induced death of hepatocyte, we observed the accumulation of round vacuoles of mCherry within the cytoplasm of hepatocytes. This likely indicates phagocytosis by live hepatocytes of dying hepatocytes and aligns well with the hepatocyte-dominated production of chemokines and adhesion molecules we observe following DT-induced hepatocyte death. This possibility is supported by studies demonstrating that healthy hepatocytes can phagocytose apoptotic hepatocytes via the asialoglycoprotein receptor (ASGPR) [171, 172]. Therefore, we speculate that the tissue-derived DAMP is signaling from within an endosomal compartment in the hepatocyte. Of the TLRs that signal from endosomal compartments—TLR3, TLR4, TLR7, TLR8, and TLR9—TLR3 aligns best with our TLR4-independent, TRIF-dependent inflammation; however, signaling via TLR7, TLR8, or TLR9 could account for the partial role we observed for MyD88 in the propagation of inflammation following hepatocyte death.

Interestingly, and in support of a model where the hepatocyte is a consistent early mediator of immune activation, in our studies of diet- and alcohol-induced liver injury, we saw the up-regulation of *Tlr4*, *Tlr7*, and *Tlr9* transcripts, but not of *Tlr3*, *Irf3*, or *Irf7* potentially indicating a role for sensing by TLR4, TLR7, or TLR9 within endosomes as well, though TLR4 also signals from the cell membrane.

We speculate that dying hepatocytes are phagocytosed by neighboring hepatocytes and that the DAMPs released by dying hepatocytes bind to intracellular PRRs. In turn, this initiates signaling through the TRIF pathway and induces production of inflammatory mediators and recruitment of myeloid cells. In our acute model of injury, resolution of inflammation is apparent by the appearance of mitotic hepatocytes at 48 hours and increased numbers at 72 hours, indicating a tissue-repair response. The transition from an early Ly6C(+) monocyte population to the later Ly6C(-) monocyte population suggests that the monocytes may participate in tissue repair, as has been extensively reviewed [17]. The importance of a tissue repair response driven by TRIF has implications for pathogen infection. Both TLR3 and TLR4, involved in the recognition of viruses and bacteria, respectively signal through TRIF to drive an immune response. If the response and ultimately, resolution, to hepatocyte death is also signaled through TRIF, one can imagine the potentially multiplying effects of hepatocyte death and pathogen signaling through the same pathways. For example, the NS3/4A protein produced by HCV inhibits type I IFN production by cleavage of both TRIF and MAVS [154]. If TRIF signaling is inhibited and hepatocytes die, monocytes involved in resolving inflammation may not be recruited. This could result in the perpetual cycles of inflammation and cell death seen in chronic viral hepatitis infections which can ultimately lead to fibrosis, cirrhosis, and hepatocellular carcinoma.

Conclusion

Acute and chronic liver diseases are global concerns that continue to grow. It is imperative that we gain a more complete understanding of the innate mechanisms and immune pathways involved in liver injury. The studies detailed in this dissertation advance our understanding of the inflammation that occurs following hepatocyte death and identify hepatocytes as key players in the response. These studies inform future research into areas of possible hepatocyte-targeted interventions or therapies for acute and chronic liver disease.

Acknowledgements

We thank the University of Washington's Department of Comparative Medicine and the Vivarium staff for excellent animal husbandry. For the gifts of gene-targeted mice, we thank Dr. Michael Gale, Jr., Dr. Alan Aderem, Dr. Andrew Oberst, and Dr. David Sherman. We also thank Dr. Keith Elkon for experimental materials; the University of Washington Histology and Imaging Core for preparation of histology samples; the Loeb, Rabinovitch, and Beavo labs for the use of equipment; and the University of Washington Pathology Flow Core, and particularly Donna Prunkard, for assistance on the Aria machines. We thank Dr. Kyle Minch for sharing his extensive expertise in microscopy and image analysis. Lastly, we thank Dr. Matthew Yeh for the scoring of histology slides and for sharing his expertise in diet- and alcohol-induced liver injury.

Special thanks are extended to Drs. Nick Crispe, Isaac Mohar, Sara Murray, Jessica B. Roberto, and Kyle Minch for all of their personal and professional support throughout the course of my graduate studies. The depth of my gratitude is unmeasurable. Thank you.

APPENDIX: ISOLATION OF NON-PARENCHYMAL CELLS FROM THE MOUSE LIVER

The Appendix presents the protocol for mouse liver perfusion, isolation of non-parenchymal cells, and assessment of cell purity. The in-text citations, references, figure and table numbers, and section headings have been updated to fit into this dissertation, but otherwise the following text and figures have not been modified from a chapter appearing in **Malaria Vaccines** [Malaria Vaccines: Methods and Protocols, Methods in Molecular Biology, Isolation of Non-parenchymal Cells from the Mouse Liver, vol. 1325, 2015, pp 3-17, Mohar, I., Brempelis K.J., Murray, S.A, Ebrahimkhani, M.R., and Crispe, I.N., (© Springer Science+Business Media New York 2015)], reprinted with permission of Springer. (DOI: 10.1007/978-1-4939-2815-6_1)

Summary

Hepatocytes comprise the majority of liver mass and cell number. However, in order to understand liver biology, the non-parenchymal cells (NPCs) must be considered. Herein, a relatively rapid and efficient method for isolating liver NPCs from a mouse is described. Using this method, liver sinusoidal endothelial cells, Kupffer cells, natural killer (NK) and NK-T cells, dendritic cells, CD4+ and CD8+ T cells, and quiescent hepatic stellate cells can be purified. This protocol permits the collection of peripheral blood, intact liver tissue, and hepatocytes, in addition to NPCs. *In situ* perfusion via the portal vein leads to efficient liver digestion. NPCs are enriched from the resulting single-cell suspension by differential and gradient centrifugation. The NPCs can by analyzed or sorted into highly-enriched populations using flow cytometry. The isolated cells are suitable for flow cytometry, protein, and mRNA analyses as well as primary culture.

Key words: liver, perfusion, cell isolation, sinusoidal endothelial cells, Kupffer cells, hepatic stellate cells

Introduction

The principle cell types in a healthy liver are hepatocytes, liver sinusoidal endothelial cells (LSEC), Kupffer cells, and hepatic stellate cells (HSC) [173-175]. Fewer in number are bile duct cells, venous and arterial endothelial cell, hepatic progenitor cells, and dendritic cells. Furthermore, the number and proportion of leukocytes can increase tremendously in an infected or damaged liver [176, 177]. As a result, granulocytes, monocytes, natural killer (NK) and NK-T cells, dendritic cells, CD4+ and CD8+ lymphocytes, and B cells are important determinants of the liver biology. Thus, the dissected dynamics of each cell type can provide powerful information to understand the pathology and immunology of the tissue. This information, in combination with serological, histological and tissue-level observations, allows for a comprehensive assessment of each experimental mouse, thus reducing the number of experimental mice while increasing the likelihood of discovery.

The purpose of this protocol is to provide a detailed description of materials and methods by which liver cell populations can be isolated from the mouse liver and studied, while also permitting the collection of blood and intact liver tissue. The liver dissociation protocol is derived from the method published by Seglen [178] for isolating rat liver cells. Dr. Seglen provides an extensive description of the theory behind rat liver dissociation that extends to the mouse. We have evolved the method of Seglen to allow rapid, yet effective, isolation of mouse liver cells, permitting the dissociation of up to five livers per hour by two skilled technicians--one conducting perfusions and dissections, the other processing cell suspensions.

The basic protocol relies upon *in situ* perfusion of the liver via the portal vein. Peripheral blood and cells are flushed from the liver in a Ca^{2+}-free buffer, prior to perfusion with the collagenase digestion solution. Following liver digestion, the liver is removed and mechanically dissociated. Hepatocytes are separated by low-speed centrifugation, and then non-parenchymal cells (NPCs) are enriched by gradient separation. The enriched NPCs allow for relatively efficient cell type-specific analysis and/or further purification by flow cytometry [179]. For purification, magnetic bead-based methods can be applied and in certain circumstances are preferred [180], however, cell sorting allows for multi-way separation from each preparation.

Although liver NPCs are the focus of this protocol, hepatocytes are readily purified and cultured with good success. In addition, it is not yet clear if this protocol is able to isolate the population of sessile Kupffer cells, which are radio-resistant and appear somewhat distinct in function from their non-sessile counterparts [174]. This caveat in mind, this protocol establishes a reproducible method to isolate and enable the study of many cell types from the mouse liver. Indeed, a parallel understanding of cell-specific responses associated with tissue immune and pathological responses offers promise of new insights into treatment and prevention of infection and disease.

Materials

All solutions and consumables should be purchased as ‘tissue culture tested’ from a trusted commercial source in order to assure minimal contamination with endotoxin and sterility. All surgical instruments should be thoroughly washed, rinsed and autoclaved for sterility, especially if primary culture is the end goal. As with any protocol involving animals, institutional guidelines for handling, anesthesia and waste disposal should be followed.

2.1. Anesthesia

1. Anesthesia approved for terminal procedures such as Avertin; 1.25% (w/v) 2,2,2-tribromomethanol, 2.5% (v/v) 2-methyl-2-butanol, sterile water. Filter sterilize then store at 4°C protected from light (see Note 1).
2. 28G ½ inch needle, suitable for intraperitoneal injections
3. 1-cc syringe

2.2. Perfusion / Liver Dissociation Hardware Components

1. Peristaltic pump; such as Gilson Minipuls3 with medium flow-rate pump head
2. Pump tubing and connectors; such as F1825113 and F1179951
3. Tubing extension with slip-tip end; such as Hospira 1265528
4. Catheter; 24G, IV, such as BD 381412 (see Note 2)
5. Scissors, straight fine-tipped dissection
6. Forceps, 2 blunt tip
7. 50-ml conical tubes
8. 15-ml conical tubes
9. 5-cm sterile petri dish (optional)
10. 10-cm sterile petri dish
11. Stainless steel mesh ‘tea strainer’
12. 10-cc syringe
13. 100-μm filter
14. 70-μm filter (optional)
15. Gauze pads, large-size
16. Surgical tape, such as 3M transpore
17. Disposable absorbent underpads
18. 37°C water bath with 50-ml conical rack

2.3. Perfusion / Liver Dissociation Solution Components

1. Hank's Balance Salt Solution (HBSS); no Ca^{2+}, no Mg^{2+}, no phenol red
2. HBSS with phenol red
3. Phosphate buffered saline (PBS), pH 7.4
4. Distilled water, TC-grade
5. PBS, 10X
6. HEPES; 1M (Stock)
7. EDTA; 0.5M (Stock)
8. $CaCl_2$; 0.5M (Stock)
9. Fetal bovine serum (FBS)
10. Collagenase; *Clostridium histolyticum*, Sigma-Aldrich C5138 (see Note 3)
11. Optiprep; 60% iodixanol solution in water
12. Tissue fixative; 4% formaldehyde in PBS
13. 70% ethanol

These solutions can be prepared in advance and stored at 4°C.

1. Perfusion Buffer, 5 – 10 ml per mouse; HBSS, 5 mM HEPES, 0.5 mM EDTA
2. Wash Buffer, 50 ml per mouse; PBS, 4% FBS, 0.5 mM EDTA
3. PBS Flow Buffer (PFB), 20 ml per mouse; PBS, 1 mM EDTA, 2% FBS

These solutions should be prepared on the day of isolation.

1. Collagenase solution, 5 – 10 ml per mouse; HBSS (w/ phenol red), 5 mM HEPES, 0.5 mM $CaCl_2$, 0.5 mg/mL collagenase
2. 40% iodixanol in PBS, 2.5 mL per mouse; 1.67 mL Optiprep + 0.25 mL 10X PBS + 0.58 mL TC-grade water

2.4. Cell Analysis and Purification Components

1. Flow cytometer; such as BD Biosciences, LSRII or Aria
2. Flow cytometry tubes (see Note 4)
3. Antibodies for sorting cell type and/or analysis (Table 1) (see Note 5)

Methods

3.1. Prepare for perfusion(s)

1. Warm perfusion and collagenase solutions to 37°C for approximately 15 min prior to beginning the perfusion.
2. Prepare tubing for perfusion (see Note 6).
3. Prepare perfusion area with absorbent pad, dissection tools, gauze, 10-cm petri dish, tea strainer, and 10-cc syringe (Figure 1).
4. Fill perfusion line with perfusion solution.

3.2. Anesthetize mouse

1. Inject mouse with appropriate amount of anesthesia.
2. Once adequate level anesthesia is obtained, proceed to section 3.3 (see Note 7).

3.3. Surgical preparation

1. Place mouse belly-up on large gauze pad.
2. Secure mouse by footpads using surgical tape in an X orientation (Figure 2A).
3. Disinfect and wet mouse fur using 70% ethanol. Wipe off excess.
4. Open skin to expose the peritoneal membrane (Figure 2B).
5. Open peritoneal membrane (Figure 2C), gently move intestines and stomach to the right and very gently ‘stick’ the liver to the diaphragm. This should expose the portal vein and descending vena cava (see Note 8) (Figure 2D).
6. Use sharp scissors to nick the portal vein; blood will flow (see Note 9).

3.4. Blood and tissue collection (optional)

1. Collect 0.2 – 0.5 ml of blood as it pools near the portal vein. Transfer to proper collection tube.
2. Locate and remove ~ 2/3 of the right posterior liver lobe (Figure 2D, 2E). Transfer to 4% formaldehyde for fixation or further divide for other assessments.

3.5. *In situ* liver dissociation

1. Turn on pump to flow of ~ 2 ml/min.
2. Drip perfusion buffer onto the cut portal vein.
3. Use gauze sponge to draw perfusion solution to the left.
4. Identify the opening in the vein (see Note 10).
5. Gently catheterize the vein; the liver should blanch (see Note 11) (Figure 2F).
6. Cut the descending vena cava; blood and buffer should visibly flow from the vena cava.
7. Relax your hand (see Note 12).
8. Perfuse liver with 5 – 10 ml of perfusion buffer. Most perfusion tubing set-ups hold about 5 ml of solution, thus once the descending vena cava is cut, proceed to step 9.
9. Stop pump.
10. Switch line to collagenase, using the left hand.
11. Resume pump flow (see Note 13).
12. Swell the liver using forceps to occlude buffer flow from the vena cava, every 45 – 60 sec for 5 – 10 sec. If part of the right posterior lobe was removed, use the forceps to occlude flow into this lobe (see Note 14).
13. Perfuse liver with 5 – 10 ml of collagenase buffer. After 3-4 minutes, the liver should soften and the left lobe will begin to fall over the portal vein. When this happens, use forceps to lift up the lobe to periodically check that the catheter is

properly positioned. After 5 minutes, the internal structure of the liver cracks. This indicates a good digestion, and is most evident in the right anterior lobe.

14. Stop the pump.
15. Remove catheter from vein.
16. Reverse pump to return unused collagenase solution to the 50-ml conical tube.
17. Switch line back to perfusion solution and refill the line in preparation for the next mouse.

3.6. Single cell suspension

1. Using wide-tipped forceps, grasp the liver just to the left of the gall bladder along the falciform ligament (Figure 2G).
2. Use scissors to separate the liver from the diaphragm and all other points of connection. Care should be taken to avoid cutting the gastrointestinal tract.
3. Transfer the digested liver into the tea strainer within a 10-cm petri dish.
4. Remove the gall bladder (see Note 15).
5. Add 30 mL of cold wash buffer to the dish.
6. Use the rubber plunger of 10-cc syringe to gently massage the liver through the tea strainer, shake the strainer to disperse the cells. The liver should easily disperse with only the capsule and ligament remaining in the strainer.
7. Use 10-cc syringe (or 10-ml pipet) to gently disperse any clumps.
8. Filter (100 μm) the cell suspension into a 50-mL conical tube.
9. Store on ice or at 4°C for no longer than 15 minutes before proceeding to section 3.8.

3.7. Isolate splenocytes (optional, see Note 16).

1. Locate and remove spleen.
2. Place spleen into 5-ml petri dish filled with 10 ml of PFB.
3. Place the spleen on the rough surface of a glass slide.

4. Use the rough surface of a second glass slide to dissociate the spleen by gentle pressure applied in a circular motion. Continue this gentle mashing until the tissue is clearly dispersed.
5. Scrape the cells into the buffer using the edge of the slide.
6. Disperse the cells by pipetting.
7. Filter (70 μm) into 50-ml conical tube.
8. Store on ice until the NPC isolation reaches step 3.10.7, then process as NPC.

3.8. Crude Liver Cell Fractionation

1. Centrifuge the cell suspension at 50 x g for 3 min at room temperature. At this speed and duration, hepatocytes and debris will pellet while most NPCs will remain in suspension.
2. Transfer the supernatant, which contains the hepatocyte-depleted NPCs, to a new 50-ml conical tube.

3.9. Hepatocyte enrichment (optional)

1. Wash the hepatocyte pellet in 40 mL of wash buffer.
2. Pellet at 50 x g for 3 minutes.
3. Resuspend in 10 mL of media.
4. The resulting hepatocytes can be further enriched by magnetic bead depletion of contaminating cells and/or plated on collagen-coated tissue culture dishes. For the mouse, anti-CD45 and anti-CD146 microbeads will deplete most immune cells and endothelial cells, respectively.

3.10. Non-parenchymal cell enrichment

1. Pellet the NPC suspension at 500 x g for 5-7 minutes at 4°C.
2. Gently resuspend in 2.5 ml of PFB.
3. Mix cell suspension with 2.5 ml of 30 - 40% iodixanol solution in 15-ml conical. A final concentration of 20% iodixanol will enrich for most if not all intact NPCs.

4. Gently overlay with 2 ml of PFB.
5. Centrifuge at 1500 x g for 25 minutes at room temperature. If available, turn the brake OFF on the centrifuge to minimize disturbance to the cell interface.
6. During the centrifugation add 10 ml of cold PFB to a 15 ml conical tube.
7. After centrifugation a well-defined interface of cells should be visible. Carefully transfer this cell layer from the iodixanol gradient to the 10 ml of PFB in order to wash away excess iodixanol.
8. Centrifuge at 500 x g for 5 min at 4°C.
9. Resuspend the enriched NPC pellet in 0.5 ml of cold PFB or appropriate buffer for desired applications.

3.11. Staining NPCs for flow cytometry

1. Prepare the necessary number of flow cytometry tubes.
2. Add anti-CD16/anti-CD36 (Fc receptor blocking) antibody to each sample to a final concentration of 1:250 (see Note 17).
3. Incubate for 5 min at room temperature.
4. Add antibody cocktail (see Table 1).
5. Vortex briefly and gently.
6. Incubate for 20 min at 4°C.
7. Wash the cells by adding 1 ml of PFB to each sample.
8. Centrifuge at 500 x g for 5 min at 4°C.
9. Aspirate supernatant.
10. Resuspend cell pellet in 0.5 ml of PFB.
11. In order to minimize clogs during cell sorting, filter the cell suspension.

3.12. Identifying and sorting liver NPC by flow cytometry.

Liver NPCs have yet to become absolute in their defining characteristics. However, many distinct cell populations can be sorted from a mouse liver. Those identified here

represent a cross-section of major cell types, including endothelial cells, macrophage, quiescent hepatic stellate cells, lymphocytes, and natural killer cells. If a population of cells appears diffuse in characteristics, separation by an additional dimension may reveal multiple cell populations. The successful isolation of pure and viable cells is as much art as science and will be aided by the direction and advice of a skilled flow cytometrist with an appreciation for the complexity of sorting from dissociated tissue. The gating strategy depicted in Figure 3 is one approach to sorting liver NPCs.

3.13. Quality control analysis of enriched liver cell populations.

Quality control analysis of enriched and sorted liver cell populations can be conducted by *in vitro* culture of the cells to confirm morphology and/or function [179]. In addition, enriched cells can be analyzed for expression of genes known to be relatively specific to cell types. The basic protocol and representative results are presented below.

The described liver cell isolation method was used to purify liver LSECs, Kupffer cells (KCs), qHSCs, and hepatocytes from 5 nine-week-old C57BL/6J male mice purchased from The Jackson Laboratory (Bar Harbor, ME). Briefly, hepatocytes were processed through Step 3.9 and enriched using anti-CD45 and anti-CD146 microbeads. Liver NPCs were processed through Step 3.10 and then stained for cell sorting on a BD Aria III, as touched upon in Step 3.12. The antibodies used to discriminate cell populations during sorting were as follows: Live/Dead Violet (Pacific Blue), CD11b (BV605), IA/IE (FITC), Tie2 (PE), Ly6C (PerCP-Cy5.5), F4/80 (APC), and Ly6G (APC-Cy7). There were minimal differences in the concentration of antibodies used in sorting (see Note 18) and while the gating strategy was similar to that shown in Figure 3, it was not identical (see Note 19).

Post-sort analyses of sorted LSECs, KCs, and qHSCs show average cell purities of 93.02%, 93.82%, and 87.02% respectively (averaged value of n=5). To further assess

the purity of these cell populations, RNA was isolated using TRIzol (Invitrogen) and then cDNA was synthesized (QIAGEN QuantiTect) and quantified using microfluidic PCR (Fluidigm Corp, South San Francisco CA, USA) with cell-type-specific TaqMan® assays (Invitrogen) (Figure 4). The qRT-PCR analysis shows that isolated hepatocytes, LSECs, KCs, and qHSCs are enriched for their cell-type-specific genes. Genes commonly associated with each cell type—*Alb* for hepatocytes, *Tek* (Tie2) for LSECs, *Emr1* (F4/80) for KCs, and *Pdgfrb* for qHSCs—are enriched in the expected populations (see Note 20).

Notes

1. Avertin becomes toxic when exposed to light. Although concentrated stock solutions can be prepared, preparation of smaller volumes of working solution minimizes the likelihood of accumulating toxic byproducts.
2. Some researchers use the needle to catheterize, others simply use a 24G needle. We prefer to use the Vialon™ catheter alone and reuse it on multiple mice.
3. Collagenase is available in many fractions and sources. We have found that collagenase from *Clostridium histolyticum*, Type IV, from Sigma-Aldrich dissociates the liver efficiently and maintains expected cell function.
4. Standard polystyrene tubes are suitable for most applications. However, prior to sorting samples, it is important to filter (40 um) each sample in order to reduce the likelihood of clumps and clogs. Use sterile tubes when necessary.
5. The choice of antibodies and fluorophores is highly dependent upon the cell(s) of interest. Those listed in Table 1 allow for separation of relatively pure populations of LSEC, Kupffer cells, CD8+ T cells, CD4+ T cell, infiltrating myeloid cells, and quiescent HSC. During inflammation or pathology, the morpohology

and cell surface molecules of most cells change, resulting in heterogeneity. Thus, additional antibodies may be necessary to achieve homogenous cell populations.

6. Prepare a perfusion tubing set using two IV extensions, two adaptors, and one length of silicon peristaltic pump tubing. Cut and discard the male end from one extension set and the female from the other; remove the slide clamps from both and discard. Connect the cut ends of the extension tubes to the pump tubing using the connectors (Figure 1A). Connect the catheter to the male end (Figure 1B). Perfusion tubing may be reused for many months with proper cleaning and storage. Flush the tubing with 5 ml of 70% ethanol followed by 15 ml of sterile distilled water. Allow the tubing to run dry then store in a plastic zip-lock bag, protected from light. Tubing will become brittle with prolonged exposure to ethanol. Upon re-use, flush the tubing with ethanol then distilled water, run dry, then fill with perfusion buffer.
7. Toe-pinch reflex is a standard method for assessing depth of anesthesia in mice. The mouse should not flinch. If flinching occurs, allow more time or administer additional Avertin.
8. Exercise care when moving the liver in order to avoid hemorrhage. Once the portal vein is exposed, place forceps in order to hold back other tissue. Excess fat (or pancreas) may partially hide the portal vein. This is more likely in older (>8 months of age) male mice.
9. It will be more difficult to catheterize the vein if it is cut clean through. A ‘nick’ in the vein will allow an entry point for a catheter without a needle, while preserving structural support.

10. Blood will generally flow from the right – the opening towards the intestines. As perfusion buffer washes the blood away, the nick in the portal vein should be clear. Gently catheterize the vein towards the liver.
11. Do not cut the descending vena cava until the portal vein is catheterized. The liver should blanch as soon as the vein is catheterized, if it doesn't the vein is not catheterized, so try again. The most likely 'miss' occurs in the smooth muscle layer surrounding the vein. This layer will puff up. If this occurs, remove the catheter and try for the vein opening again. The catheter is visible within the vein.
12. It is important to maintain a steady hand or else the catheter will slip, tear or puncture (if pushed too far toward the liver) the vein. Mindful relaxation of the right hand will minimize shaking and fatigue, which is especially important for multiple mouse experiments. If with time and practice, shaking persists and is the cause of failed perfusions, consider the method of Seglen and secure the catheter with a noose. Alternatively, with practice, the catheter can be fully released from grip, once the mouse has expired.
13. When switching the line from perfusion buffer to collagenase, air bubbles are occasionally introduced. A small bubble (< 3 mm) in the line is not an issue. Larger bubbles may occlude the perfusion of regions of the liver, but not always. If a very large bubble (> 2 cm) is seen in the line, it is best to remove the catheter just before the bubble reaches the catheter, run the bubble out, then catheterize the vein again. With practice, this is easily done. When in doubt, let the bubble run its course.
14. The liver should swell. The left lobe, in particular, should clearly swell and fall over the portal vein. If the liver does not swell, inspect the catheter in the portal vein. Diseased livers (i.e. fibrotic) do not digest or swell very well.

15. The gall bladder contains bile acid salts, digestive enzymes, and fat-soluble compounds destine for excretion in the feces. Ideally, the gall bladder is removed intact. However, we have not observed a difference in NPC phenotype due to gall bladder rupture. If working with an assistant, pass the digested liver to the assistant to complete the processing, then continue with section 3.7 or begin another mouse.
16. Although optional, removal and isolation of cells from the spleen is useful for preparing compensations for flow cytometry and providing additional (and validating) immunological information. The cell surface staining of lymphocytes isolated from the liver often shows a bias towards mixed activation and polarization states. By contrasting the immunophenotype of cells in the liver to those of the spleen, one is better able to assure: 1) an intact and 'proper' immune system, 2) proper staining protocol, and 3) proper gating strategy in flow cytometry.
17. A concentration of 1:250 Fc block is generally adequate to identify populations of liver NPCs with proper compensation. Increasing the concentration of Fc block will reduce the amount of non-specific antibody binding, and has the potential to further resolve cell populations. LSEC and KC are abundant liver NPC and show affinity for most flow cytometry antibodies.
18. Anti-CD16/anti-CD36 (Fc receptor blocking) was used at a final concentration of 1:50 to increase the resolution between cell populations. The Live/Dead Violet stain was used at a final concentration of 1:1000. All other antibodies were used at a final concentration of 1:200.
19. Cells were sorted in the manner illustrated in Figure 3, with modification. In brief, following size gating on the FSC-A vs. SSC-A plot, Live/Dead was used to exclude dead cells. Cells staining $CD11b^{int/hi}Tie2^{int/lo}$ CD11b vs. Tie2 plot were

further gated on CD11b vs. Ly6G to gate out the Ly6G^{hi} neutrophils then selecting Kupffer cells by CD11b vs. F4/80. Of note, since the size gate from the FSC-A vs. SSC-A plot is mostly sufficient to separate qHSC from LSEC and KC, this panel uses the Pacific Blue channel to sort qHSC as the highly auto-fluorescent population and to define dead cells as the Pacific Blue positive population. The qHSC are generally more Pacific Blue "positive" than dead cells.

20. The low-level expression of LSEC- and KC-specific genes in the qHSC population is likely due to a small contaminating fraction of dead LSECs and KCs, and resulting from the use of the Pacific Blue channel for both qHSC auto-fluorescence and the Live/Dead-violet stain. We suspect this issue to be solved if a different channel for Live/Dead discrimination is used. Auto-fluorescence from debris, however, renders many other channels frustratingly non-specific for absolute exclusion of dead cells. As a result, exclusion of dead cells should be considered on a case-by-case basis.

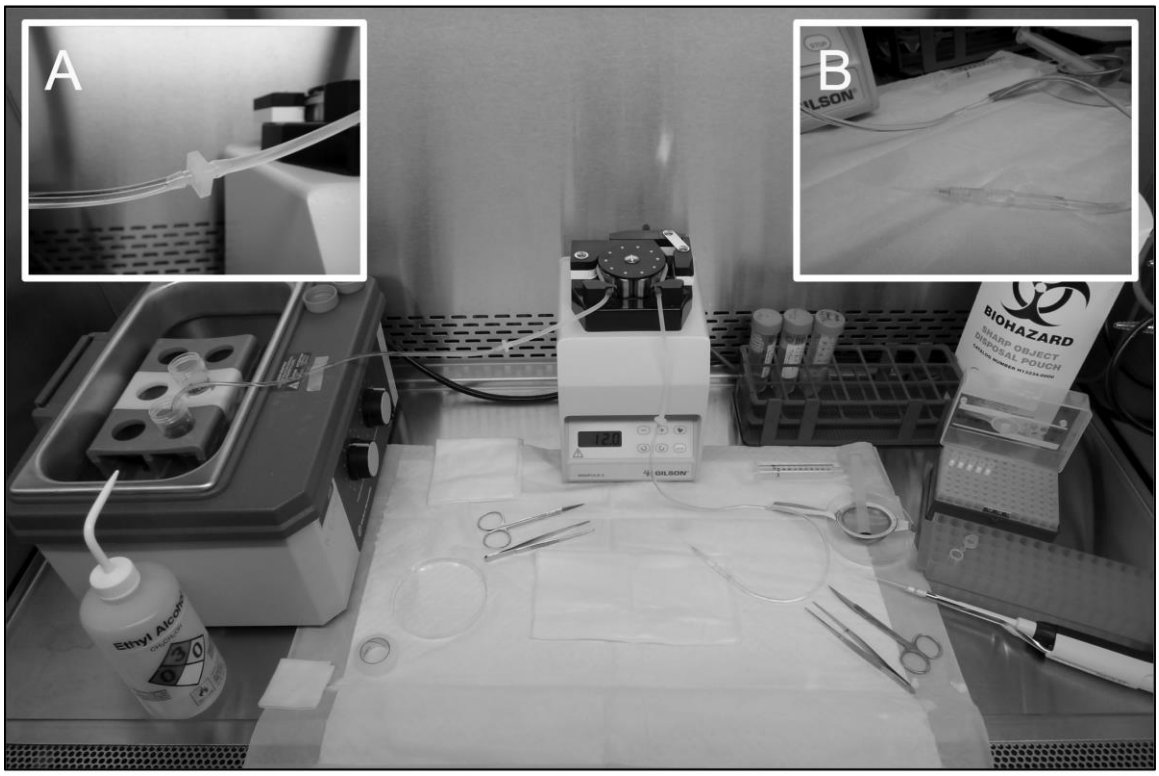

Figure A-1. Suggested workspace set-up. Position the water bath and pump to allow the perfusion tubing to reach the bottom of the 50-ml conical tubes. The water bath should be to the left, in order to allow switching of the perfusion line while holding the catheter with the right hand. Place absorbent pad on the work surface; this pad will both absorb perfusion solutions and act as the foundation to adhere the mouse. Place large gauze pad in the center of the work area; this small pad will absorb most of the perfusion solutions as well as blood and should be changed after every other if not every mouse. Place tea strainer in a 10-cm petri dish. Place the lid of the dish to the left of the smaller gauze pad. Place one pair of sharp scissors and forceps above the gauze. Place the other scissors and forceps to the right of the gauze. Position the surgical tape, small gauze pads, and 70% ethanol within easy reach. Inset A illustrates the connection between extension tubing and silicon peristaltic pump tubing. Inset B illustrates the catheter connected to the male end of the extension tubing.

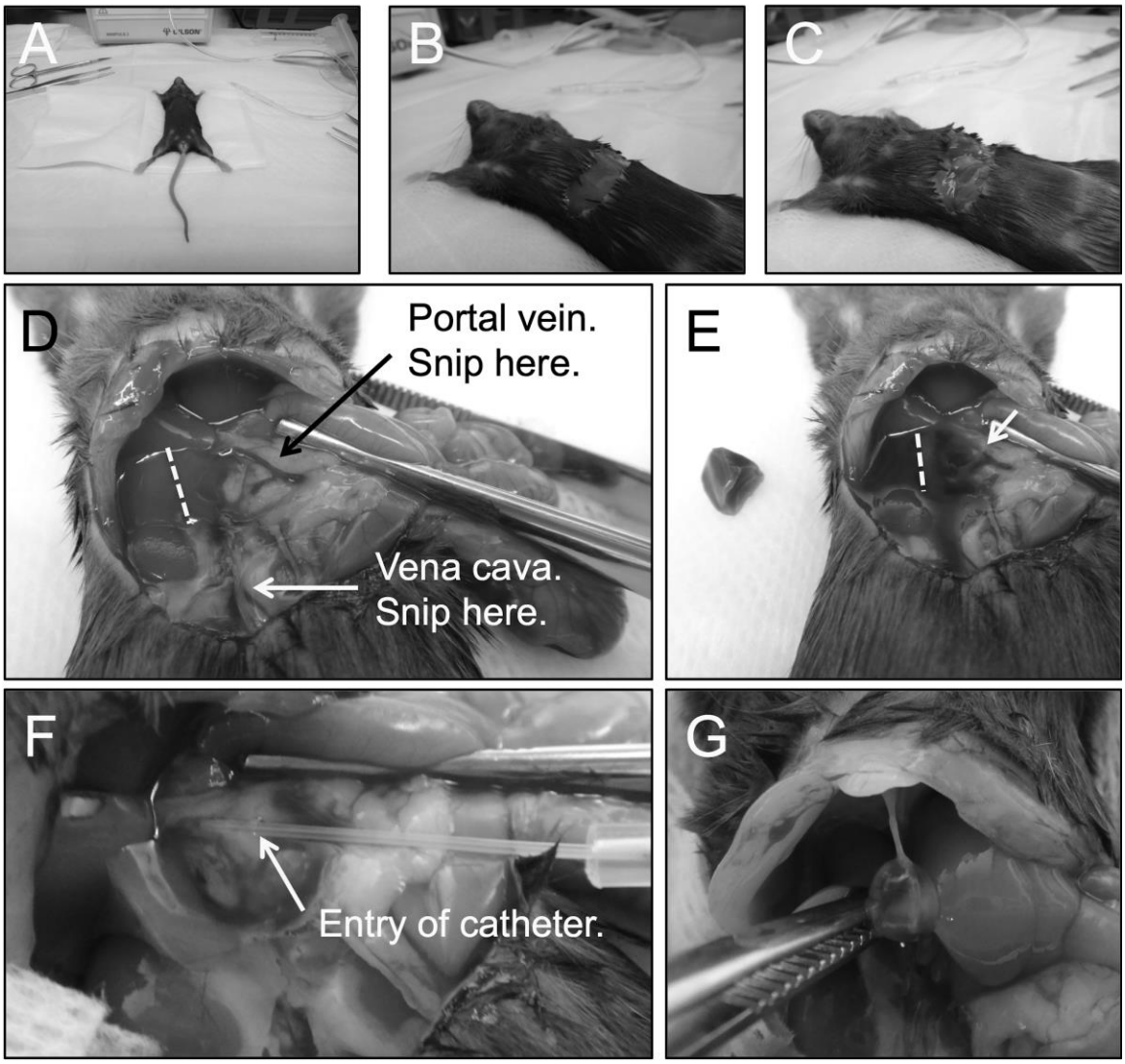

Figure A-2. General perfusion anatomy and procedure.A) Adhere anesthetized mouse overtop of the gauze in an X-configuration. B) Make a crosswise incision through the mouse skin to reveal the peritoneum. C) Being careful to avoid cutting internal organs, make a crosswise incision through the peritoneum. D) Move the gastrointestinal organs to the left, revealing the portal vein. Place forceps to hold tissue off of the vein. E) Snip the portal vein (collect blood if desired), then remove a portion of the intact right posterior lobe. Catheterize the portal vein, then immediately cut the descending vena cava. F) The liver will blanch once the portal vein is catheterized, and will fully perfuse once the vena cava is cut. Avoid pushing the catheter too far into the vein. The tip of the catheter should be easily observed within the vein. G) Once digested, remove the liver by the falciform ligament, along the top of the medial lobe. The gall bladder is a good landmark for identifying the ligament.

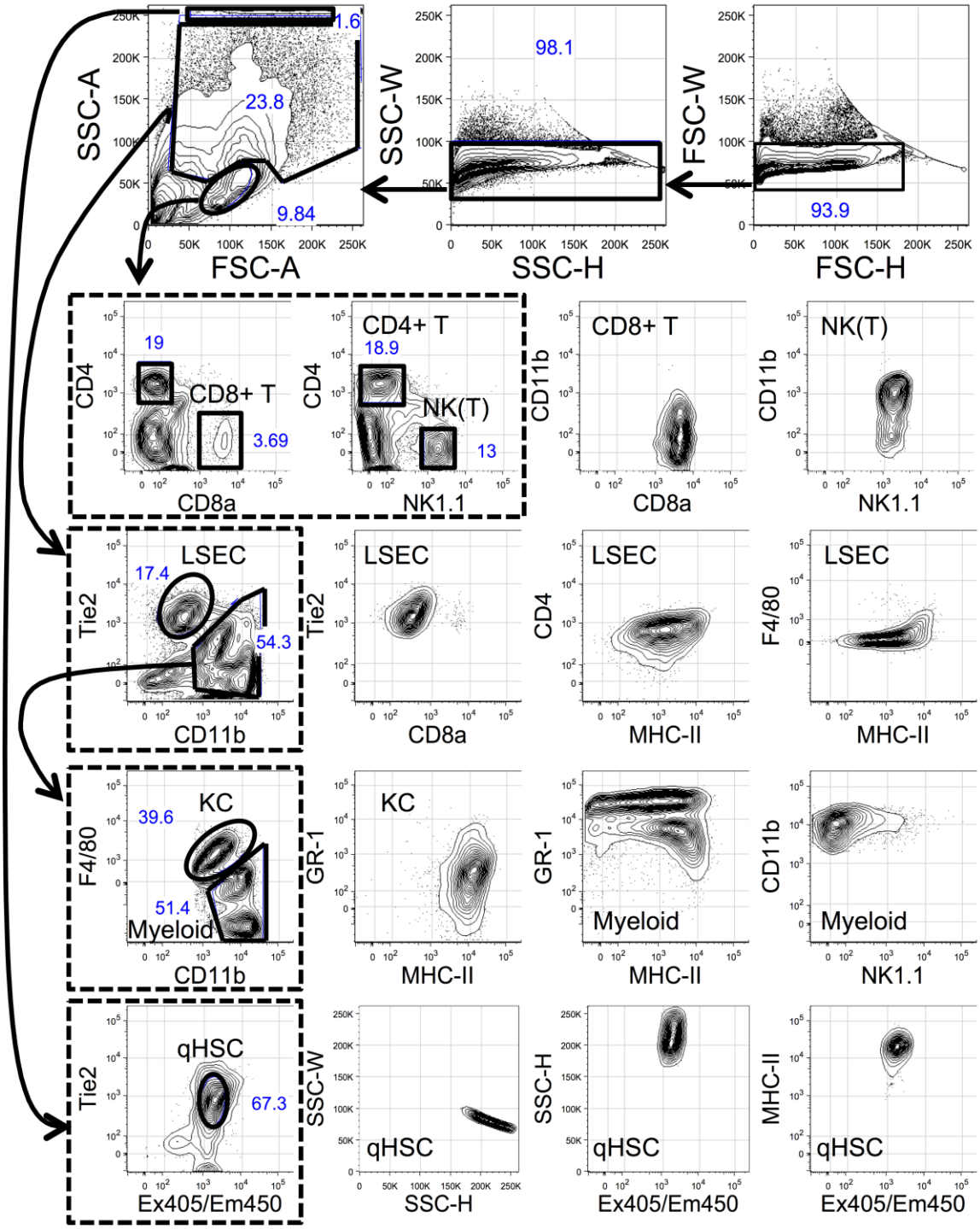

Figure A-3. NPC sort strategy. Representative NPC sorting strategy from a C57BL/6J mouse 68 h following injection of 50,000 *P. yoelii* sporozoites. Labeled gates are sorted populations. Exclude doublets by FSC-H vs. FSC-W and SSC-H vs. SSC-W, but if quiescent hepatic stellate (qHSC) are desired, be sure to include the SSC-H events. From a standard FSC-A vs. SSC-A scatter plot, separate lymphocyte-sized cells from cells with high granularity (SSC) and larger size (FSC). Hepatic stellate cells contain highly refractive retinol droplets and are auto-fluorescent when excited with 405nm and

(Figure A-3 legend, continued)
emitting at 450nm. Lymphocytes can be separated into many populations. Here, CD8+ T cells are collected against CD8a vs. CD4. CD4+ T cells and NK(T) cells are collected against NK1.1 vs. CD4. A significant population of NK-T cells are CD4+ in the mouse. The best identifier of NK-T cells is CD1d (stained by tetramer, not conducted here). NK(T) cells induce CD11b expression when activated. From the larger cells, LSEC, Kupffer cells (KC), and infiltrating myeloid cells (including monocytes and granulocytes) can be collected. LSEC are selected against CD11b vs. Tie2. From the $CD11b^{int/hi}$ $Tie2^{int/lo}$ cells, KC and general myeloid cells can be distinguished by CD11b vs. F4/80 staining. Here we see that KC are MHC class-II high and GR-1 (Ly6G/Ly6C) intermediate. The myeloid infiltrate contains $GR1^{hi}$ and $GR1i^{int}$ population with varying degree of MHC-II staining. Lastly, qHSC show very high SSC and auto-fluorescence (Ex 405nm / Em 450nm) and often show auto-fluorescence in many channels. Since many of these characteristics are that of dead cells or debris, the best validation of sorted qHSC is direct observation under a light microscope. In all cases, heterogeneity may exist in these populations, and further selection or validation of purity may be needed.

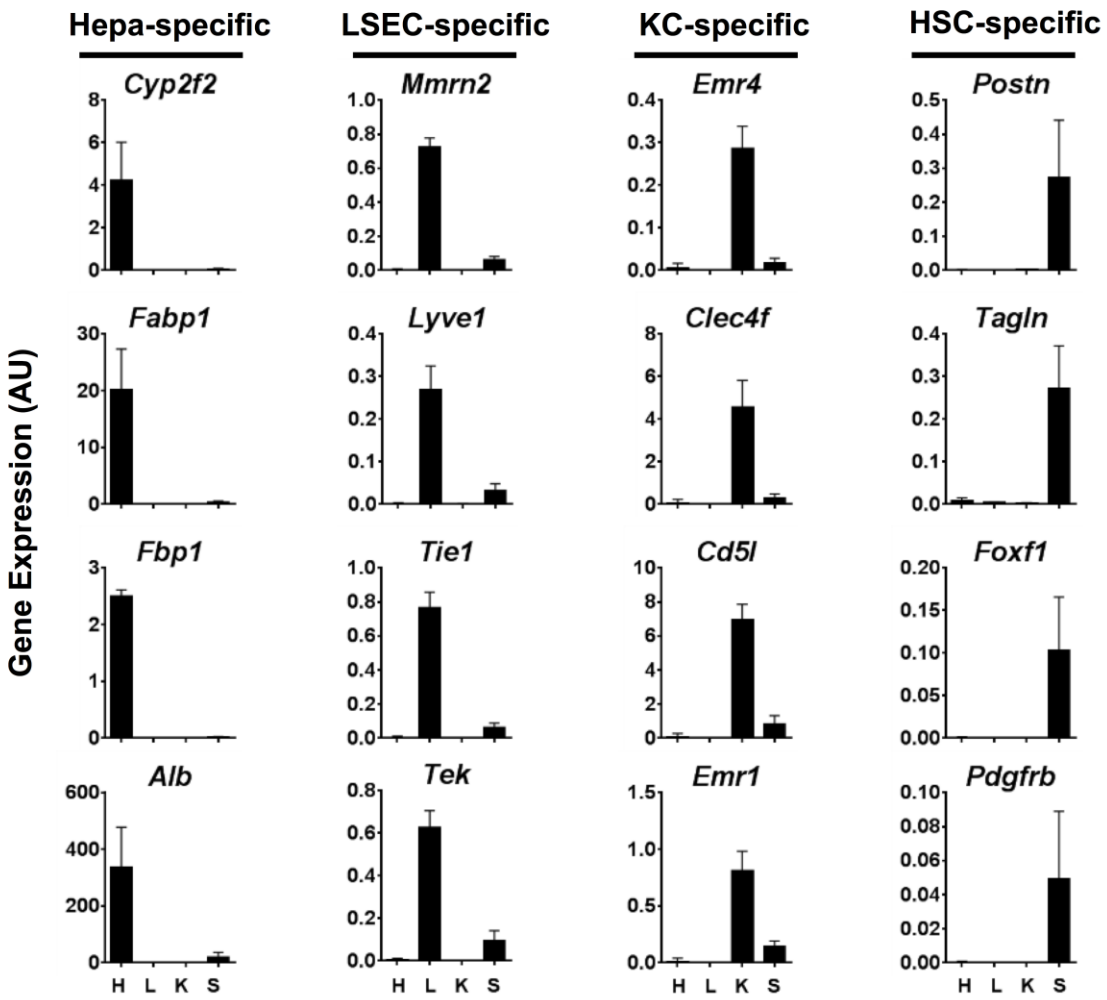

Figure A-4. Quality control by qRT-PCR of hepatocytes and sorted liver NPCs. The relative expression of genes in enriched liver cell types illustrates the efficacy of the method. Gene expression is normalized to the average of three house-keeping genes: *Gapdh*, *Actb*, and *Hprt*. Each bar is the mean (+SD) of n=5 mice. H=Hepatocyte, L=LSEC, K= Kupffer cell, and S=Hepatic stellate cell. Graphed using Prism6 (GraphPad Software, San Diego CA, USA).

Epitope	Fluorophore	Clone	Dilution
CD8a	Pacific Blue	53-6-7	1:250
CD4	PerCP-Cy5.5	RM4-5	1:250
CD11b	FITC	M1/70	1:200
NK1.1	Per-Cy7	PK136	1:200
Tie2	PE	TEK4	1:250
F4/80	APC	BM8	1:200
GR1	APC-Cy7	RB6-8C5	1:200
N/A	Live/Dead Violet	N/A	1:1000

Table A-1. Antibodies for FACS-based purification of some of the major liver NPC and leukocytes. The antibodies listed here will allow for selection or analysis of some of the most numerous liver NPC as well as some leukocytes.

Acknowledgements

This protocol was developed under support by the National Institutes of Health grants

R21AI099872 and T32AI007411 and Seattle Biomedical Research Institute.

REFERENCES

1. Mortality, G. B. D. & Causes of Death, C. Global, regional, and national age-sex specific all-cause and cause-specific mortality for 240 causes of death, 1990-2013: a systematic analysis for the Global Burden of Disease Study 2013. *Lancet* **385**, 117-171, doi:10.1016/S0140-6736(14)61682-2 (2015).
2. *Hepatitis B, Fact sheet N°204*, <http://www.who.int/mediacentre/factsheets/fs204/en/> (2015).
3. *Hepatitis C: Fact sheet N°164*, <http://www.who.int/mediacentre/factsheets/fs164/en/> (2015).
4. Te, H. S. & Jensen, D. M. Epidemiology of hepatitis B and C viruses: a global overview. *Clin Liver Dis* **14**, 1-21, vii, doi:10.1016/j.cld.2009.11.009 (2010).
5. Sebastiani, G., Gkouvatsos, K. & Pantopoulos, K. Chronic hepatitis C and liver fibrosis. *World J Gastroenterol* **20**, 11033-11053, doi:10.3748/wjg.v20.i32.11033 (2014).
6. Perz, J. F., Armstrong, G. L., Farrington, L. A., Hutin, Y. J. & Bell, B. P. The contributions of hepatitis B virus and hepatitis C virus infections to cirrhosis and primary liver cancer worldwide. *J Hepatol* **45**, 529-538, doi:10.1016/j.jhep.2006.05.013 (2006).
7. Lee, W. M. Acute liver failure. *Semin Respir Crit Care Med* **33**, 36-45, doi:10.1055/s-0032-1301733 (2012).
8. Shen, X. D., Ke, B., Zhai, Y., Gao, F., Tsuchihashi, S., Lassman, C. R., Busuttil, R. W. & Kupiec-Weglinski, J. W. Absence of toll-like receptor 4 (TLR4) signaling in the donor organ reduces ischemia and reperfusion injury in a murine liver transplantation model. *Liver Transpl* **13**, 1435-1443, doi:10.1002/lt.21251 (2007).
9. Neuschwander-Tetri, B. A. & Caldwell, S. H. Nonalcoholic steatohepatitis: summary of an AASLD Single Topic Conference. *Hepatology* **37**, 1202-1219, doi:10.1053/jhep.2003.50193 (2003).
10. Szabo, G., Petrasek, J. & Bala, S. Innate immunity and alcoholic liver disease. *Dig Dis* **30 Suppl 1**, 55-60, doi:10.1159/000341126 (2012).
11. Heron, M., Hoyert, D. L., Murphy, S. L., Xu, J., Kochanek, K. D. & Tejada-Vera, B. Deaths: final data for 2006. *Natl Vital Stat Rep* **57**, 1-134 (2009).
12. Kumar, H., Kawai, T. & Akira, S. Toll-like receptors and innate immunity. *Biochem Biophys Res Commun* **388**, 621-625, doi:10.1016/j.bbrc.2009.08.062 (2009).
13. Chen, G. Y. & Nunez, G. Sterile inflammation: sensing and reacting to damage. *Nat Rev Immunol* **10**, 826-837, doi:10.1038/nri2873 (2010).
14. Enomoto, N., Ikejima, K., Bradford, B., Rivera, C., Kono, H., Brenner, D. A. & Thurman, R. G. Alcohol causes both tolerance and sensitization of rat Kupffer cells via mechanisms dependent on endotoxin. *Gastroenterology* **115**, 443-451 (1998).
15. Nanji, A. A., Khettry, U., Sadrzadeh, S. M. & Yamanaka, T. Severity of liver injury in experimental alcoholic liver disease. Correlation with plasma endotoxin, prostaglandin E2, leukotriene B4, and thromboxane B2. *Am J Pathol* **142**, 367-373 (1993).
16. Uesugi, T., Froh, M., Arteel, G. E., Bradford, B. U. & Thurman, R. G. Toll-like receptor 4 is involved in the mechanism of early alcohol-induced liver injury in mice. *Hepatology* **34**, 101-108, doi:10.1053/jhep.2001.25350 (2001).
17. Zimmermann, H. W., Trautwein, C. & Tacke, F. Functional role of monocytes and macrophages for the inflammatory response in acute liver injury. *Front Physiol* **3**, 56, doi:10.3389/fphys.2012.00056 (2012).

18. Liaskou, E., Wilson, D. V. & Oo, Y. H. Innate immune cells in liver inflammation. *Mediators Inflamm* **2012**, 949157, doi:10.1155/2012/949157 (2012).
19. Mosher, B., Dean, R., Harkema, J., Remick, D., Palma, J. & Crockett, E. Inhibition of Kupffer cells reduced CXC chemokine production and liver injury. *J Surg Res* **99**, 201-210, doi:10.1006/jsre.2001.6217 (2001).
20. Pellicoro, A., Ramachandran, P., Iredale, J. P. & Fallowfield, J. A. Liver fibrosis and repair: immune regulation of wound healing in a solid organ. *Nat Rev Immunol* **14**, 181-194, doi:10.1038/nri3623 (2014).
21. Chen, Y. & Sun, R. Toll-like receptors in acute liver injury and regeneration. *Int Immunopharmacol* **11**, 1433-1441, doi:10.1016/j.intimp.2011.04.023 (2011).
22. Arumugam, T. V., Okun, E., Tang, S. C., Thundyil, J., Taylor, S. M. & Woodruff, T. M. Toll-like receptors in ischemia-reperfusion injury. *Shock* **32**, 4-16, doi:10.1097/SHK.0b013e318193e333 (2009).
23. Hinson, J. A., Roberts, D. W. & James, L. P. Mechanisms of acetaminophen-induced liver necrosis. *Handb Exp Pharmacol*, 369-405, doi:10.1007/978-3-642-00663-0_12 (2010).
24. Wang, K. Molecular mechanisms of liver injury: apoptosis or necrosis. *Exp Toxicol Pathol* **66**, 351-356, doi:10.1016/j.etp.2014.04.004 (2014).
25. Krenkel, O., Mossanen, J. C. & Tacke, F. Immune mechanisms in acetaminophen-induced acute liver failure. *Hepatobiliary Surg Nutr* **3**, 331-343, doi:10.3978/j.issn.2304-3881.2014.11.01 (2014).
26. Gujral, J. S., Knight, T. R., Farhood, A., Bajt, M. L. & Jaeschke, H. Mode of cell death after acetaminophen overdose in mice: apoptosis or oncotic necrosis? *Toxicol Sci* **67**, 322-328 (2002).
27. Brenner, C., Galluzzi, L., Kepp, O. & Kroemer, G. Decoding cell death signals in liver inflammation. *J Hepatol* **59**, 583-594, doi:10.1016/j.jhep.2013.03.033 (2013).
28. Malhi, H. & Gores, G. J. Molecular mechanisms of lipotoxicity in nonalcoholic fatty liver disease. *Semin Liver Dis* **28**, 360-369, doi:10.1055/s-0028-1091980 (2008).
29. Yin, M., Wheeler, M. D., Kono, H., Bradford, B. U., Gallucci, R. M., Luster, M. I. & Thurman, R. G. Essential role of tumor necrosis factor alpha in alcohol-induced liver injury in mice. *Gastroenterology* **117**, 942-952 (1999).
30. Malhi, H. & Gores, G. J. Cellular and molecular mechanisms of liver injury. *Gastroenterology* **134**, 1641-1654, doi:10.1053/j.gastro.2008.03.002 (2008).
31. Huet, P. M., Nagaoka, M. R., Desbiens, G., Tarrab, E., Brault, A., Bralet, M. P. & Bilodeau, M. Sinusoidal endothelial cell and hepatocyte death following cold ischemia-warm reperfusion of the rat liver. *Hepatology* **39**, 1110-1119, doi:10.1002/hep.20157 (2004).
32. van Golen, R. F., van Gulik, T. M. & Heger, M. The sterile immune response during hepatic ischemia/reperfusion. *Cytokine Growth Factor Rev* **23**, 69-84, doi:10.1016/j.cytogfr.2012.04.006 (2012).
33. Gujral, J. S., Bucci, T. J., Farhood, A. & Jaeschke, H. Mechanism of cell death during warm hepatic ischemia-reperfusion in rats: apoptosis or necrosis? *Hepatology* **33**, 397-405, doi:10.1053/jhep.2001.22002 (2001).
34. Yang, S. Q., Lin, H. Z., Lane, M. D., Clemens, M. & Diehl, A. M. Obesity increases sensitivity to endotoxin liver injury: implications for the pathogenesis of steatohepatitis. *Proc Natl Acad Sci U S A* **94**, 2557-2562 (1997).
35. Solga, S. F. & Diehl, A. M. Non-alcoholic fatty liver disease: lumen-liver interactions and possible role for probiotics. *J Hepatol* **38**, 681-687 (2003).
36. Matzinger, P. Tolerance, danger, and the extended family. *Annu Rev Immunol* **12**, 991-1045, doi:10.1146/annurev.iy.12.040194.005015 (1994).

37. Matzinger, P. The danger model: a renewed sense of self. *Science* **296**, 301-305, doi:10.1126/science.1071059 (2002).
38. Scaffidi, P., Misteli, T. & Bianchi, M. E. Release of chromatin protein HMGB1 by necrotic cells triggers inflammation. *Nature* **418**, 191-195, doi:10.1038/nature00858 (2002).
39. Tsung, A., Sahai, R., Tanaka, H., Nakao, A., Fink, M. P., Lotze, M. T., Yang, H., Li, J., Tracey, K. J., Geller, D. A. & Billiar, T. R. The nuclear factor HMGB1 mediates hepatic injury after murine liver ischemia-reperfusion. *J Exp Med* **201**, 1135-1143, doi:10.1084/jem.20042614 (2005).
40. Bell, C. W., Jiang, W., Reich, C. F., 3rd & Pisetsky, D. S. The extracellular release of HMGB1 during apoptotic cell death. *Am J Physiol Cell Physiol* **291**, C1318-1325, doi:10.1152/ajpcell.00616.2005 (2006).
41. Kawai, T. & Akira, S. Toll-like receptors and their crosstalk with other innate receptors in infection and immunity. *Immunity* **34**, 637-650, doi:10.1016/j.immuni.2011.05.006 (2011).
42. Yamamoto, M., Sato, S., Hemmi, H., Hoshino, K., Kaisho, T., Sanjo, H., Takeuchi, O., Sugiyama, M., Okabe, M., Takeda, K. & Akira, S. Role of adaptor TRIF in the MyD88-independent toll-like receptor signaling pathway. *Science* **301**, 640-643, doi:10.1126/science.1087262 (2003).
43. Yamamoto, M., Sato, S., Mori, K., Hoshino, K., Takeuchi, O., Takeda, K. & Akira, S. Cutting Edge: A Novel Toll/IL-1 Receptor Domain-Containing Adapter That Preferentially Activates the IFN- Promoter in the Toll-Like Receptor Signaling. *The Journal of Immunology* **169**, 6668-6672, doi:10.4049/jimmunol.169.12.6668 (2002).
44. Seki, E. & Brenner, D. A. Toll-like receptors and adaptor molecules in liver disease: update. *Hepatology* **48**, 322-335, doi:10.1002/hep.22306 (2008).
45. Yamamoto, M., Sato, S., Hemmi, H., Uematsu, S., Hoshino, K., Kaisho, T., Takeuchi, O., Takeda, K. & Akira, S. TRAM is specifically involved in the Toll-like receptor 4-mediated MyD88-independent signaling pathway. *Nat Immunol* **4**, 1144-1150, doi:10.1038/ni986 (2003).
46. Yamamoto, M., Sato, S., Hemmi, H., Sanjo, H., Uematsu, S., Kaisho, T., Hoshino, K., Takeuchi, O., Kobayashi, M., Fujita, T., Takeda, K. & Akira, S. Essential role for TIRAP in activation of the signalling cascade shared by TLR2 and TLR4. *Nature* **420**, 324-329, doi:10.1038/nature01182 (2002).
47. Feng, Y. & Chao, W. Toll-like receptors and myocardial inflammation. *Int J Inflam* **2011**, 170352, doi:10.4061/2011/170352 (2011).
48. Liu, S., Gallo, D. J., Green, A. M., Williams, D. L., Gong, X., Shapiro, R. A., Gambotto, A. A., Humphris, E. L., Vodovotz, Y. & Billiar, T. R. Role of toll-like receptors in changes in gene expression and NF-kappa B activation in mouse hepatocytes stimulated with lipopolysaccharide. *Infect Immun* **70**, 3433-3442 (2002).
49. Wu, J., Meng, Z., Jiang, M., Zhang, E., Trippler, M., Broering, R., Bucchi, A., Krux, F., Dittmer, U., Yang, D., Roggendorf, M., Gerken, G., Lu, M. & Schlaak, J. F. Toll-like receptor-induced innate immune responses in non-parenchymal liver cells are cell type-specific. *Immunology* **129**, 363-374, doi:10.1111/j.1365-2567.2009.03179.x (2010).
50. Wang, B., Trippler, M., Pei, R., Lu, M., Broering, R., Gerken, G. & Schlaak, J. F. Toll-like receptor activated human and murine hepatic stellate cells are potent regulators of hepatitis C virus replication. *J Hepatol* **51**, 1037-1045, doi:10.1016/j.jhep.2009.06.020 (2009).

51. Szabo, G., Dolganiuc, A. & Mandrekar, P. Pattern recognition receptors: a contemporary view on liver diseases. *Hepatology* **44**, 287-298, doi:10.1002/hep.21308 (2006).
52. Li, K., Chen, Z., Kato, N., Gale, M., Jr. & Lemon, S. M. Distinct poly(I-C) and virus-activated signaling pathways leading to interferon-beta production in hepatocytes. *J Biol Chem* **280**, 16739-16747, doi:10.1074/jbc.M414139200 (2005).
53. Weiskirchen, R. & Tacke, F. Cellular and molecular functions of hepatic stellate cells in inflammatory responses and liver immunology. *Hepatobiliary Surg Nutr* **3**, 344-363, doi:10.3978/j.issn.2304-3881.2014.11.03 (2014).
54. Sawaki, J., Tsutsui, H., Hayashi, N., Yasuda, K., Akira, S., Tanizawa, T. & Nakanishi, K. Type 1 cytokine/chemokine production by mouse NK cells following activation of their TLR/MyD88-mediated pathways. *Int Immunol* **19**, 311-320, doi:10.1093/intimm/dxl148 (2007).
55. Asselin-Paturel, C., Brizard, G., Chemin, K., Boonstra, A., O'Garra, A., Vicari, A. & Trinchieri, G. Type I interferon dependence of plasmacytoid dendritic cell activation and migration. *J Exp Med* **201**, 1157-1167, doi:10.1084/jem.20041930 (2005).
56. Shu, S. A., Lian, Z. X., Chuang, Y. H., Yang, G. X., Moritoki, Y., Comstock, S. S., Zhong, R. Q., Ansari, A. A., Liu, Y. J. & Gershwin, M. E. The role of CD11c(+) hepatic dendritic cells in the induction of innate immune responses. *Clin Exp Immunol* **149**, 335-343, doi:10.1111/j.1365-2249.2007.03419.x (2007).
57. Lukacs-Kornek, V. & Schuppan, D. Dendritic cells in liver injury and fibrosis: shortcomings and promises. *J Hepatol* **59**, 1124-1126, doi:10.1016/j.jhep.2013.05.033 (2013).
58. Tian, Z., Chen, Y. & Gao, B. Natural killer cells in liver disease. *Hepatology* **57**, 1654-1662, doi:10.1002/hep.26115 (2013).
59. Kubes, P. & Mehal, W. Z. Sterile inflammation in the liver. *Gastroenterology* **143**, 1158-1172, doi:10.1053/j.gastro.2012.09.008 (2012).
60. Holt, M. P., Cheng, L. & Ju, C. Identification and characterization of infiltrating macrophages in acetaminophen-induced liver injury. *J Leukoc Biol* **84**, 1410-1421, doi:10.1189/jlb.0308173 (2008).
61. You, Q., Holt, M., Yin, H., Li, G., Hu, C. J. & Ju, C. Role of hepatic resident and infiltrating macrophages in liver repair after acute injury. *Biochem Pharmacol* **86**, 836-843, doi:10.1016/j.bcp.2013.07.006 (2013).
62. Williams, C. D., Bajt, M. L., Farhood, A. & Jaeschke, H. Acetaminophen-induced hepatic neutrophil accumulation and inflammatory liver injury in CD18-deficient mice. *Liver Int* **30**, 1280-1292, doi:10.1111/j.1478-3231.2010.02284.x (2010).
63. Marques, P. E., Oliveira, A. G., Pereira, R. V., David, B. A., Gomides, L. F., Saraiva, A. M., Pires, D. A., Novaes, J. T., Patricio, D. O., Cisalpino, D., Menezes-Garcia, Z., Leevy, W. M., Chapman, S. E., Mahecha, G., Marques, R. E., Guabiraba, R., Martins, V. P., Souza, D. G., Mansur, D. S., Teixeira, M. M., Leite, M. F. & Menezes, G. B. Hepatic DNA deposition drives drug-induced liver injury and inflammation in mice. *Hepatology* **61**, 348-360, doi:10.1002/hep.27216 (2015).
64. Imaeda, A. B., Watanabe, A., Sohail, M. A., Mahmood, S., Mohamadnejad, M., Sutterwala, F. S., Flavell, R. A. & Mehal, W. Z. Acetaminophen-induced hepatotoxicity in mice is dependent on Tlr9 and the Nalp3 inflammasome. *J Clin Invest* **119**, 305-314, doi:10.1172/JCI35958 (2009).
65. Williams, C. D., Antoine, D. J., Shaw, P. J., Benson, C., Farhood, A., Williams, D. P., Kanneganti, T. D., Park, B. K. & Jaeschke, H. Role of the Nalp3

inflammasome in acetaminophen-induced sterile inflammation and liver injury. *Toxicol Appl Pharmacol* **252**, 289-297, doi:10.1016/j.taap.2011.03.001 (2011).
66. Williams, C. D., Farhood, A. & Jaeschke, H. Role of caspase-1 and interleukin-1beta in acetaminophen-induced hepatic inflammation and liver injury. *Toxicol Appl Pharmacol* **247**, 169-178, doi:10.1016/j.taap.2010.07.004 (2010).
67. Yohe, H. C., O'Hara, K. A., Hunt, J. A., Kitzmiller, T. J., Wood, S. G., Bement, J. L., Bement, W. J., Szakacs, J. G., Wrighton, S. A., Jacobs, J. M., Kostrubsky, V., Sinclair, P. R. & Sinclair, J. F. Involvement of Toll-like receptor 4 in acetaminophen hepatotoxicity. *Am J Physiol Gastrointest Liver Physiol* **290**, G1269-1279, doi:10.1152/ajpgi.00239.2005 (2006).
68. Shah, N., Montes de Oca, M., Jover-Cobos, M., Tanamoto, K., Muroi, M., Sugiyama, K., Davies, N. A., Mookerjee, R. P., Dhar, D. K. & Jalan, R. Role of toll-like receptor 4 in mediating multiorgan dysfunction in mice with acetaminophen induced acute liver failure. *Liver Transpl* **19**, 751-761, doi:10.1002/lt.23655 (2013).
69. Fisher, J. E., McKenzie, T. J., Lillegard, J. B., Yu, Y., Juskewitch, J. E., Nedredal, G. I., Brunn, G. J., Yi, E. S., Malhi, H., Smyrk, T. C. & Nyberg, S. L. Role of Kupffer cells and toll-like receptor 4 in acetaminophen-induced acute liver failure. *J Surg Res* **180**, 147-155, doi:10.1016/j.jss.2012.11.051 (2013).
70. Possamai, L. A., McPhail, M. J., Khamri, W., Wu, B., Concas, D., Harrison, M., Williams, R., Cox, R. D., Cox, I. J., Anstee, Q. M. & Thursz, M. R. The role of intestinal microbiota in murine models of acetaminophen-induced hepatotoxicity. *Liver Int* **35**, 764-773, doi:10.1111/liv.12689 (2015).
71. Su, G. L., Hoesel, L. M., Bayliss, J., Hemmila, M. R. & Wang, S. C. Lipopolysaccharide binding protein inhibitory peptide protects against acetaminophen-induced hepatotoxicity. *Am J Physiol Gastrointest Liver Physiol* **299**, G1319-1325, doi:10.1152/ajpgi.00140.2010 (2010).
72. Zhai, Y., Shen, X. D., O'Connell, R., Gao, F., Lassman, C., Busuttil, R. W., Cheng, G. & Kupiec-Weglinski, J. W. Cutting edge: TLR4 activation mediates liver ischemia/reperfusion inflammatory response via IFN regulatory factor 3-dependent MyD88-independent pathway. *J Immunol* **173**, 7115-7119 (2004).
73. Bamboat, Z. M., Balachandran, V. P., Ocuin, L. M., Obaid, H., Plitas, G. & DeMatteo, R. P. Toll-like receptor 9 inhibition confers protection from liver ischemia-reperfusion injury. *Hepatology* **51**, 621-632, doi:10.1002/hep.23365 (2010).
74. Huang, H., Evankovich, J., Yan, W., Nace, G., Zhang, L., Ross, M., Liao, X., Billiar, T., Xu, J., Esmon, C. T. & Tsung, A. Endogenous histones function as alarmins in sterile inflammatory liver injury through Toll-like receptor 9 in mice. *Hepatology* **54**, 999-1008, doi:10.1002/hep.24501 (2011).
75. Shen, X. D., Ke, B., Ji, H., Gao, F., Freitas, M. C., Chang, W. W., Lee, C., Zhai, Y., Busuttil, R. W. & Kupiec-Weglinski, J. W. Disruption of Type-I IFN pathway ameliorates preservation damage in mouse orthotopic liver transplantation via HO-1 dependent mechanism. *Am J Transplant* **12**, 1730-1739, doi:10.1111/j.1600-6143.2012.04021.x (2012).
76. Yang, Q. W., Lu, F. L., Zhou, Y., Wang, L., Zhong, Q., Lin, S., Xiang, J., Li, J. C., Fang, C. Q. & Wang, J. Z. HMBG1 mediates ischemia-reperfusion injury by TRIF-adaptor independent Toll-like receptor 4 signaling. *J Cereb Blood Flow Metab* **31**, 593-605, doi:10.1038/jcbfm.2010.129 (2011).
77. Sharma, M., Mitnala, S., Vishnubhotla, R. K., Mukherjee, R., Reddy, D. N. & Rao, P. N. The Riddle of Nonalcoholic Fatty Liver Disease: Progression From

Nonalcoholic Fatty Liver to Nonalcoholic Steatohepatitis. *J Clin Exp Hepatol* **5**, 147-158, doi:10.1016/j.jceh.2015.02.002 (2015).
78. Farrell, G. C., van Rooyen, D., Gan, L. & Chitturi, S. NASH is an Inflammatory Disorder: Pathogenic, Prognostic and Therapeutic Implications. *Gut Liver* **6**, 149-171, doi:10.5009/gnl.2012.6.2.149 (2012).
79. Dyson, J. K., Anstee, Q. M. & McPherson, S. Non-alcoholic fatty liver disease: a practical approach to treatment. *Frontline Gastroenterol* **5**, 277-286, doi:10.1136/flgastro-2013-100404 (2014).
80. Day, C. P. & James, O. F. Steatohepatitis: a tale of two "hits"? *Gastroenterology* **114**, 842-845 (1998).
81. Paschos, P. & Paletas, K. Non alcoholic fatty liver disease and metabolic syndrome. *Hippokratia* **13**, 9-19 (2009).
82. Tilg, H. & Moschen, A. R. Evolution of inflammation in nonalcoholic fatty liver disease: the multiple parallel hits hypothesis. *Hepatology* **52**, 1836-1846, doi:10.1002/hep.24001 (2010).
83. Szabo, G., Velayudham, A., Romics, L., Jr. & Mandrekar, P. Modulation of non-alcoholic steatohepatitis by pattern recognition receptors in mice: the role of toll-like receptors 2 and 4. *Alcohol Clin Exp Res* **29**, 140S-145S (2005).
84. Rivera, C. A., Adegboyega, P., van Rooijen, N., Tagalicud, A., Allman, M. & Wallace, M. Toll-like receptor-4 signaling and Kupffer cells play pivotal roles in the pathogenesis of non-alcoholic steatohepatitis. *J Hepatol* **47**, 571-579, doi:10.1016/j.jhep.2007.04.019 (2007).
85. Li, L., Chen, L., Hu, L., Liu, Y., Sun, H. Y., Tang, J., Hou, Y. J., Chang, Y. X., Tu, Q. Q., Feng, G. S., Shen, F., Wu, M. C. & Wang, H. Y. Nuclear factor high-mobility group box1 mediating the activation of Toll-like receptor 4 signaling in hepatocytes in the early stage of nonalcoholic fatty liver disease in mice. *Hepatology* **54**, 1620-1630, doi:10.1002/hep.24552 (2011).
86. Cohen, J. I. & Nagy, L. E. Pathogenesis of alcoholic liver disease: interactions between parenchymal and non-parenchymal cells. *J Dig Dis* **12**, 3-9, doi:10.1111/j.1751-2980.2010.00468.x (2011).
87. Mencin, A., Kluwe, J. & Schwabe, R. F. Toll-like receptors as targets in chronic liver diseases. *Gut* **58**, 704-720, doi:10.1136/gut.2008.156307 (2009).
88. Yin, M., Bradford, B. U., Wheeler, M. D., Uesugi, T., Froh, M., Goyert, S. M. & Thurman, R. G. Reduced early alcohol-induced liver injury in CD14-deficient mice. *J Immunol* **166**, 4737-4742 (2001).
89. Hritz, I., Mandrekar, P., Velayudham, A., Catalano, D., Dolganiuc, A., Kodys, K., Kurt-Jones, E. & Szabo, G. The critical role of toll-like receptor (TLR) 4 in alcoholic liver disease is independent of the common TLR adapter MyD88. *Hepatology* **48**, 1224-1231, doi:10.1002/hep.22470 (2008).
90. Zhao, X. J., Dong, Q., Bindas, J., Piganelli, J. D., Magill, A., Reiser, J. & Kolls, J. K. TRIF and IRF-3 binding to the TNF promoter results in macrophage TNF dysregulation and steatosis induced by chronic ethanol. *J Immunol* **181**, 3049-3056 (2008).
91. Petrasek, J., Iracheta-Vellve, A., Csak, T., Satishchandran, A., Kodys, K., Kurt-Jones, E. A., Fitzgerald, K. A. & Szabo, G. STING-IRF3 pathway links endoplasmic reticulum stress with hepatocyte apoptosis in early alcoholic liver disease. *Proc Natl Acad Sci U S A* **110**, 16544-16549, doi:10.1073/pnas.1308331110 (2013).
92. Roh, Y. S., Zhang, B., Loomba, R. & Seki, E. TLR2 and TLR9 contribute to alcohol-mediated liver injury through induction of CXCL1 and neutrophil

infiltration. *Am J Physiol Gastrointest Liver Physiol* **309**, G30-41, doi:10.1152/ajpgi.00031.2015 (2015).
93. Byun, J. S., Suh, Y. G., Yi, H. S., Lee, Y. S. & Jeong, W. I. Activation of toll-like receptor 3 attenuates alcoholic liver injury by stimulating Kupffer cells and stellate cells to produce interleukin-10 in mice. *J Hepatol* **58**, 342-349, doi:10.1016/j.jhep.2012.09.016 (2013).
94. Aoyama, T., Paik, Y. H. & Seki, E. Toll-like receptor signaling and liver fibrosis. *Gastroenterol Res Pract* **2010**, doi:10.1155/2010/192543 (2010).
95. Roh, Y. S. & Seki, E. Toll-like receptors in alcoholic liver disease, non-alcoholic steatohepatitis and carcinogenesis. *J Gastroenterol Hepatol* **28 Suppl 1**, 38-42, doi:10.1111/jgh.12019 (2013).
96. DeLeve, L. D., Wang, X., Kaplowitz, N., Shulman, H. M., Bart, J. A. & van der Hoek, A. Sinusoidal endothelial cells as a target for acetaminophen toxicity. Direct action versus requirement for hepatocyte activation in different mouse strains. *Biochem Pharmacol* **53**, 1339-1345 (1997).
97. Ito, Y., Bethea, N. W., Abril, E. R. & McCuskey, R. S. Early hepatic microvascular injury in response to acetaminophen toxicity. *Microcirculation* **10**, 391-400, doi:10.1038/sj.mn.7800204 (2003).
98. McCuskey, R. S., Bethea, N. W., Wong, J., McCuskey, M. K., Abril, E. R., Wang, X., Ito, Y. & DeLeve, L. D. Ethanol binging exacerbates sinusoidal endothelial and parenchymal injury elicited by acetaminophen. *J Hepatol* **42**, 371-377, doi:10.1016/j.jhep.2004.11.033 (2005).
99. Knolle, P. A., Gerken, G., Loser, E., Dienes, H. P., Gantner, F., Tiegs, G., Meyer zum Buschenfelde, K. H. & Lohse, A. W. Role of sinusoidal endothelial cells of the liver in concanavalin A-induced hepatic injury in mice. *Hepatology* **24**, 824-829, doi:10.1002/hep.510240413 (1996).
100. Tiegs, G., Hentschel, J. & Wendel, A. A T cell-dependent experimental liver injury in mice inducible by concanavalin A. *J Clin Invest* **90**, 196-203, doi:10.1172/JCI115836 (1992).
101. Watanabe, Y., Morita, M. & Akaike, T. Concanavalin A induces perforin-mediated but not Fas-mediated hepatic injury. *Hepatology* **24**, 702-710, doi:10.1053/jhep.1996.v24.pm0008781346 (1996).
102. Datta, G., Fuller, B. J. & Davidson, B. R. Molecular mechanisms of liver ischemia reperfusion injury: insights from transgenic knockout models. *World J Gastroenterol* **19**, 1683-1698, doi:10.3748/wjg.v19.i11.1683 (2013).
103. Hokeness, K. L., Kuziel, W. A., Biron, C. A. & Salazar-Mather, T. P. Monocyte chemoattractant protein-1 and CCR2 interactions are required for IFN-alpha/beta-induced inflammatory responses and antiviral defense in liver. *J Immunol* **174**, 1549-1556 (2005).
104. Lee, P. Y., Li, Y., Kumagai, Y., Xu, Y., Weinstein, J. S., Kellner, E. S., Nacionales, D. C., Butfiloski, E. J., van Rooijen, N., Akira, S., Sobel, E. S., Satoh, M. & Reeves, W. H. Type I interferon modulates monocyte recruitment and maturation in chronic inflammation. *Am J Pathol* **175**, 2023-2033, doi:10.2353/ajpath.2009.090328 (2009).
105. Majer, O., Bourgeois, C., Zwolanek, F., Lassnig, C., Kerjaschki, D., Mack, M., Muller, M. & Kuchler, K. Type I interferons promote fatal immunopathology by regulating inflammatory monocytes and neutrophils during Candida infections. *PLoS Pathog* **8**, e1002811, doi:10.1371/journal.ppat.1002811 (2012).
106. Seo, S. U., Kwon, H. J., Ko, H. J., Byun, Y. H., Seong, B. L., Uematsu, S., Akira, S. & Kweon, M. N. Type I interferon signaling regulates Ly6C(hi) monocytes and

neutrophils during acute viral pneumonia in mice. *PLoS Pathog* **7**, e1001304, doi:10.1371/journal.ppat.1001304 (2011).
107. Seya, T., Oshiumi, H., Sasai, M., Akazawa, T. & Matsumoto, M. TICAM-1 and TICAM-2: toll-like receptor adapters that participate in induction of type 1 interferons. *Int J Biochem Cell Biol* **37**, 524-529, doi:10.1016/j.biocel.2004.07.018 (2005).
108. Sato, S., Sugiyama, M., Yamamoto, M., Watanabe, Y., Kawai, T., Takeda, K. & Akira, S. Toll/IL-1 Receptor Domain-Containing Adaptor Inducing IFN- (TRIF) Associates with TNF Receptor-Associated Factor 6 and TANK-Binding Kinase 1, and Activates Two Distinct Transcription Factors, NF- B and IFN-Regulatory Factor-3, in the Toll-Like Receptor Signaling. *The Journal of Immunology* **171**, 4304-4310, doi:10.4049/jimmunol.171.8.4304 (2003).
109. Nakai, H., Fuess, S., Storm, T. A., Muramatsu, S., Nara, Y. & Kay, M. A. Unrestricted hepatocyte transduction with adeno-associated virus serotype 8 vectors in mice. *J Virol* **79**, 214-224, doi:10.1128/JVI.79.1.214-224.2005 (2005).
110. Cooper, M., Nayak, S., Hoffman, B. E., Terhorst, C., Cao, O. & Herzog, R. W. Improved induction of immune tolerance to factor IX by hepatic AAV-8 gene transfer. *Hum Gene Ther* **20**, 767-776, doi:10.1089/hum.2008.161 (2009).
111. Zaiss, A. K., Liu, Q., Bowen, G. P., Wong, N. C. W., Bartlett, J. S. & Muruve, D. A. Differential Activation of Innate Immune Responses by Adenovirus and Adeno-Associated Virus Vectors. *Journal of Virology* **76**, 4580-4590, doi:10.1128/jvi.76.9.4580-4590.2002 (2002).
112. Cavassani, K. A., Moreira, A. P., Habiel, D., Ito, T., Coelho, A. L., Allen, R. M., Hu, B., Raphelson, J., Carson, W. F. t., Schaller, M. A., Lukacs, N. W., Omary, M. B., Hogaboam, C. M. & Kunkel, S. L. Toll like receptor 3 plays a critical role in the progression and severity of acetaminophen-induced hepatotoxicity. *PLoS One* **8**, e65899, doi:10.1371/journal.pone.0065899 (2013).
113. Xiao, X., Zhao, P., Rodriguez-Pinto, D., Qi, D., Henegariu, O., Alexopoulou, L., Flavell, R. A., Wong, F. S. & Wen, L. Inflammatory regulation by TLR3 in acute hepatitis. *J Immunol* **183**, 3712-3719, doi:10.4049/jimmunol.0901221 (2009).
114. Jayandharan, G. R., Aslanidi, G., Martino, A. T., Jahn, S. C., Perrin, G. Q., Herzog, R. W. & Srivastava, A. Activation of the NF-kappaB pathway by adeno-associated virus (AAV) vectors and its implications in immune response and gene therapy. *Proc Natl Acad Sci U S A* **108**, 3743-3748, doi:10.1073/pnas.1012753108 (2011).
115. Kariko, K., Ni, H., Capodici, J., Lamphier, M. & Weissman, D. mRNA is an endogenous ligand for Toll-like receptor 3. *J Biol Chem* **279**, 12542-12550, doi:10.1074/jbc.M310175200 (2004).
116. Tang, Y., Bian, Z., Zhao, L., Liu, Y., Liang, S., Wang, Q., Han, X., Peng, Y., Chen, X., Shen, L., Qiu, D., Li, Z. & Ma, X. Interleukin-17 exacerbates hepatic steatosis and inflammation in non-alcoholic fatty liver disease. *Clin Exp Immunol* **166**, 281-290, doi:10.1111/j.1365-2249.2011.04471.x (2011).
117. Affo, S., Rodrigo-Torres, D., Blaya, D., Morales-Ibanez, O., Coll, M., Millan, C., Altamirano, J., Arroyo, V., Caballeria, J., Bataller, R., Gines, P. & Sancho-Bru, P. Chemokine Receptor Ccr6 Deficiency Alters Hepatic Inflammatory Cell Recruitment and Promotes Liver Inflammation and Fibrosis. *PLoS One* **10**, e0145147, doi:10.1371/journal.pone.0145147 (2015).
118. Hammerich, L., Bangen, J. M., Govaere, O., Zimmermann, H. W., Gassler, N., Huss, S., Liedtke, C., Prinz, I., Lira, S. A., Luedde, T., Roskams, T., Trautwein, C., Heymann, F. & Tacke, F. Chemokine receptor CCR6-dependent

accumulation of gammadelta T cells in injured liver restricts hepatic inflammation and fibrosis. *Hepatology* **59**, 630-642, doi:10.1002/hep.26697 (2014).
119. Saelens, X., Festjens, N., Parthoens, E., Vanoverberghe, I., Kalai, M., van Kuppeveld, F. & Vandenabeele, P. Protein synthesis persists during necrotic cell death. *J Cell Biol* **168**, 545-551, doi:10.1083/jcb.200407162 (2005).
120. Saito, K., Dai, Y. & Ohtsuka, K. Enhanced expression of heat shock proteins in gradually dying cells and their release from necrotically dead cells. *Exp Cell Res* **310**, 229-236, doi:10.1016/j.yexcr.2005.07.014 (2005).
121. Vanden Berghe, T., Kalai, M., Denecker, G., Meeus, A., Saelens, X. & Vandenabeele, P. Necrosis is associated with IL-6 production but apoptosis is not. *Cell Signal* **18**, 328-335, doi:10.1016/j.cellsig.2005.05.003 (2006).
122. Cullen, S. P., Henry, C. M., Kearney, C. J., Logue, S. E., Feoktistova, M., Tynan, G. A., Lavelle, E. C., Leverkus, M. & Martin, S. J. Fas/CD95-induced chemokines can serve as "find-me" signals for apoptotic cells. *Mol Cell* **49**, 1034-1048, doi:10.1016/j.molcel.2013.01.025 (2013).
123. Yatim, N., Jusforgues-Saklani, H., Orozco, S., Schulz, O., Barreira da Silva, R., Reis e Sousa, C., Green, D. R., Oberst, A. & Albert, M. L. RIPK1 and NF-kappaB signaling in dying cells determines cross-priming of CD8(+) T cells. *Science* **350**, 328-334, doi:10.1126/science.aad0395 (2015).
124. Allen, K., Jaeschke, H. & Copple, B. L. Bile acids induce inflammatory genes in hepatocytes: a novel mechanism of inflammation during obstructive cholestasis. *Am J Pathol* **178**, 175-186, doi:10.1016/j.ajpath.2010.11.026 (2011).
125. Takahashi, Y., Soejima, Y. & Fukusato, T. Animal models of nonalcoholic fatty liver disease/nonalcoholic steatohepatitis. *World J Gastroenterol* **18**, 2300-2308, doi:10.3748/wjg.v18.i19.2300 (2012).
126. Vos, M. B. & Lavine, J. E. Dietary fructose in nonalcoholic fatty liver disease. *Hepatology* **57**, 2525-2531, doi:10.1002/hep.26299 (2013).
127. Lim, J. S., Mietus-Snyder, M., Valente, A., Schwarz, J. M. & Lustig, R. H. The role of fructose in the pathogenesis of NAFLD and the metabolic syndrome. *Nat Rev Gastroenterol Hepatol* **7**, 251-264, doi:10.1038/nrgastro.2010.41 (2010).
128. Abid, A., Taha, O., Nseir, W., Farah, R., Grosovski, M. & Assy, N. Soft drink consumption is associated with fatty liver disease independent of metabolic syndrome. *J Hepatol* **51**, 918-924, doi:10.1016/j.jhep.2009.05.033 (2009).
129. Assy, N., Nasser, G., Kamayse, I., Nseir, W., Beniashvili, Z., Djibre, A. & Grosovski, M. Soft drink consumption linked with fatty liver in the absence of traditional risk factors. *Can J Gastroenterol* **22**, 811-816 (2008).
130. Machado, M. V., Michelotti, G. A., Xie, G., Almeida Pereira, T., Boursier, J., Bohnic, B., Guy, C. D. & Diehl, A. M. Mouse models of diet-induced nonalcoholic steatohepatitis reproduce the heterogeneity of the human disease. *PLoS One* **10**, e0127991, doi:10.1371/journal.pone.0127991 (2015).
131. Ito, M., Suzuki, J., Tsujioka, S., Sasaki, M., Gomori, A., Shirakura, T., Hirose, H., Ito, M., Ishihara, A., Iwaasa, H. & Kanatani, A. Longitudinal analysis of murine steatohepatitis model induced by chronic exposure to high-fat diet. *Hepatol Res* **37**, 50-57, doi:10.1111/j.1872-034X.2007.00008.x (2007).
132. Kawasaki, T., Igarashi, K., Koeda, T., Sugimoto, K., Nakagawa, K., Hayashi, S., Yamaji, R., Inui, H., Fukusato, T. & Yamanouchi, T. Rats fed fructose-enriched diets have characteristics of nonalcoholic hepatic steatosis. *J Nutr* **139**, 2067-2071, doi:10.3945/jn.109.105858 (2009).
133. Spruss, A., Kanuri, G., Wagnerberger, S., Haub, S., Bischoff, S. C. & Bergheim, I. Toll-like receptor 4 is involved in the development of fructose-induced hepatic steatosis in mice. *Hepatology* **50**, 1094-1104, doi:10.1002/hep.23122 (2009).

134. Wagnerberger, S., Spruss, A., Kanuri, G., Volynets, V., Stahl, C., Bischoff, S. C. & Bergheim, I. Toll-like receptors 1-9 are elevated in livers with fructose-induced hepatic steatosis. *Br J Nutr* **107**, 1727-1738, doi:10.1017/S0007114511004983 (2012).
135. Armutcu, F., Coskun, O., Gurel, A., Kanter, M., Can, M., Ucar, F. & Unalacak, M. Thymosin alpha 1 attenuates lipid peroxidation and improves fructose-induced steatohepatitis in rats. *Clin Biochem* **38**, 540-547, doi:10.1016/j.clinbiochem.2005.01.013 (2005).
136. Ackerman, Z., Oron-Herman, M., Grozovski, M., Rosenthal, T., Pappo, O., Link, G. & Sela, B. A. Fructose-induced fatty liver disease: hepatic effects of blood pressure and plasma triglyceride reduction. *Hypertension* **45**, 1012-1018, doi:10.1161/01.HYP.0000164570.20420.67 (2005).
137. Bergheim, I., Weber, S., Vos, M., Kramer, S., Volynets, V., Kaserouni, S., McClain, C. J. & Bischoff, S. C. Antibiotics protect against fructose-induced hepatic lipid accumulation in mice: role of endotoxin. *J Hepatol* **48**, 983-992, doi:10.1016/j.jhep.2008.01.035 (2008).
138. Sookoian, S., Castano, G. O. & Pirola, C. J. Modest alcohol consumption decreases the risk of non-alcoholic fatty liver disease: a meta-analysis of 43 175 individuals. *Gut* **63**, 530-532, doi:10.1136/gutjnl-2013-305718 (2014).
139. Hashimoto, Y., Hamaguchi, M., Kojima, T., Ohshima, Y., Ohbora, A., Kato, T., Nakamura, N. & Fukui, M. Modest alcohol consumption reduces the incidence of fatty liver in men: a population-based large-scale cohort study. *J Gastroenterol Hepatol* **30**, 546-552, doi:10.1111/jgh.12786 (2015).
140. Kwon, H. K., Greenson, J. K. & Conjeevaram, H. S. Effect of lifetime alcohol consumption on the histological severity of non-alcoholic fatty liver disease. *Liver Int* **34**, 129-135, doi:10.1111/liv.12230 (2014).
141. Dunn, W., Xu, R. & Schwimmer, J. B. Modest wine drinking and decreased prevalence of suspected nonalcoholic fatty liver disease. *Hepatology* **47**, 1947-1954, doi:10.1002/hep.22292 (2008).
142. Ekstedt, M., Franzen, L. E., Holmqvist, M., Bendtsen, P., Mathiesen, U. L., Bodemar, G. & Kechagias, S. Alcohol consumption is associated with progression of hepatic fibrosis in non-alcoholic fatty liver disease. *Scand J Gastroenterol* **44**, 366-374, doi:10.1080/00365520802555991 (2009).
143. Song, M., Chen, T., Prough, R. A., Cave, M. C. & McClain, C. J. Chronic Alcohol Consumption Causes Liver Injury in High-Fructose-Fed Male Mice Through Enhanced Hepatic Inflammatory Response. *Alcohol Clin Exp Res*, doi:10.1111/acer.12994 (2016).
144. Duarte, N., Coelho, I. C., Patarrao, R. S., Almeida, J. I., Penha-Goncalves, C. & Macedo, M. P. How Inflammation Impinges on NAFLD: A Role for Kupffer Cells. *Biomed Res Int* **2015**, 984578, doi:10.1155/2015/984578 (2015).
145. Elpek, G. O. Cellular and molecular mechanisms in the pathogenesis of liver fibrosis: An update. *World J Gastroenterol* **20**, 7260-7276, doi:10.3748/wjg.v20.i23.7260 (2014).
146. Donohue, T. M., Jr., Curry-McCoy, T. V., Todero, S. L., White, R. L., Kharbanda, K. K., Nanji, A. A. & Osna, N. A. L-Buthionine (S,R) sulfoximine depletes hepatic glutathione but protects against ethanol-induced liver injury. *Alcohol Clin Exp Res* **31**, 1053-1060, doi:10.1111/j.1530-0277.2007.00393.x (2007).
147. Lu, Y., Zhuge, J., Wang, X., Bai, J. & Cederbaum, A. I. Cytochrome P450 2E1 contributes to ethanol-induced fatty liver in mice. *Hepatology* **47**, 1483-1494, doi:10.1002/hep.22222 (2008).

148. Clugston, R. D., Yuen, J. J., Hu, Y., Abumrad, N. A., Berk, P. D., Goldberg, I. J., Blaner, W. S. & Huang, L. S. CD36-deficient mice are resistant to alcohol- and high-carbohydrate-induced hepatic steatosis. *J Lipid Res* **55**, 239-246, doi:10.1194/jlr.M041863 (2014).
149. Mandrekar, P., Ambade, A., Lim, A., Szabo, G. & Catalano, D. An essential role for monocyte chemoattractant protein-1 in alcoholic liver injury: regulation of proinflammatory cytokines and hepatic steatosis in mice. *Hepatology* **54**, 2185-2197, doi:10.1002/hep.24599 (2011).
150. Obstfeld, A. E., Sugaru, E., Thearle, M., Francisco, A. M., Gayet, C., Ginsberg, H. N., Ables, E. V. & Ferrante, A. W., Jr. C-C chemokine receptor 2 (CCR2) regulates the hepatic recruitment of myeloid cells that promote obesity-induced hepatic steatosis. *Diabetes* **59**, 916-925, doi:10.2337/db09-1403 (2010).
151. Suraweera, D. B., Weeratunga, A. N., Hu, R. W., Pandol, S. J. & Hu, R. Alcoholic hepatitis: The pivotal role of Kupffer cells. *World J Gastrointest Pathophysiol* **6**, 90-98, doi:10.4291/wjgp.v6.i4.90 (2015).
152. Suh, Y. G. & Jeong, W. I. Hepatic stellate cells and innate immunity in alcoholic liver disease. *World J Gastroenterol* **17**, 2543-2551, doi:10.3748/wjg.v17.i20.2543 (2011).
153. Lieber, C. S., Leo, M. A., Mak, K. M., Xu, Y., Cao, Q., Ren, C., Ponomarenko, A. & DeCarli, L. M. Model of nonalcoholic steatohepatitis. *Am J Clin Nutr* **79**, 502-509 (2004).
154. Crispe, I. N. Hepatocytes as Immunological Agents. *J Immunol* **196**, 17-21, doi:10.4049/jimmunol.1501668 (2016).
155. Thompson, A. J. & Locarnini, S. A. Toll-like receptors, RIG-I-like RNA helicases and the antiviral innate immune response. *Immunol Cell Biol* **85**, 435-445, doi:10.1038/sj.icb.7100100 (2007).
156. Wree, A., Mehal, W. Z. & Feldstein, A. E. Targeting Cell Death and Sterile Inflammation Loop for the Treatment of Nonalcoholic Steatohepatitis. *Semin Liver Dis* **36**, 27-36, doi:10.1055/s-0035-1571272 (2016).
157. Liu, W., Baker, R. D., Bhatia, T., Zhu, L. & Baker, S. S. Pathogenesis of nonalcoholic steatohepatitis. *Cell Mol Life Sci*, doi:10.1007/s00018-016-2161-x (2016).
158. Mehal, W. Z. The inflammasome in liver injury and non-alcoholic fatty liver disease. *Dig Dis* **32**, 507-515, doi:10.1159/000360495 (2014).
159. Cavassani, K. A., Ishii, M., Wen, H., Schaller, M. A., Lincoln, P. M., Lukacs, N. W., Hogaboam, C. M. & Kunkel, S. L. TLR3 is an endogenous sensor of tissue necrosis during acute inflammatory events. *J Exp Med* **205**, 2609-2621, doi:10.1084/jem.20081370 (2008).
160. Zhou, R., Wei, H., Sun, R. & Tian, Z. Recognition of double-stranded RNA by TLR3 induces severe small intestinal injury in mice. *J Immunol* **178**, 4548-4556 (2007).
161. Jeyaseelan, S., Young, S. K., Fessler, M. B., Liu, Y., Malcolm, K. C., Yamamoto, M., Akira, S. & Worthen, G. S. Toll/IL-1 Receptor Domain-Containing Adaptor Inducing IFN- (TRIF)-Mediated Signaling Contributes to Innate Immune Responses in the Lung during Escherichia coli Pneumonia. *The Journal of Immunology* **178**, 3153-3160, doi:10.4049/jimmunol.178.5.3153 (2007).
162. Shi, H., Kokoeva, M. V., Inouye, K., Tzameli, I., Yin, H. & Flier, J. S. TLR4 links innate immunity and fatty acid-induced insulin resistance. *J Clin Invest* **116**, 3015-3025, doi:10.1172/JCI28898 (2006).

163. Cullberg, K. B., Larsen, J. O., Pedersen, S. B. & Richelsen, B. Effects of LPS and dietary free fatty acids on MCP-1 in 3T3-L1 adipocytes and macrophages in vitro. *Nutr Diabetes* **4**, e113, doi:10.1038/nutd.2014.10 (2014).
164. Suganami, T., Tanimoto-Koyama, K., Nishida, J., Itoh, M., Yuan, X., Mizuarai, S., Kotani, H., Yamaoka, S., Miyake, K., Aoe, S., Kamei, Y. & Ogawa, Y. Role of the Toll-like receptor 4/NF-kappaB pathway in saturated fatty acid-induced inflammatory changes in the interaction between adipocytes and macrophages. *Arterioscler Thromb Vasc Biol* **27**, 84-91, doi:10.1161/01.ATV.0000251608.09329.9a (2007).
165. Lee, J. Y., Sohn, K. H., Rhee, S. H. & Hwang, D. Saturated fatty acids, but not unsaturated fatty acids, induce the expression of cyclooxygenase-2 mediated through Toll-like receptor 4. *J Biol Chem* **276**, 16683-16689, doi:10.1074/jbc.M011695200 (2001).
166. Schaeffler, A., Gross, P., Buettner, R., Bollheimer, C., Buechler, C., Neumeier, M., Kopp, A., Schoelmerich, J. & Falk, W. Fatty acid-induced induction of Toll-like receptor-4/nuclear factor-kappaB pathway in adipocytes links nutritional signalling with innate immunity. *Immunology* **126**, 233-245, doi:10.1111/j.1365-2567.2008.02892.x (2009).
167. Erridge, C. & Samani, N. J. Saturated fatty acids do not directly stimulate Toll-like receptor signaling. *Arterioscler Thromb Vasc Biol* **29**, 1944-1949, doi:10.1161/ATVBAHA.109.194050 (2009).
168. Harte, A. L., da Silva, N. F., Creely, S. J., McGee, K. C., Billyard, T., Youssef-Elabd, E. M., Tripathi, G., Ashour, E., Abdalla, M. S., Sharada, H. M., Amin, A. I., Burt, A. D., Kumar, S., Day, C. P. & McTernan, P. G. Elevated endotoxin levels in non-alcoholic fatty liver disease. *J Inflamm (Lond)* **7**, 15, doi:10.1186/1476-9255-7-15 (2010).
169. Wong, V. W., Wong, G. L., Chan, H. Y., Yeung, D. K., Chan, R. S., Chim, A. M., Chan, C. K., Tse, Y. K., Woo, J., Chu, W. C. & Chan, H. L. Bacterial endotoxin and non-alcoholic fatty liver disease in the general population: a prospective cohort study. *Aliment Pharmacol Ther* **42**, 731-740, doi:10.1111/apt.13327 (2015).
170. Jurgens, H., Haass, W., Castaneda, T. R., Schurmann, A., Koebnick, C., Dombrowski, F., Otto, B., Nawrocki, A. R., Scherer, P. E., Spranger, J., Ristow, M., Joost, H. G., Havel, P. J. & Tschop, M. H. Consuming fructose-sweetened beverages increases body adiposity in mice. *Obes Res* **13**, 1146-1156, doi:10.1038/oby.2005.136 (2005).
171. Dini, L., Pagliara, P. & Carla, E. C. Phagocytosis of apoptotic cells by liver: a morphological study. *Microsc Res Tech* **57**, 530-540, doi:10.1002/jemt.10107 (2002).
172. Dini, L., Autuori, F., Lentini, A., Oliverio, S. & Piacentini, M. The clearance of apoptotic cells in the liver is mediated by the asialoglycoprotein receptor. *FEBS Lett* **296**, 174-178 (1992).
173. Baratta, J. L., Ngo, A., Lopez, B., Kasabwalla, N., Longmuir, K. J. & Robertson, R. T. Cellular organization of normal mouse liver: a histological, quantitative immunocytochemical, and fine structural analysis. *Histochem Cell Biol* **131**, 713-726, doi:10.1007/s00418-009-0577-1 (2009).
174. Klein, I., Cornejo, J. C., Polakos, N. K., John, B., Wuensch, S. A., Topham, D. J., Pierce, R. H. & Crispe, I. N. Kupffer cell heterogeneity: functional properties of bone marrow derived and sessile hepatic macrophages. *Blood* **110**, 4077-4085, doi:10.1182/blood-2007-02-073841 (2007).

175. Winau, F., Quack, C., Darmoise, A. & Kaufmann, S. H. Starring stellate cells in liver immunology. *Curr Opin Immunol* **20**, 68-74, doi:10.1016/j.coi.2007.10.006 (2008).
176. Wynn, T. A. & Ramalingam, T. R. Mechanisms of fibrosis: therapeutic translation for fibrotic disease. *Nat Med* **18**, 1028-1040, doi:10.1038/nm.2807 (2012).
177. Crispe, I. N. The liver as a lymphoid organ. *Annu Rev Immunol* **27**, 147-163, doi:10.1146/annurev.immunol.021908.132629 (2009).
178. Seglen, P. O. Preparation of isolated rat liver cells. *Methods Cell Biol* **13**, 29-83 (1976).
179. Ebrahimkhani, M. R., Mohar, I. & Crispe, I. N. Cross-presentation of antigen by diverse subsets of murine liver cells. *Hepatology* **54**, 1379-1387, doi:10.1002/hep.24508 (2011).
180. Brownell, J., Wagoner, J., Lovelace, E. S., Thirstrup, D., Mohar, I., Smith, W., Giugliano, S., Li, K., Crispe, I. N., Rosen, H. R. & Polyak, S. J. Independent, parallel pathways to CXCL10 induction in HCV-infected hepatocytes. *J Hepatol* **59**, 701-708, doi:10.1016/j.jhep.2013.06.001 (2013).